

WASHINGTON UNIVERSITY  
THE HENRY EDWIN SEVER GRADUATE SCHOOL  
DEPARTMENT OF CIVIL ENGINEERING

---

A STRUCTURAL HEALTH MONITORING FRAMEWORK  
FOR CIVIL STRUCTURES

by

Diego F. Giraldo

Prepared under the direction of Professor Shirley J. Dyke

---

A dissertation presented to the Henry Edwin Sever Graduate School of  
Washington University in partial fulfillment of the  
requirements of the degree of  
DOCTOR OF SCIENCE

May 2006

Saint Louis, Missouri

WASHINGTON UNIVERSITY  
THE HENRY EDWIN SERVER GRADUATE SCHOOL  
DEPARTMENT OF CIVIL ENGINEERING

---

ABSTRACT

---

A STRUCTURAL HEALTH MONITORING FRAMEWORK  
FOR CIVIL STRUCTURES

by

Diego F. Giraldo

---

ADVISOR: Professor Shirley J. Dyke

---

May 2006

Saint Louis, Missouri

---

A health monitoring framework that detects and localizes damage in civil structures is proposed in this dissertation. Dynamic measurements of the systems as they vibrate under the influence of ambient and service loads are used to characterize the structural condition at any given time. Localization of damage is achieved by comparing characterizations in the pre and post damage states from a statistical point of view. Damage is localized regardless of the environmental conditions that affect the structures' dynamic behavior. Full automation of the data analysis is pursued. The methodology is tested with simulated responses of a finite element model that represents a typical highway bridge. Several uncertainties and modeling errors typically found in real applications were considered in this numerical example. The main advantages and limitations of the proposed framework are explained. The research emphasizes realistic applicability to civil structures in which only a few low vibrational modes can be measured with relatively high accuracy, and noise in sensors is unavoidable. However, the proposed framework as a whole (or in part) is likely to perform well in other engineering fields.

# Contents

<b>List of Tables .....</b>	<b>v</b>
<b>List of Figures.....</b>	<b>vi</b>
<b>Acknowledgments .....</b>	<b>ix</b>
<b>1 Introduction .....</b>	<b>1</b>
1.1 Classification of SHM Techniques .....	2
1.2 Remaining Challenges .....	6
1.3 General Trends.....	7
1.4 Main Objective .....	8
1.5 Overview.....	8
<b>2 Modal Identification Through Ambient Vibration .....</b>	<b>10</b>
2.1 Time-invariant Linear Systems.....	13
2.1.1 Discrete Systems .....	14
2.1.2 Modal Properties .....	16
2.2 The Methodologies .....	18
2.2.1 Free Response Estimation Techniques.....	18
2.2.2 Modal Identification Techniques.....	23
2.2.3 Data Management .....	33
2.3 The Benchmark Structure .....	35
2.3.1 Experimental Setup .....	36
2.3.2 Analytical Model.....	37
2.4 Analytical Analysis and Results .....	39
2.4.1 Free Response Estimation.....	39
2.4.2 Modal Identification.....	42
2.4.3 Comparison of Results .....	49
2.5 Experimental Results .....	54
2.5.1 Hammer Testing (Implementation of ERA/DC).....	55
2.5.2 Comparison of Results .....	56
2.6 Conclusions.....	58

<b>3</b>	<b>Structural Health Monitoring Through Model Updating .....</b>	<b>60</b>
3.1	Methodology .....	62
3.1.1	The Objective Function.....	64
3.1.2	Optimization Technique .....	65
3.1.3	Gradients and Hessian of Objective Function.....	67
3.1.4	Sensitivities of Mode Shapes .....	69
3.1.5	Derivatives of the Stiffness Matrix .....	73
3.1.6	Implementation Issues.....	74
3.2	Validation through Analytical Model .....	76
3.2.1	The Identification Model .....	79
3.2.2	Convergence of Mode Shape Sensitivities.....	80
3.2.3	Optimization Results.....	81
3.2.4	Convergence Rate .....	83
3.3	Conclusions.....	84
<b>4</b>	<b>Accommodating Varying Environmental Conditions .....</b>	<b>86</b>
4.1	Methodology .....	88
4.1.1	Stiffness Characterization Through Least Squares .....	89
4.1.2	Principal Component Analysis.....	90
4.2	Validation Through Analytical Model .....	99
4.2.1	Identification Model.....	101
4.2.2	Applying PCA.....	102
4.3	Conclusions.....	108
<b>5</b>	<b>SHM Framework Definition and Validation .....</b>	<b>110</b>
5.1	The Structural Health Monitoring Framework .....	111
5.1.1	Identification of Dynamic Properties.....	111
5.1.2	Building an Identification Model.....	114
5.1.3	Forming an Accurate Baseline .....	115
5.1.4	Setting up the Optimization Algorithm.....	116
5.1.5	Multiple Characterizations of the Healthy Structure .....	118
5.1.6	Outlier Analysis and Issuing Warnings.....	118
5.2	Numerical Example .....	120
5.2.1	The Finite Element Model .....	121
5.2.2	Damage Scenarios.....	123
5.2.3	Simulating Dynamic Responses.....	126
5.3	Implementation of the SHM Framework.....	127
5.3.1	Identification of Dynamic Properties .....	127
5.3.2	The Identification Model .....	130

5.3.3	The Search for a Baseline .....	133
5.3.4	Setting up the Optimization Algorithm.....	135
5.3.5	Multiple Characterizations of the Healthy Structure .....	136
5.3.6	Outlier Analysis and Issuing Warnings.....	136
5.4	Conclusions.....	142
<b>6</b>	<b>Conclusions .....</b>	<b>145</b>
6.1	Future Work .....	147
	<b>References.....</b>	<b>149</b>
	<b>Vita .....</b>	<b>156</b>

## List of Tables

Table 2.1	Member properties of benchmark experiment.....	36
Table 2.2	Theoretical natural frequencies and damping ratios.....	39
Table 2.3	Evaluation criteria.....	49
Table 2.4	Evaluation criteria for constant noise level .....	52
Table 2.5	Evaluation criteria for variable noise level.....	54
Table 2.6	Identified modal properties.....	57
Table 3.1	Damage scenarios .....	77
Table 3.2	Expected stiffness reduction on ID-model .....	79
Table 4.1	Damage patterns investigated in this study .....	99
Table 4.2	Warnings issued.....	106
Table 4.3	Warnings issued for unbraced cases .....	108
Table 5.1	Damage scenarios .....	124
Table 5.2	Expected damaged elements of ID-model.....	132
Table 5.3	Warnings issued.....	137

## List of Figures

Figure 1.1	Classification of SHM techniques .....	3
Figure 2.1	The benchmark structure .....	35
Figure 2.2	Analytical model of the benchmark problem .....	38
Figure 2.3	Comparison of estimated free responses by NExT and RDD .....	41
Figure 2.4	Numerical implementation of ERA/DC .....	43
Figure 2.5	Typical stabilization diagram for ERA/DC .....	45
Figure 2.6	Accuracy of first natural frequency for different ARMAv model orders ...	46
Figure 2.7	Numerical implementation of PEM/LS .....	47
Figure 2.8	Accuracy of first natural frequency for different truncations .....	48
Figure 2.9	Numerical implementation of SSI .....	49
Figure 2.10	Deviation of identified natural frequencies ( $J_1$ ) .....	51
Figure 2.11	Deviation of identified damping ratios ( $J_3$ ) .....	51
Figure 2.12	Computational modes detected with ERA/DC ( $J_2$ ).....	51
Figure 2.13	Accuracy of identified natural frequencies as a function of noise level.....	53
Figure 2.14	Accuracy of identified mode shapes ( $J_2$ ) as a function of noise level.....	53
Figure 2.15	Accuracy of identified damping ratios ( $J_3$ ) as a function of noise level ...	54
Figure 2.16	Typical impulse responses .....	56

Figure 2.17 Experimentally identified mode shapes.....	58
Figure 3.1 Conjugate gradients algorithm with Newton-Ramphson and Fletcher-Reeves (From [67]) .....	67
Figure 3.2 Shear model with 3 DOF .....	73
Figure 3.3 Finite element model of the continuous beam with three supports (512 elements) .....	77
Figure 3.4 Mass-normalized mode shapes of the healthy model .....	78
Figure 3.5 ID-model with three supports (32 elements) .....	79
Figure 3.6 Convergence of mode shape sensitivities .....	80
Figure 3.7 Optimization results (ideal conditions).....	81
Figure 3.8 Optimization results (noisy mode shapes).....	82
Figure 3.9 Convergence rate of three optimization algorithms.....	83
Figure 4.1 Identified stiffness values of the two dimensional example (E1 and E2)...	94
Figure 4.2 Residual error after projection .....	96
Figure 4.3 Prediction model based on healthy elements.....	97
Figure 4.4 Young's modulus of steel vs. temperature (after [76]) .....	100
Figure 4.5 Association between members of the finite element model and elements of the identification model .....	101
Figure 4.6 Identified stiffnesses in the healthy state .....	102
Figure 4.7 Residual error ( $e_p$ ) of two elements of the first floor before and after damage (case 2) .....	104

Figure 4.8 Variation of stiffness values detected of two elements of the first floor before and after damage (case 2) .....	105
Figure 4.9 Outlier samples of residual error ( $> 2\%$ ) .....	107
Figure 5.1 Typical highway bridge with three simple supports .....	120
Figure 5.2 Finite element model .....	121
Figure 5.3 Damage scenarios .....	125
Figure 5.4 Frequency content of random inputs .....	126
Figure 5.5 Sensor placement .....	128
Figure 5.6 Accelerations recorded from three sensors .....	128
Figure 5.7 Identified modal properties of the healthy structure .....	130
Figure 5.8 Identification model .....	131
Figure 5.9 Identified baseline for the optimization process .....	134
Figure 5.10 Modal properties of the updated ID-model .....	134
Figure 5.11 Convergence of mode shape sensitivities .....	135
Figure 5.12 100 characterizations of the healthy structure .....	136
Figure 5.13 Outlier samples of residual error ( $> 5\%$ ) .....	138
Figure 5.14 Residual error (PCA) and Young's moduli reduction (no-PCA) (Averaged values over 20 samples) .....	141

## Acknowledgments

Special thanks to Dr. Shirley Dyke for her support and patience during all this time. Without her ideas, critiques, and unscheduled help, this dissertation would not have become a reality. I would also like to thank all members of the committee for taking some of their time to revise this document and to all graduate students who worked with me during all this time and provided ideas that were materialized here.

Lastly, I would like to thank the National Science Foundation which funded this research through grants No. CMS-0245402 and CMS 97-33272.

Diego F. Giraldo

*Washington University in St. Louis*

*May 2006*

# Chapter 1

## Introduction

Structural health monitoring (SHM) has become an important area of research within the civil engineering community in recent years. Its potential is so promising that hundreds of scientists from around the world are trying to develop techniques to assess damage in structures by using response measurements and complex algorithms. However, our community is still far from obtaining a framework that effectively detects damage in structures that have been heavily excited by a natural phenomenon, or have suffered from regular daily use and display conditions such as corrosion or fatigue, all within a reasonable budget. Until this vision is realized, significant funds are being spent on visual and enhanced visual inspections that often require the removal of non-structural components and can be affected by the inspector's subjective judgment. Moreover, due to the highly qualified personnel they require, these type of inspections might not be possible immediately after a major event. For instance, the city of Seattle has more than 150 bridges to inspect in the case of a catastrophic event. As our infrastructure grows at higher rates than ever before, and larger and more complex structures are being constructed, the need to reduce costs, improve the reliability, and accelerate the process of inspecting our most important structures, becomes more evident.

Some of the desired features of SHM techniques include automating the data analysis process to minimize the need for human supervision, and the capability to identify damage in the structure while it is in service as well as after a major event. It is also desirable

that different degrees and types of damage be identified accurately as they occur regardless of the environmental conditions that may affect the structure's behavior. However, it is unrealistic to think that a single technique would be capable of detecting damage of different natures such as a loss of stiffness in a structural element, corrosion in a steel connection, or an overstress due to a static deflection. Therefore, a combination of methodologies that optimally combines their outputs and takes full advantage of the information available should be the final goal of the research in this area.

The research performed in this dissertation attempts to combine two complementary techniques in order to accurately detect and localize structural damage. Ambient vibrations constitute the only source of information and the effects of the unknown environmental conditions are systematically accommodated. The resulting structural health monitoring framework does not attempt to quantify the damage or state a prognosis of the structure's condition. Moreover, the emphasis is limited to the localization of structurally deficient elements capable of changing the global dynamic properties of the structures.

## **1.1 Classification of SHM Techniques**

SHM techniques can be classified according to several characteristics. For instance, in 1993, Rytter [65] established four levels of techniques determined by the information provided to the user (see Fig. 1.1). Under this distinction, level 1 simply determines whether damage has occurred, whereas level 4 also determines the location, severity and remaining life of the structure. Another important method for classification is associated with the type of input required to analyze the status of the structure. Here, SHM techniques are classified as vibration-based, statically-based, and those that perform a direct inspection of the structural elements. This last category includes approaches such as the use of fatigue sensors, crack recognition through digital imaging, crack detection in concrete with embedded sensors, and corrosion detection procedures. Although promising

results are being obtained by some researchers working in those areas, direct inspection techniques are usually localized and expensive and their use in large civil structures is not always feasible.

Statically-based procedures use static deflections under specific load conditions to determine the changes on the stiffness of the structure. An example of these types of methods was proposed by Johnson [46] who developed an optimization technique to detect damage in frames using previously known static loads and the deflections produced in the healthy and damaged structures. In his work, the stiffness matrix of a finite element

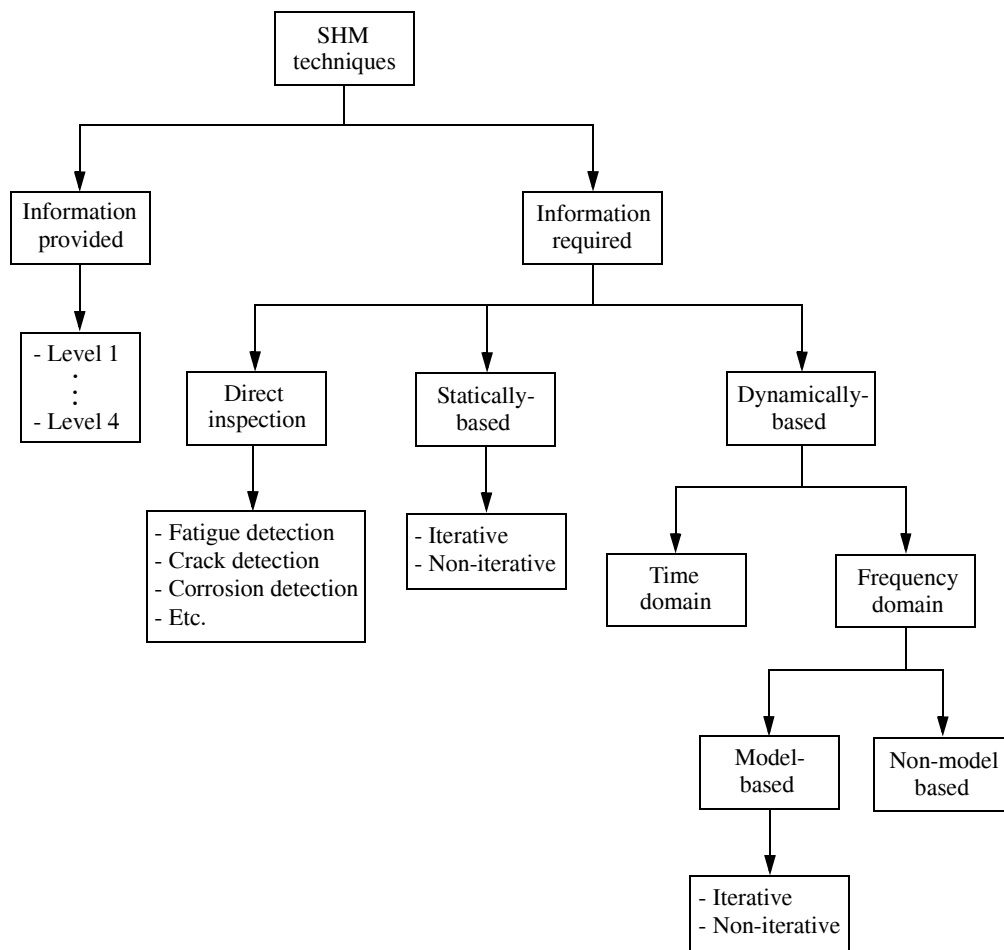


**Figure 1.1 Classification of SHM techniques**

model representative of the structure is updated until its response matches the measured deflection. Hu and Shenton [37] used genetic algorithms to detect damage in an analytical two-span continuous beam with a uniformly distributed load. The concept of redistribution of dead load when damage occurs is used in their work. Yokoyama and Rafiquzzaman [78], on the other hand, developed a damage identification technique that uses the static deflections and support reactions produced by a moving load on several types of bridges including simply supported beams, girder systems and slabs. The variability of the curvature is analyzed to detect damaged elements. In general, statically-based SHM methods are limited regarding the information obtained from the structure and are difficult to implement due to the large static loads required.

Unlike the slow development of statically-based methods, vibration-based SHM techniques for civil structures has been growing rapidly during the last two decades. In 1998 Doebling *et al.* [23] provided a broad review of the literature in this area, exposing the advantages and capabilities of several methodologies. Under this classification, time-dependent response measurements are obtained from the structure to analyze its behavior. Most of these methods use the characteristics of a healthy structure and compare them to those displayed at any given time to detect the existence of damage and localize the weakness with certain accuracy. Lei *et al.* [51], for example, proposed the Time Series Analysis, a technique in which a localized analysis of the outputs of the structure is used to determine the proximity of damage.

The work performed by Lei *et al.*, however, differs from the majority of the research being developed in vibration-based SHM, in which time-history responses of the structure are used to find its dynamic properties (i.e. natural frequencies, mode shapes and damping ratios), which are later used to localize damage. Three typical steps are used in these techniques. First, the modal properties of the healthy structure are identified using recorded responses to dynamic loads. Dynamic loads may include forced vibrations obtained with dynamic shakers or actuators, as well as ambient vibrations generated

with the normal operation of the structure. Although forced vibrations typically provide better modal information, the use of ambient vibrations constitutes an attractive alternative for modal identification as it does not require artificially loading the structure or stopping its use in order to test it. The second step consists of characterizing the structure according to the identified modal information. Here, the estimation of structural parameters such as stiffness or flexibility is often used along with a simplified finite element model representative of the structure. Some techniques, however, characterize the modal properties themselves. The third and final step consists of repeating the first two steps at any given time and comparing the characterization of the structure to the original properties in the undamaged state.

Several techniques can be found in the literature that follow this trend. For instance Bernal [9] developed a technique that uses damage location vectors (DLV). In his work, Bernal estimated the flexibility matrix of the structure for both the undamaged and damaged states based on their detected dynamic properties. Based on these flexibility matrices damage location vectors are calculated to reveal the proximity of damage. Pandey *et al.* [60] attempted to localize damage by comparing the curvature of the mode shapes before and after damage. The technique, however, is very sensitive to noise in the sensors and is limited regarding the type of structures to which it can be applied. Parloo *et al.* [61] developed a technique that localizes damage using the sensitivities of the mode shapes to changes of mass and stiffness. Although accurate detection of damage is obtained, the need for a high number of mode shapes makes the technique not always feasible for civil structures.

Unlike the work performed by Bernal, Pandey *et al.*, and Parloo *et al.* in which no mathematical model of the system is needed, some techniques make use of an identification model to localize damage. Ching and Beck [18], for example, proposed a two-stage Bayesian approach in which the most likely dynamic properties of the structure are found by reducing the error between the measured response of the structure and the cal-

culated response from a numerical model. Mass and stiffness matrices are then identified by updating a model of the structure using a Bayesian probabilistic framework. With a similar approach, Caicedo and Dyke [15] developed a technique to localize damage in elastic structures using the dynamic properties identified with ambient vibration. In this methodology, stiffness values of an identification model are calculated using its characteristic equation and the modal properties detected. Even though more information from the structure is being used in modal based methodologies (e.g. mass, geometry), the use of an identification model always introduces modeling errors into the problem.

## 1.2 Remaining Challenges

Although encouraging results have been obtained in both analytical and small scale experiments, several challenges have to be overcome before SHM becomes a reality in full-scale civil structures. Among those, a well known challenge is the uncertainty in the measured modal parameters, affected by external and uncontrollable environmental conditions such as temperature, temperature gradients, and humidity. To meet this challenge Sohn *et al.* [69] proposed a method based on an outlier analysis by Worden *et al.* [74]. This method consists of a statistical analysis that determines the distribution of the dynamic properties of the system over an undetermined number of environmental factors that affect its behavior. The method effectively eliminates the effects of the surrounding conditions and an accurate detection of damage is achieved. Kullaa [50] and Yan *et al.* [76] both took further steps with this methodology, the former applying it to civil structures, and the latter doing some experimental work with scaled models. However, the methodology is still classified as level 1 (as described by Rytter [65]) and is unable to locate the damage on the structure. The statistical nature of the method also helps to minimize the impact of unavoidable noise in sensors.

Perhaps visual inspection will not be replaced for a long time. However, the implementation of a reliable SHM framework should allow us to considerably reduce the amount

of periodic inspections needed in key structures and, more importantly, provide fast and accurate information on their state after extreme loads have been applied. Yet the biggest challenge for the research community is the search for collaboration from the industry both to fund further investigations and to involve them in the design process. To become more attractive to the industry and finally become a reality in our infrastructure, SHM systems must combine various techniques with different capabilities. Moreover, studies of the potential costs and benefits need to be carried out.

### 1.3 General Trends

Due to their importance for the normal functioning of our civilization, bridges have become an important target for research in SHM. Some challenges are associated with the implementation of such techniques in these type of structures. For instance, the typical high flexibility of long span bridges constitutes a difficulty to accurately identify modal properties. Full scale implementations of various techniques are already under development and preliminary results have been published. Abe and Siringoringo [1], for example, applied a method based on the global dynamic properties of the Hakucho Bridge (Japan) to detect changes in the stiffness of a simplified model of the bridge. Other full scale application were developed by Xiang *et al.* [75], who applied a statistically-based method to the Wenhui Bridge using several types of sensors, and Sumitro *et al.* [70], who used actual-stress measurements to detect damage in the Ashidagawa Bridge with a localized technique. All these applications are still under development, and although damage is detected with relative accuracy using analytical models, real damage is still to be detected.

Acceleration records have become the most popular measurement within the research community for structural health monitoring purposes. Simplicity, relative low price, and reliability are the most important advantages of these type of measurements. However, recent technological advances have provided engineers with a variety of sensors capable

of measuring accurate dynamic responses. Laser displacement measurements, for instance, have been used in several fields and are commercially available. However, complexity, difficulties associated with long distances, and high price constitute important drawbacks for SHM applications. Other types of measurements include the use of high resolution digital imaging to measure displacements and strain measurements using optical fibers. In the former, Paudel *et al.* [63] developed an “edge recognition” method capable of recording dynamic displacements within the frequency range of interest for civil structures. Ito *et al.* [41], in the latter, used strain measurements obtained with optical fiber sensors to avoid fatigue damage and detect shear failure in concrete slabs. While the possibilities are expanding, acceleration sensors are also developing quickly reducing consistently their size, price, and power required.

## 1.4 Main Objective

This research aims to develop a vibration-based SHM framework capable of detecting and localizing damage within a structure regardless of the surrounding environmental conditions that affect its dynamic behavior. Ambient vibrations will constitute the only source of information to characterize the stiffness of the structures at any given time. Localization of damage will be achieved by comparing characterizations in the pre and post damage states from a statistical point of view.

The research will emphasize realistic applicability to civil structures in which only a few low frequencies can be measured with relatively high accuracy, and noise in sensors is unavoidable. Moreover, the automation of the data analysis is pursued.

## 1.5 Overview

The dissertation is organized as follows. In the second chapter, a comparison of three of the most popular modal identification techniques for estimating modal properties of

structures as they vibrate in their natural environment is carried out. Both simulated as well as experimental data obtained from of a four-storey steel building known as the SHM benchmark problem is used for this purpose. The use of an optimization algorithm for model updating is proposed in Chapter 3 as a way to characterize the stiffness of a structure and localize damage by observing the changes of the identified values. Characterizations are obtained by updating a representative finite element model such that the correlation of its mode shapes with those estimated from the structure is optimized. The mathematical tools required to implement such optimization are derived here.

A principal component analysis is proposed in Chapter 4 in an attempt to accommodate the effects of unknown and varying environmental conditions over the numerical characterizations. This type of analysis requires multiple characterizations of the healthy structure under a wide range of environmental conditions in order to accurately map the influence and reduce it in post-damage characterizations. Finally, the conclusions reached and methodologies proposed in Chapters 2, 3 and 4 are combined in a six-step framework in Chapter 5. The framework is then tested using a finite element model of a typical highway bridge. Several uncertainties typically found in real-world applications are considered in this numerical example. A summary of the conclusions and possible paths for future research are discussed in Chapter 6.

## **Chapter 2**

### **Modal Identification Through Ambient Vibration**

As mentioned in Chapter 1, a significant amount of research has been done in the area of structural health monitoring (SHM) using the global dynamic properties of civil structures. In this context, the accurate identification of modal properties plays a fundamental role in the evaluation of the state of the structures. Before engaging in a discussion about the identification of these properties, it is important to underscore that, although closely related, system and modal identification are not the same. Whereas modal identification refers to the process of estimating the dynamic properties of a system (i.e. natural frequencies, damping ratios and mode shapes), with system identification an input-output model capable of reproducing or even predicting the outputs of a system is pursued. Although we are only concerned with the identification of dynamic properties in this chapter (modal identification), most recent methodologies perform system identification. Therefore, an extra step has to be implemented in order to obtain the dynamic properties as shown later in this chapter. The term modal identification will be used throughout this dissertation regardless of the fact that system identification is performed as an intermediate step.

Although impulse responses and forced vibrations have long been used in several engineering fields as reliable means to obtain modal properties, the use of these tests is not always feasible in civil engineering applications due to massive sizes and safety concerns. Moreover, civil structures are irremediably subjected to unmeasurable external

loads such as wind and soil vibrations. For these reasons, as well as cost and simplicity, the use of ambient vibrations constitutes an attractive alternative for modal identification in this field. However, several obstacles exist that make the use of ambient vibrations challenging as a source of information. Among these are the assumptions that the unmeasured loads have certain statistical properties and that a significant number of dynamic modes are excited. In addition, low amplitudes are sometimes insufficient to overcome nonlinear behavior due to internal friction [29]. Therefore, the use of ambient loading may not be applicable in all cases.

A number of techniques have been developed in the last four decades for modal identification using ambient responses. The classification of the techniques documented in the literature, however, has always been an arguable matter. For instance, depending on how the time records are employed, some authors have classified the techniques as time domain and frequency domain techniques. This classification becomes vague as some of the techniques are comprised by intermediate steps that involve complementary approaches. The scope of this study is limited to those techniques whose main algorithm is classified as time domain, allowing the use of frequency domain approaches as an initial step. Moreover, only techniques that are capable of estimating full sets of modal properties (i.e. natural frequencies, damping ratios and mode shapes) are considered.

Although widely reported in the literature, our knowledge of the relative advantages and disadvantages of the techniques with respect to similar algorithms remains limited. Several authors have published comparisons with certain restrictions and Monte-Carlo results are scarcely reported. For instance, in 1993, Lew *et al.* [52] compared the techniques derived from the eigensystem realization algorithm (ERA) while trying to keep the computational effort needed at the same level. Although this is an attractive feature to use as a baseline, by doing so some techniques were at a disadvantage. In 1995, Deforges *et al.* [22] made a comparison in which only natural frequencies and damping ratios were considered. More recently, Kinkegaard and Andersen [49] compared three of

the most popular techniques by using a rather simple dynamic system. Other comparative studies have been published by Brinker *et al.* [12], and Abdeghani *et al.* [2]. In general, complete comparisons are difficult to achieve due to the amount of technical parameters needed to carry out the techniques (e.g. model order estimation and record lengths). However, comparison studies are rarely redundant, providing different insight into certain applications and conditions.

This chapter makes an attempt to statistically compare three of the most popular modal identification techniques available in the literature. This comparison is performed on the basis of “best possible results” regardless of the computational power required. All evaluations carried out in this study use both analytically simulated data as well as experimental acceleration records from a structure selected by a working group formed by the American Society of Civil Engineers (ASCE) and the International Association of Structural Control and Monitoring (IASCM). The structure, known as the SHM benchmark problem, is a four-storey steel frame scaled at 1:3 [44]. Specifically, simulated data is employed to assess and compare, via Monte-Carlo simulations, three modal identification methods to determine which of these algorithms performs best in an entirely automated environment. Only the first six vibrational modes are targeted in the identification and the effects of noise are evaluated. Additionally, experimental data is used to analyze the viability of detecting reliable dynamic properties using typical ambient vibrations of civil structures. With this in mind, the modal properties obtained from executing the best technique to ambient vibration records are compared to those obtained with more traditional hammer testing in the experimental phase of the benchmark structure.

The chapter is organized as follows. In the first section, a brief review of time-invariant linear systems, state representations, and the mathematical meaning of modal properties is provided. The second section is devoted to presenting the modal identification methodologies evaluated. It is important to emphasize, however, that detailed mathematical derivations of the techniques are not intended. Original references are provided for the

interested reader. In the third section, both the analytical model and the experimental structure of the benchmark problem are introduced. The fourth section is dedicated to the analysis of the analytical data. All selected parameters used to carry out the identification and the evaluation of the different techniques via Monte-Carlo simulations are explained in detail. Results of this analytical study are statistically presented here with a discussion of the main conclusions. The final section is devoted to the experimental case, providing insight on the results obtained and the parameters selected to execute the identification of both ambient vibration records and hammer tests. Conclusions about this comparison are also presented in this section.

## 2.1 Time-invariant Linear Systems

When subjected to external forces, the dynamic equilibrium of a lumped linear system with  $n$ -degrees of freedom is described by the differential equation

$$\mathbf{M}\ddot{\mathbf{X}}(t) + \mathbf{C}_s\dot{\mathbf{X}}(t) + \mathbf{K}\mathbf{X}(t) = \mathbf{F}(t), \quad (2-1)$$

where  $\mathbf{M}$ ,  $\mathbf{C}_s$  and  $\mathbf{K}$  are  $n \times n$  time-invariant matrices defining the mass, damping and stiffness of the system, whereas  $\mathbf{X}(t)$  and  $\mathbf{F}(t)$  are  $n \times 1$  vectors describing the displacement and external excitation, respectively. Here, derivatives with respect to time are symbolized with (  $\dot{\phantom{x}}$  ).

To simplify the numerical simulations of dynamic systems, Eq. (2-1) is usually rewritten as a system of first-order differential equations. This transformation can be performed in a number of ways. However, the most widely used is the so-called state-space representation given by

$$\dot{\mathbf{Z}}(t) = \mathbf{A}_c \mathbf{Z}(t) + \mathbf{B}_c \mathbf{F}(t) \quad (2-2)$$

where  $\mathbf{Z}(t) = \begin{bmatrix} \mathbf{X} & \dot{\mathbf{X}} \end{bmatrix}^T$  is known as the state vector, whereas the system matrix  $\mathbf{A}_c$ , and the input influence matrix  $\mathbf{B}_c$  are defined, respectively, as

$$\mathbf{A}_c = \begin{bmatrix} \mathbf{0} & \mathbf{I} \\ -\mathbf{M}^{-1}\mathbf{K} & -\mathbf{M}^{-1}\mathbf{C}_s \end{bmatrix} \quad \text{and} \quad \mathbf{B}_c = \begin{bmatrix} \mathbf{0} \\ \mathbf{M}^{-1} \end{bmatrix}. \quad (2-3)$$

Furthermore, to evaluate Eq. (2-1) at any time, the state-space representation of the system is complemented with the output equation

$$\mathbf{Y}(t) = \mathbf{C} \mathbf{Z}(t) + \mathbf{D} \mathbf{F}(t), \quad (2-4)$$

where  $\mathbf{Y}(t)$  can be deliberately selected from all outputs of the system that are linear combinations of the state and the input vectors. For instance, if accelerations of the system are pursued, then the observation and direct term matrices ( $\mathbf{C}$  and  $\mathbf{D}$ , respectively) are defined as

$$\mathbf{C} = \begin{bmatrix} -\mathbf{M}^{-1}\mathbf{K} & -\mathbf{M}^{-1}\mathbf{C}_s \end{bmatrix} \quad \text{and} \quad \mathbf{D} = \begin{bmatrix} \mathbf{M}^{-1} \end{bmatrix}. \quad (2-5)$$

### 2.1.1 Discrete Systems

Together, Eqs. (2-2) and (2-4) constitute a continuous-time state-space model. This means that the system response can be evaluated at any particular time. Because experimental data is discrete in nature, a discretized version of this system is necessary to numerically simulate its behavior. The model can then be discretized every  $\Delta t$  and expressed as

$$\begin{aligned} \mathbf{Z}_{k+1} &= \mathbf{A} \mathbf{Z}_k + \mathbf{B} \mathbf{F}_k \\ \mathbf{Y}_k &= \mathbf{C} \mathbf{Z}_k + \mathbf{D} \mathbf{F}_k \end{aligned}, \quad (2-6)$$

where the system and input influence matrices ( $\mathbf{A}$  and  $\mathbf{C}$ , respectively) can be obtained by applying a zero-order hold approximation (see [49])

$$\mathbf{A} = \exp(\mathbf{A}_c \Delta t) \quad \text{and} \quad \mathbf{B} = \mathbf{A}_c^{-1} [\mathbf{A} - \mathbf{I}] \mathbf{B}_c . \quad (2-7)$$

When implementing system identification techniques based on output measurements, typically a discrete state-space realization of the structure is obtained. However, it is important to emphasize that the states of these resulting realizations do not have any physical meaning. In other words, the coefficient matrices are not comprised of products of the structural matrices  $\mathbf{M}$ ,  $\mathbf{K}$  and  $\mathbf{C}_s$  (or their inverses), but of real scalars whose combination produces the same output displayed by the system.

### **Free Response and Markov Parameters**

Assume now that a discretized system described by Eq. (2-6) is vibrating in free response (i.e.  $\mathbf{F}_k = 0$ ) due to an unknown set of initial conditions  $\mathbf{Z}_1$ . When  $k = 1$ , the states and output of the system are given by  $\mathbf{Z}_2 = \mathbf{A} \mathbf{Z}_1$  and  $\mathbf{Y}_1 = \mathbf{C} \mathbf{A} \mathbf{Z}_1$ , respectively. In general, the states and output of the system can be expressed as

$$\mathbf{Z}_k = \mathbf{A}^{k-1} \mathbf{Z}_1 \quad \text{and} \quad \mathbf{Y}_k = \mathbf{C} \mathbf{A}^k \mathbf{Z}_1 , \quad (2-8)$$

for  $k = 1, 2, \dots$ . The discretized samples of the free response of the system are known as the Markov parameters, and are widely used in modal identification.

### **Stochastic Inputs and Measurement Noise**

When dealing with ambient vibrations of civil structures, the excitation is produced by unknown forces, while the measurements (usually accelerations) are corrupted by

unavoidable noise in sensors. In this case, the system can be viewed as a purely stochastic process described by the discrete state-space representation

$$\begin{aligned}\mathbf{Z}_{k+1} &= \mathbf{A} \mathbf{Z}_k + \mathbf{W}_k \\ \mathbf{Y}_k &= \mathbf{C} \mathbf{Z}_k + \mathbf{V}_k\end{aligned}\tag{2-9}$$

where  $\mathbf{W}_k$  and  $\mathbf{V}_k$  represent the unmeasurable input and the noise in the sensors, respectively. In order to analyze these type of systems, some assumptions are made. Therefore, it is assumed here that the processes  $\mathbf{W}_k$  and  $\mathbf{V}_k$  have zero mean, are statistically independent, and are uncorrelated with their previous values. In other words, the covariance matrices can be expressed as

$$E \left[ \begin{pmatrix} \mathbf{W}_p \\ \mathbf{V}_p \end{pmatrix} \begin{pmatrix} \mathbf{W}_q^T & \mathbf{V}_q^T \end{pmatrix} \right] = \begin{bmatrix} \mathbf{Q} & \mathbf{S} \\ \mathbf{S}^T & \mathbf{R} \end{bmatrix} \delta_{pq}\tag{2-10}$$

where  $E[\ ]$  represents the expectance operator and  $\delta$  is the Kronecker delta.

### 2.1.2 Modal Properties

The modal properties of a linear dynamic system described by Eq. (2-1) can be obtained from its characteristic equation, given by

$$(\lambda_i^2 \mathbf{M} + \lambda_i \mathbf{C}_s + \mathbf{K}) \phi_i = 0,\tag{2-11}$$

where  $\lambda_i$  is the  $i$ -th root of the equation and  $\phi_i$  is the  $i$ -th mode shape of the dynamic system.  $\lambda_i$  and the elements of  $\phi_i$  are real for overdamped modes, but for underdamped modes (as most civil structures), they are complex and occur in conjugate pairs. For each

pair of roots  $\lambda = a \pm bj$ , the damped and undamped natural frequencies as well as the associated damping ratio can be obtained, respectively, as

$$\omega_d = b, \quad \omega = \sqrt{a^2 + b^2} \quad \text{and} \quad \zeta = \frac{a}{\sqrt{a^2 + b^2}}. \quad (2-12)$$

The modal properties can also be extracted from the system and output matrices of a state-space representation of a dynamic system, even in those cases in which the states are not physically meaningful. In the case of a discrete representation, the roots of the characteristic equation are equivalent to the eigenvalues of the system matrix  $\mathbf{A}$ , whereas the mode shapes can be obtained multiplying the eigenvectors of  $\mathbf{A}$  by the output matrix  $\mathbf{C}$ .

### Modal Assurance Criteria (MAC)

At multiple locations throughout this thesis it will be necessary to numerically evaluate the similarity of two mode shapes. In these cases, a correlation technique known as modal assurance criterion (MAC) will be used. The MAC has established itself as a key correlation measure ever since it was first proposed by in 1982 by Allemang and Brown [3]. The MAC between two mode shapes  $\phi_a$  and  $\phi_b$  is defined as,

$$\text{MAC}(\phi_a, \phi_b) = \frac{\left\{ \sum_{r=1}^N (\phi_{a_r})(\phi_{b_r}^*) \right\}}{\sqrt{\sum_{r=1}^N (\phi_{a_r})^2 \sum_{r=1}^N (\phi_{b_r}^*)^2}} \quad (2-13)$$

where  $r$  indicates the  $r$ -th component of a total of  $N$  components describing the mode shape. A value close to 1.0 suggests that the two mode shapes are well correlated, whereas a value close to 0 indicates that they are uncorrelated and are probably associated with different frequencies.

## 2.2 The Methodologies

As mentioned previously, the modal identification of civil structures using ambient vibrations has emerged as a convenient alternative in terms of safety, cost and simplicity. However, several difficulties arise as the statistical properties of the unknown inputs play a significant role in the success or failure of the identification. It was believed that modal identification would succeed only if the inputs were white noise with a Gaussian distribution. Using different approaches, Andersen [5] and Ibrahim *et al.* [39] reduced the limitations imposed by this requirement. In their work, it was shown that, as long as the input can be generated by filtering Gaussian white noise through a linear filter, then the original system can be substituted by an alternative state-space representation with Gaussian white noise excitation whose modal properties remain unchanged [5]. Experimentally, Caicedo *et al.* [17] showed that modal identification can be carried out using band-limited ambient vibrations with questionable stationarity, as in the case of some civil structures.

### 2.2.1 Free Response Estimation Techniques

Early developments on modal identification using time domain techniques rely heavily on free responses and Markov parameters. For instance, in 1977, Ibrahim and Mikulcik-wen [40] developed a technique (known as the Ibrahim Time Domain (ITD) method) that retrieves modal properties of linear systems by performing an eigenvalue decomposition of a special arrangement of the free response. In the last two decades, the estimation of such responses using the vibrations of civil structures as they operate in a normal basis has allowed researchers to implement this type of modal identification methodology. Therefore, as a first step in this comparative study, the two most common techniques for the estimation of free responses are compared in terms of the quality of their results and the ability to deal with noisy measurements. However, even in an analytical study, the evaluation of the estimated free responses is not easy because the set of initial

conditions that generates the estimated free response is unknown. To overcome this difficulty, the results obtained from both techniques are visually inspected in both the time and the frequency domain (by means of spectral density functions). Simulated ambient vibrations from the analytical model of the benchmark problem are used to accomplish this goal.

### **Natural Excitation Technique (NExT)**

Although auto- and cross-correlation functions had already been used to produce free decaying functions of systems subjected to unknown inputs (see for instance Bendat and Piersol [8]), it was in 1993 when James *et al.* [43] provided the mathematical background for this practice. In their work, it was shown that when forced vibration data is available from tests conducted with certain types of excitation, the cross-correlation functions between the response measurements and a single reference measurement satisfy the homogeneous differential equation of motion of the linear system and, therefore, can be treated as free responses. The technique is known as NExT (Natural Excitation Technique) and assumes that the excitation is weakly stationary, broad-band, and uncorrelated to prior system responses.

Consider the  $n$ -degree of freedom, time-invariant, linear system described by Eq. (2-1) (and repeated here for convenience)

$$\mathbf{M}\mathbf{X}(t) + \mathbf{C}_s\mathbf{X}(t) + \mathbf{K}\mathbf{X}(t) = \mathbf{F}(t). \quad (2-14)$$

Post multiplying Eq. (2-14) by the displacement of any of the degrees of freedom measured  $\mathbf{X}_i(s)$  (referred to as the reference signal), and taking the expected value of each side yields

$$\mathbf{M}\mathbf{R}_{\mathbf{X}\mathbf{X}_i}^{\cdot}(t, s) + \mathbf{C}_s\mathbf{R}_{\mathbf{X}\mathbf{X}_i}^{\cdot}(t, s) + \mathbf{K}\mathbf{R}_{\mathbf{X}\mathbf{X}_i}(t, s) = \mathbf{R}_{\mathbf{F}\mathbf{X}_i}(t, s), \quad (2-15)$$

where  $\mathbf{R}(\cdot)$  denotes the vector of correlation functions. For weakly stationary processes it can be shown that [8]

$$\mathbf{R}_{XX_i}(\tau) = \mathbf{R}_{XX_i}^{\cdot}(\tau) = -\mathbf{R}_{XX_i}^{\cdot}(\tau), \quad (2-16)$$

where  $\tau = t - s$ . Assuming that the displacement, velocity and acceleration processes are weakly stationary and uncorrelated with future disturbances (i.e.  $\mathbf{R}_{FX_i}(t, s) = 0$ ), and taking the fourth derivative of Eq. (2-15) we obtain

$$\mathbf{M}\mathbf{R}_{XX_i}^{\cdot\cdot\cdot\cdot}(\tau) + \mathbf{C}_s\mathbf{R}_{XX_i}^{\cdot\cdot\cdot\cdot}(\tau) + \mathbf{K}\mathbf{R}_{XX_i}^{\cdot\cdot\cdot\cdot}(\tau) = \mathbf{0}. \quad (2-17)$$

Equation (2-17) shows that the cross-correlation function of the responses of the structure with a reference signal satisfies the homogeneous equation of motion and can be treated as free response. Since the calculation of cross-correlation functions are obtained by performing an inverse Fourier transform to the cross-spectral density functions, NExT is considered to be a frequency domain technique.

### *Known Issues*

The successful implementation of NExT highly depends on two factors, namely: 1) the capability of the unknown input to excite all the modes of the structure; and 2) the length of the records used. Since cross spectral density functions are usually obtained by “windowing” data records and averaging results in the frequency domain, lengthy records provide more samples to be averaged, and therefore, better results.

The main drawback in the implementation of the natural excitation technique is related to the fact that one singular sensor has to be selected as reference for the entire set of measurements. Several problems are derived from this requirement. For instance, when the selected reference sensor is located at a point of the structure where a vibrational

mode does not have high participation, the estimated free response contains little or no information of that mode. This phenomenon occurs when the sensor is located near a modal node or when the motion of the mode is orthogonal to the measurements of the sensor. In these cases, the chances of not detecting the mode or miscalculating it are highly increased. Moreover, for every channel selected as reference, a different free response for an unknown set of initial conditions is obtained. To overcome these problems, modal identification based on free responses obtained from NExT have to be applied repeatedly, using several channels as reference.

### **Random Decrement Technique (RDD)**

The random decrement technique was developed at NASA by Henry Cole [19-21] in the late sixties and early seventies, while trying to develop methodologies to identify damage in aerospace structures subjected to ambient loads. The mathematical background of the technique as well as the implementation issues have been provided by several authors throughout the years [38, 72]. It is now accepted that the random decrement (RDD) is a fast method to estimate auto and cross-correlation functions.

As clearly stated by Asmussen [6], the basis of the RDD technique is that, when driven by a stationary input, the random response of a linear system starting at some arbitrary time  $t_o$  is composed of three parts, namely: 1) the free response from the initial displacement at  $t_o$ , 2) the impulse response due to the initial velocity, and 3) a random component which is due to the load applied to the structure in the time following  $t_o$ . Let us now assume that every time the displacement equals certain value  $a$  (referred to as the trig level), a record of the response is taken for a period of time. If  $N$  of these segments are averaged we obtain the random decrement signature described as

$$D_{XX}(\tau) = \frac{1}{N} \sum_{i=1}^N X(t_o + \tau) | X(t_o) = a, \quad (2-18)$$

where  $X$  represents the random displacement. As the number of averaged segments increases, the random response will decrease and eventually cancel itself. Similarly, since the velocity at each triggering point is a random variable, the impulse response becomes negligible. Therefore, the result is a free decaying response due to an initial displacement  $a$ .

In 1977, Ibrahim [38] extended the applicability of the random decrement technique by introducing the auto and cross-RDD signatures, allowing the analysis of multichannel measurements and, therefore, the search for mode shapes. Then, in 1982, Vandiver *et al.* [72] showed that the RDD signature, expressed now as a conditional expectation, is simply proportional to the auto correlation function. Bedewi [7] later generalized the work of both Ibrahim and Vandever *et al.* and set the following relations between the random decrement signatures and the correlation functions

$$D_{XX}(\tau) = E[X(t_o + \tau) | X(t_o) = a] = \frac{R_{XX}(\tau)}{\sigma_X^2} a \quad (2-19)$$

$$D_{YX}(\tau) = E[Y(t_o + \tau) | X(t_o) = a, \dot{X}(t_o) = v] = \frac{R_{YX}(\tau)}{\sigma_X^2} a - \frac{R'_{YX}(\tau)}{\sigma_X^2} v, \quad (2-20)$$

where  $E[\ ]$  represents the expectance operator,  $R'_{YX}(\tau)$  is the derivative of the cross-correlation function and  $\sigma_X^2$  is the variance of the derivative of the process  $X$ . When the trig condition is chosen so that  $X(t_o) = a$  for any  $\dot{X}(t_o)$ , then for Gaussian processes the last term of Eq. (2-20) vanishes since  $X(t_o)$  and  $\dot{X}(t_o)$  are independent. Therefore, the cross-RDD is proportional to the cross-correlation function. When dealing with multichannel measurements, however, the initial conditions of all measured DOF's are not known, but a set of initial conditions does exist giving a free response for which, the RDD signature is an unbiased estimate [12].

### *Known Issues*

The numerical implementation of the random decrement technique becomes a challenge as the measured responses of the systems are discrete. This fact implies that the probability of having the value  $X(t) = a$  is zero. In his dissertation, Asmussen [6] detailed the different triggering conditions that researchers have used to overcome this difficulty. The most popular approach is to set a small range around the established threshold  $a$  and consider all points that lie within this range as triggering points.

Similar to NExT, the implementation of the random decrement technique also requires the selection of one reference sensor from which the triggering points are obtained. This condition arises the same problems described previously. Also similar to NExT, but perhaps more critical in the random signature, is the high noise to signal ratio of the estimated response towards the end of the decay.

## **2.2.2 Modal Identification Techniques**

Four modal identification techniques are compared under similar conditions in this study. Although the mathematical basis of each technique is presented on this thesis, it is not intended to derive every detail of these algorithms. Interested readers are referred to the original articles where the algorithms have been introduced. However, details are provided regarding the numerical implementation of the techniques for the numerical example used.

### **Eigensystem Realization Algorithm with Data Correlations (ERA/DC)**

To obtain mathematical models capable of reproducing responses measured from physical systems, Juang and Pappa [48] developed a technique that uses the so-called Markov parameters to build state-space representations of linear systems. The methodology was based on the earlier Ibrahim time domain (ITD) method which was limited by the need

of a large number of sensors to form a square arrangement of the free response. Due to its efficacy for lightly damped systems, the eigensystem realization algorithm (ERA) was extensively used in the late 80's and early 90's for advanced control and health monitoring of civil structures. Although the ERA was first proposed to be applied using impulse responses, it can be shown that, when free responses with unknown initial conditions are used, the system and output matrices of the state-space realization (i.e.  $\mathbf{A}$  and  $\mathbf{C}$ ) are obtained. Thus, despite the inability to calculate the input influence matrices ( $\mathbf{B}$  and  $\mathbf{D}$ ), the calculation of modal properties is not affected.

In 1988 Juang *et al.* [47] proposed an alternative approach to the ERA called ERA/DC, where DC indicates that it makes use of data correlations. The improved algorithm has shown to be at least as effective as its predecessor (see Lew *et al.* [52]). The algorithm uses the discretized free response  $\mathbf{h}$  (e.g.  $\mathbf{R}_{XX_i}$  from NExT) to form a matrix known as the Hankel matrix

$$\mathbf{H}_{k-1} = \begin{bmatrix} \mathbf{h}_k & \mathbf{h}_{k+1} & \cdots & \mathbf{h}_{k+c} \\ \mathbf{h}_{k+1} & \mathbf{h}_{k+2} & \cdots & \vdots \\ \vdots & \vdots & & \vdots \\ \mathbf{h}_{k+r} & \cdots & \cdots & \mathbf{h}_{k+c+r} \end{bmatrix}. \quad (2-21)$$

Using the Markov parameters of Eq. (2-8), the Hankel matrix can also be expressed as

$$\mathbf{H}_{k-1} = \begin{bmatrix} \mathbf{CA}^k \mathbf{Z}_1 & \mathbf{CA}^{k+1} \mathbf{Z}_1 & \cdots & \mathbf{CA}^{k+c} \mathbf{Z}_1 \\ \mathbf{CA}^{k+1} \mathbf{Z}_1 & \mathbf{CA}^{k+2} \mathbf{Z}_1 & \cdots & \vdots \\ \vdots & \vdots & & \vdots \\ \mathbf{CA}^{k+r} \mathbf{Z}_1 & \cdots & \cdots & \mathbf{CA}^{k+r+c} \mathbf{Z}_1 \end{bmatrix}, \quad (2-22)$$

where  $\mathbf{A}$  is the system matrix of a state space realization of the linear system, and  $\mathbf{Z}_1$  is the vector of unknown initial conditions. Alternatively, Eq. (2-22) is expressed as

$$\mathbf{H}_{k-1} = \begin{bmatrix} \mathbf{C} \\ \mathbf{CA} \\ \vdots \\ \mathbf{CA}^r \end{bmatrix} \mathbf{A}^{k-1} \begin{bmatrix} \mathbf{AZ}_1 & \mathbf{A}^2\mathbf{Z}_1 & \dots & \mathbf{A}^{c+1}\mathbf{Z}_1 \end{bmatrix} = \mathbf{UA}^{k-1}\mathbf{V}, \quad (2-23)$$

where  $\mathbf{C}$  is the output matrix of the system. Using two different Hankel matrices formed from the same free response, the correlation matrix  $\mathbf{R}_k$  is defined as

$$\mathbf{R}_k = \mathbf{H}_k \mathbf{H}_0^T = \mathbf{UA}^k\mathbf{U}^T. \quad (2-24)$$

The block correlation matrix is then formed as

$$\mathcal{U}_k = \begin{bmatrix} \mathbf{R}_k & \mathbf{R}_{k+\gamma} & \dots & \mathbf{R}_{k+\beta\gamma} \\ \mathbf{R}_{k+\gamma} & \mathbf{R}_{k+2\gamma} & \dots & \vdots \\ \vdots & \vdots & & \vdots \\ \mathbf{R}_{k+\alpha\gamma} & \dots & \dots & \mathbf{R}_{k+\alpha\gamma+\beta\gamma} \end{bmatrix}, \quad (2-25)$$

Combining  $\mathcal{U}_k$  with Eq. (2-24), the block correlation matrix can be expressed as

$$\mathcal{U}_k = \begin{bmatrix} \mathbf{UA}^k \\ \mathbf{UA}^{k+\gamma} \\ \vdots \\ \mathbf{UA}^{k+\alpha\gamma} \end{bmatrix} \mathbf{A}^k \begin{bmatrix} \mathbf{A}^k\mathbf{U}^T & \mathbf{A}^{k+\gamma}\mathbf{U}^T & \dots & \mathbf{A}^{k+\alpha\gamma}\mathbf{U}^T \end{bmatrix} = \mathbf{PA}^k\mathbf{Q}. \quad (2-26)$$

A singular value decomposition of  $\mathcal{U}_0$  is performed yielding

$$\mathcal{U}_0 = \mathbf{G}\Psi\mathbf{S}^T \quad (2-27)$$

where  $\Psi$  is a diagonal matrix with the singular values in the diagonal, and the matrices  $\mathbf{G}$  and  $\mathbf{S}$  are square and unitary. The matrices  $\Psi_N$ ,  $\mathbf{G}_N$  and  $\mathbf{S}_N$  are obtained eliminating the rows and columns corresponding to small singular values produced by computational modes. Since  $\Psi_N$  is a diagonal matrix, Eq. (2-27) can be expressed as

$$\mathcal{U}_0 = (\mathbf{G}_N\Psi_N^{1/2})(\Psi_N^{1/2}\mathbf{S}_N^T). \quad (2-28)$$

From Eqs. (2-26) and (2-28), when  $k = 0$

$$\mathbf{P} = \mathbf{G}_N\Psi_N^{1/2} \quad \text{and} \quad \mathbf{Q} = \Psi_N^{1/2}\mathbf{S}_N^T. \quad (2-29)$$

For  $k = 1$ , Eq. (2-26) takes the form

$$\mathcal{U}_1 = \mathbf{P}\mathbf{A}\mathbf{Q} \quad (2-30)$$

Combining Eqs. (2-23), (2-29) and (2-30), the system and output matrices can be found

$$\mathbf{A} = \Psi_N^{-1/2} \mathbf{G}_N^T \mathcal{U}_1 \mathbf{S}_N \Psi_N^{-1/2} \quad \text{and} \quad \mathbf{C} = \begin{bmatrix} \mathbf{I} & \mathbf{0} \end{bmatrix} \mathbf{G}_N \Psi_N^{-1/2}, \quad (2-31)$$

where  $\mathbf{I}$  is the identity matrix, and  $\mathbf{0}$  is a zero matrix, both of proper dimensions for the necessary matrix products. While natural frequencies can be obtained directly from the system matrix ( $\mathbf{A}$ ), mode shapes are obtained multiplying the eigenvectors of  $\mathbf{A}$  (associated with non-physical states) by the output matrix ( $\mathbf{C}$ ).

### *Known Issues*

Successful implementation of the ERA/DC usually requires some general knowledge of the structural system as well as some experience with the algorithm. For instance the number of samples used to form the Hankel matrix and its relative dimensions have an important impact on the results. Juang and Pappa [48] suggested using a Hankel matrix whose number of columns is 10 times the number of poles expected (i.e. 20 times the number of frequencies) and whose number of rows is 2-3 times the number of columns. Another commonly used practice to select these dimensions is associated with the quality of the free responses. Under this criterion, the Hankel matrix is built making full use of the decaying signal provided the signal to noise ratio is high. However, the selection of these parameters highly depends on the experience of the user, making the algorithm difficult to implement successfully for first-time users.

The selection of the number of singular values used to truncate matrices  $\Psi$ ,  $\mathbf{R}$  and  $\mathbf{S}$  is crucial to obtain accurate results. The underestimation of this parameter translates into overlooking vibrational modes, whereas a larger number may lead to obtaining non-existent, computational modes or even modes that are linear combinations of those pursued. Although, in theory, this number should be equal to the number of desired poles from the structural system, a number of factors may lead to undesirable results. For instance, if the free response contains little participation of one particular mode, an erroneous mode is introduced. In general, however, the overestimation of the truncation is preferable as numerical tools can later be used to distinguish true modes from those due to noise.

As pointed out previously, the methodologies to estimate free responses of systems when excited by unknown stationary inputs requires the selection of a single reference channel to execute the process. Therefore, when implementing the ERA/DC with estimated free responses, a different set of results is obtained for each channel selected.

While this repeated process helps in detecting all true modes of the structure, it also leads to obtaining different sets of values for each mode. In this case, numerical tools known as stabilization diagrams are helpful to determine similar modes and improve the accuracy by averaging the results. Stabilization of modes will be discussed later in this chapter.

### **Prediction Error Method Through Least Squares (PEM/LS)**

Prediction error methods (PEM) have been widely reported in the literature (see, for instance, [5] and [53]). The main idea is to identify a system of linear equations that, based on past inputs and outputs, can predict any output. For the special case of multivariate output-only measurements, these models are known as auto-regressive with moving average vector (ARMAv). In this case, the prediction is based not only on past outputs but also on past errors of the prediction. Several algorithms have been proposed to implement prediction error methods. Nonlinear optimization and multi-stage least squares are among the possibilities. In this study, the prediction error method is carried out using a two-stage least squares approach (PEM/LS).

As a first step, a long auto-regressive (AR) model is fitted to the measurements using least squares. The auto-regressive model is of the form

$$\hat{\mathbf{y}}_k = -\mathbf{A}_1 \mathbf{y}_{k-1} - \mathbf{A}_2 \mathbf{y}_{k-2} - \dots - \mathbf{A}_n \mathbf{y}_{k-n}, \quad (2-32)$$

where  $\hat{\mathbf{y}}$  and  $\mathbf{y}$  are the predicted and true outputs of the system, and  $\mathbf{A}_i$  is the  $i$ -th auto-regressive coefficient of the  $n$ -order AR model. In the case of multiple channels, the auto-regressive coefficients can be estimated as

$$\begin{bmatrix} -\mathbf{A}_1^T \\ -\mathbf{A}_2^T \\ \vdots \\ -\mathbf{A}_n^T \end{bmatrix} = \begin{bmatrix} \mathbf{y}_n^T & \mathbf{y}_{n-1}^T & \cdots & \mathbf{y}_1^T \\ \mathbf{y}_{n+1}^T & \mathbf{y}_n^T & \cdots & \mathbf{y}_2^T \\ \vdots & \vdots & & \vdots \\ \mathbf{y}_{j-1}^T & \mathbf{y}_{j-2}^T & \cdots & \mathbf{y}_{j-n}^T \end{bmatrix}^+ \begin{bmatrix} \mathbf{y}_{n+1}^T \\ \mathbf{y}_{n+2}^T \\ \vdots \\ \mathbf{y}_j^T \end{bmatrix}, \quad (2-33)$$

where  $j$  is the length of the recorded measurements and  $^+$  represents the pseudo inverse. The error of this AR model can be calculated by subtracting the predicted output (using Eq. 2-32) from the true output of the system (i.e.  $\mathbf{e}_k = \mathbf{y}_k - \hat{\mathbf{y}}_k$ ). In the second step, a pseudo-ARX (auto-regressive with exogenous input) model is estimated using the error obtained from the AR model as the pseudo-input. This ARX model takes the form

$$\hat{\mathbf{y}}_k = -\mathbf{A}_1 \mathbf{y}_{k-1} - \cdots - \mathbf{A}_{n_a} \mathbf{y}_{k-n_a} + \mathbf{C}_1 \mathbf{e}_{k-1} + \cdots + \mathbf{C}_{n_c} \mathbf{e}_{k-n_c}, \quad (2-34)$$

from which  $n_a$  auto-regressive and  $n_c$  moving average matrix coefficients can be estimated using, again, a least squares approach

$$\begin{bmatrix} -\mathbf{A}_1^T \\ \vdots \\ -\mathbf{A}_{n_a}^T \\ \mathbf{C}_1^T \\ \vdots \\ \mathbf{C}_{n_c}^T \end{bmatrix} = \begin{bmatrix} \mathbf{y}_{n_a}^T & \cdots & \mathbf{y}_1^T & \mathbf{e}_{n_a}^T & \cdots & \mathbf{e}_{n_a-n_c+1}^T \\ \mathbf{y}_{n_a+1}^T & \cdots & \mathbf{y}_2^T & \mathbf{e}_{n_a+2}^T & \cdots & \mathbf{e}_{n_a-n_c+2}^T \\ \vdots & \vdots & \vdots & \vdots & & \vdots \\ \mathbf{y}_{j-1}^T & \cdots & \mathbf{y}_{j-n_a}^T & \mathbf{e}_{j-1}^T & \cdots & \mathbf{e}_{j-n_c}^T \end{bmatrix}^+ \begin{bmatrix} \mathbf{y}_{n_a+1}^T \\ \mathbf{y}_{n_a+2}^T \\ \vdots \\ \mathbf{y}_j^T \end{bmatrix}. \quad (2-35)$$

The system and output matrices of a state space realization associated with this ARMAV model of order  $(n_a, n_c)$  can be formed as

$$\mathbf{A} = \begin{bmatrix} \mathbf{0} & \mathbf{I} & \dots & \mathbf{0} & \mathbf{0} \\ \vdots & \vdots & & \vdots & \vdots \\ \mathbf{0} & \mathbf{0} & \dots & \mathbf{0} & \mathbf{I} \\ \mathbf{A}_{na} & \mathbf{A}_{na-1} & \dots & \mathbf{A}_2 & \mathbf{A}_1 \end{bmatrix} \quad \text{and} \quad \mathbf{C} = [\mathbf{I} \quad \mathbf{0} \quad \dots \quad \mathbf{0}], \quad (2-36)$$

and the dynamic properties can be extracted in the same manner described previously.

### *Known Issues*

The sizes of the system and output matrices of the estimated state-space realization are significantly larger than those estimated with other techniques. As a result, along with the desired modal properties, several computational modal parameters are calculated. This phenomenon constitutes the main drawback in the use of ARMAv models for modal identification. To overcome this problem, the use of stabilization diagrams is helpful to separate true structural modes from non-physical ones. However, several models of different orders must be estimated. The automation of this process is discussed later in this chapter.

Some authors have employed this technique simply to calculate initial values for more complex non-linear optimization algorithms (see, for instance, Andersen [5]). However, the computational power required to execute such algorithms is considerable and grows exponentially as the number of sensors increases. Moreover, since the estimation of several ARMAv models of different orders is necessary, the implementation of non-linear optimization algorithms becomes impractical. Numerical evaluations (not reported here) showed that only marginal improvements (if any) on the quality of the detected modal properties are gained when optimization algorithms are implemented. In general, lengthy records allow an accurate fitting of the data with simple least squares techniques, making the implementation of optimization algorithms unnecessary.

### Stochastic Subspace Identification (SSI)

Subspace identification algorithms have slowly evolved over the last three decades, combining more mathematical tools and becoming more powerful and computationally efficient. In 1997, Van Overschee and De Moor [73] provided a common mathematical background for all subspace algorithms existing in the literature, including those used to identify input-output systems, stochastic output-only systems and the combination of the two. When applied to linear systems driven by stochastic and unmeasurable inputs, the algorithm is known as the stochastic subspace identification (SSI) technique. Here, the Kalman filter states of a realization are obtained by means of row space projection of Hankel matrices. Once the states are known, the identification problem is reduced to a linear set of equations from which the system and output matrices of the realization can be easily estimated.

Consider the Hankel matrix of the form

$$\mathbf{Y}_{0|i-1} = \begin{bmatrix} \mathbf{y}_0 & \mathbf{y}_1 & \cdots & \mathbf{y}_{j-1} \\ \mathbf{y}_1 & \mathbf{y}_2 & \cdots & \mathbf{y}_j \\ \vdots & \vdots & & \vdots \\ \mathbf{y}_{i-1} & \cdots & \cdots & \mathbf{y}_{i+j-2} \end{bmatrix}, \quad (2-37)$$

where  $\mathbf{y}_k$  is the random response of the system at time  $k$ , and the two subscripts on  $\mathbf{Y}$  denote the time index of the upper left and bottom left elements respectively. It is assumed herein that the number of columns of the Hankel matrix approaches infinity ( $j \rightarrow \infty$ ). Let us now define  $\mathbf{Z}_i$  as the orthogonal projection of the row space of  $\mathbf{Y}_{i|2i-1}$  (known as the future) onto the row space of  $\mathbf{Y}_{0|i-1}$  (known as the past)

$$\mathbf{Z}_i = \mathbf{Y}_{i|2i-1} \begin{matrix} \diagdown \\ \mathbf{Y}_{0|i-1} \end{matrix}. \quad (2-38)$$

Through a singular value decomposition of this projection, it can be shown that [49]

$$\mathbf{Z}_i = \mathbf{Q}_i \hat{\mathbf{X}}_i, \quad (2-39)$$

where  $\mathbf{Q}_i$  is the observability matrix and  $\hat{\mathbf{X}}_i$  is the Kalman state sequence

$$\mathbf{Q}_i = \begin{bmatrix} \mathbf{C}^T & (\mathbf{CA})^T & (\mathbf{CA}^2)^T & \dots & (\mathbf{CA}^{j-1})^T \end{bmatrix}^T \quad (2-40)$$

$$\hat{\mathbf{X}}_i = \begin{bmatrix} \hat{x}_t & \hat{x}_{t+1} & \dots & \hat{x}_{t+j-1} \end{bmatrix}. \quad (2-41)$$

Similarly, it can be shown that the projection

$$\mathbf{Z}_{i+1} = \frac{\mathbf{Y}_{i+1|2i}}{\mathbf{Y}_{0|i-1}} \quad (2-42)$$

can be expressed as

$$\mathbf{Z}_i = \mathbf{Q}_{i-1} \hat{\mathbf{X}}_{i+1}. \quad (2-43)$$

From Eqs. (2-40) and (2-43), the Kalman states can be obtained from output data using a singular value decomposition. As a result, the system and output matrices  $\mathbf{A}$  and  $\mathbf{C}$  can be estimated from the following set of linear equations

$$\begin{bmatrix} \hat{\mathbf{X}}_{i+1} \\ \mathbf{Y}_{i|i} \end{bmatrix} = \begin{bmatrix} \mathbf{A} \\ \mathbf{C} \end{bmatrix} \hat{\mathbf{X}}_i. \quad (2-44)$$

### *Known Issues*

The dimensions of the Hankel matrices used in the orthogonal projections have an important impact in the computational power required to execute the identification. An appropriate selection of these dimensions must take into account both the quality and amplitude level of the recorded measurements as well as the computational power available. As in all modal identification techniques, the selection of a model order becomes complicated when noisy measurements are employed and non-stationary inputs excite the structure. The use of several model orders and the stabilization of the results has been recommended by various researchers and employed in this study.

### **2.2.3 Data Management**

One of the objectives of this research is to fully automate the modal identification techniques, allowing the online evaluation of the state of the structures (discussed in later chapters) and eliminating the subjective judgement of different users. This automation can be a challenging process for several reasons. For instance, identified modal properties are often not associated with the true dynamic behavior of the structure. This phenomenon is usually a consequence of noisy sensors, overestimation of the model order, or the inability of the unknown inputs to significantly excite a particular vibrational mode. In some cases, the identified modes have clear signs of not being associated with the system (e.g. unexpectedly high damping ratios). To systematically eliminate these modes, some criteria have to be established. General knowledge of the system is fundamental for carry out this process. The criteria used for the elimination of doubtful modes are discussed in the sections devoted to the numerical implementation of the algorithms.

But perhaps the most difficult problem for automating the modal identification of structures, is to deal with those cases when the identified properties are associated with noise but do not have clear signs of this fact. This problem is aggravated by techniques such as

the combination of NExT and ERA that require repeated implementations while changing parameters of the algorithm (e.g. using different channels as reference). This practice usually results in multiple sets of repeated modal properties from which it is difficult to select the most accurate ones. To determine the true modes of the systems, researchers have used the so-called “stabilization diagrams” for years. Since no actual diagrams are required to automate this process, it is referred here as “stabilization of modes” and is described in the following section.

### **Stabilization of Vibrational Modes**

A stabilization diagram is an useful tool with which the user can easily visualize the frequencies that have been detected in a consistent manner and discard those that appear to be unrelated with the true dynamic behavior of the structure. The automation of this process is somewhat affected by subjectivity as some thresholds have to be set. Basically, the detection of similar vibrational modes is based on two criteria, namely, 1) the proximity of the frequencies and, 2) the correlation of the mode shapes. The first criterion was simply evaluated by determining a 2% threshold. Here, two frequencies are considered similar if their values are within 2% of each other. The correlation of the mode shapes was evaluated by calculating the modal assurance criterion (MAC) of the two vectors. The established threshold for this criterion was set equal to 0.9. The automated algorithm then recognizes two vibrational modes as similar if both criteria are met. Although the proximity of the detected damping ratios has also been used by some researchers, it is well known that the variation of these ratios is usually high compared to the variation of the frequencies. Therefore, it was decided to ignore these parameters in this study. Finally, stable modes are determined by searching, in descending order, those modes with the most similar sets, while averaging the corresponding frequencies, mode shapes and damping ratios.

## 2.3 The Benchmark Structure

To enhance the understanding of SHM techniques, a task group of the IASC-ASCE has developed a series of benchmark problems that allow researchers to compare results of the different techniques, improve the methodologies, and identify their capabilities and limitations. These studies are based on a structure constructed at the University of British Columbia, and, as described by Johnson *et al.* [44], it is a 4-story, 2-bay by 2-bay steel frame, scaled at 1:3 (see Fig. 2.3). In this study, data collected from the experimental structure itself as well as a finite element model that closely represents it are used. The identification of modal properties is limited to the six lowest frequencies and the associated damping ratios and mode shapes. Moreover, although multiple damage scenarios were considered by the task group, this chapter is concerned with the healthy (fully braced) condition only. All damage scenarios will be addressed in Chapter 4 when damage detection under different environmental conditions is pursued. In the following sections detailed descriptions of the experimental setup as well as the analytical model



**Figure 2.1** The benchmark structure

are provided. More information of the benchmark problem can be found in: <http://wustl.cive.wustl.edu/asce.shm/>

### 2.3.1 Experimental Setup

The structure has a 2.5m×2.5m plan and is 3.6m tall. The members are hot rolled grade 300W steel (nominal yield stress  $3e8\text{N/m}^2$ ). The sections are unusual, designed for a scale model, with properties as given in Table 2.1. Four steel plates were attached to each floor to represent the mass of the building. Each plate on floors one through three has a nominal mass of 1000Kg, and the masses on the fourth floor have a mass of 750Kg. The placement of these plates is identical at each floor, with masses being distributed asymmetrically so that the motions are coupled in every mode.

Because the structure was placed outdoors, ambient vibration was induced by several factors such as wind, and ground excitation produced by traffic, working machinery and people walking near the structure. Hammer impacts were all located in the southwest corner at the first floor (between first and second stories), and responses were recorded for both, impacts directed in the north-south and east-west directions.

**Table 2.1 Member properties of benchmark experiment**

Property	Columns	Floor beams	Braces
Section type	B100×9	S75×11	L25×25×3
Cross-sectional area $A$ [m <sup>2</sup> ]	$1.133 \times 10^{-3}$	$1.43 \times 10^{-3}$	$0.141 \times 10^{-3}$
Moment of inertia (strong direction) $I_y$ [m <sup>4</sup> ]	$1.97 \times 10^{-6}$	$1.22 \times 10^{-6}$	0
Moment of inertia (weak direction) $I_z$ [m <sup>4</sup> ]	$0.664 \times 10^{-6}$	$0.249 \times 10^{-6}$	0
St. Venant torsion constant $J$ [m <sup>4</sup> ]	$8.01 \times 10^{-9}$	$38.2 \times 10^{-9}$	0
Young's Modulus $E$ [Pa]	$2 \times 10^{11}$	$2 \times 10^{11}$	$2 \times 10^{11}$
Mass per unit length $\rho$ [kg/m]	8.89	11.0	1.11

A total of 16 uniaxial accelerometers were placed on the structure to record its response under all load cases. Each floor (including the base) was equipped with three sensors, two of which measured accelerations in the north-south direction at opposite sides of the structure, and the third measured east-west accelerations. Only the accelerometers placed on the floors are used in this study (for a total of 12 sensors). Ambient vibration was recorded for a period of five minutes with a sampling frequency of 200Hz. Hammer impacts were recorded with a sampling frequency of 1000Hz for approximately two minutes, time during which three or four impacts were applied to the structure. More information on the experimental setup can be found in Dyke *et al.* [25].

### 2.3.2 Analytical Model

132 beam elements were employed to construct a finite element model to simulate the behavior of the benchmark structure (See Fig. 2.2). Geometry, cross-sectional areas, material properties, and mass distribution of all members were based on the experimental model (see Table 2.1). Moreover, the mass associated with the steel plates attached to the structure, was carefully distributed as lumped masses along the nodes. However, some assumptions were made to simplify the analysis and reduce the computational effort needed to simulate dynamic responses. For instance, the properties of the inter-story diagonals were purposely limited so that only axial forces were developed on these members. In addition, fixed conditions in all directions were provided to the nodes connected to the ground. But perhaps the main assumption is that all floors behave like rigid membranes with no in-plane deformation. This assumption is based on the fact that, as seen in Fig. 2.2b., 16 beam elements provide stiffness to each floor. Moreover, the steel plates attached to the experimental structure provide not only the intended mass, but also some additional stiffness to the plane. As a result, all in-plane nodes were expected to have similar behavior. With this in mind, displacements along each axis as well as rotations with respect to the vertical axis of all external nodes were constrained to be dependent on the central node. Rotations with respect to the  $x$  and  $y$  axes were allowed for all

nodes. By condensing these degrees of freedom the finite element model is simplified in such a way that 88 DOF are active. Finally, damping ratios of 1% were introduced to each mode of the analytical model.

Ambient disturbance responses were simulated by introducing three bandwidth-limited, statistically-independent and normally distributed random inputs acting as horizontal ground excitation to the model in the  $x$  and  $y$  directions as well as a rotation with respect to the  $z$  axis. Similar to the studies performed by the IASC-ASCE working group on SHM, only three acceleration responses per floor were recorded (same locations as in the experimental case). Each simulation consisted of seven minute inputs from which data was obtained with a sampling frequency of 200Hz. The first two minutes of each simulation were discarded to ensure no transient response was being considered. In addition, simulated sensor noise was introduced to each sensor as white noise. The signal to noise ratio ranged between 0.03 and 0.1 (in a standard deviation sense) depending on the amplitude of the records themselves.

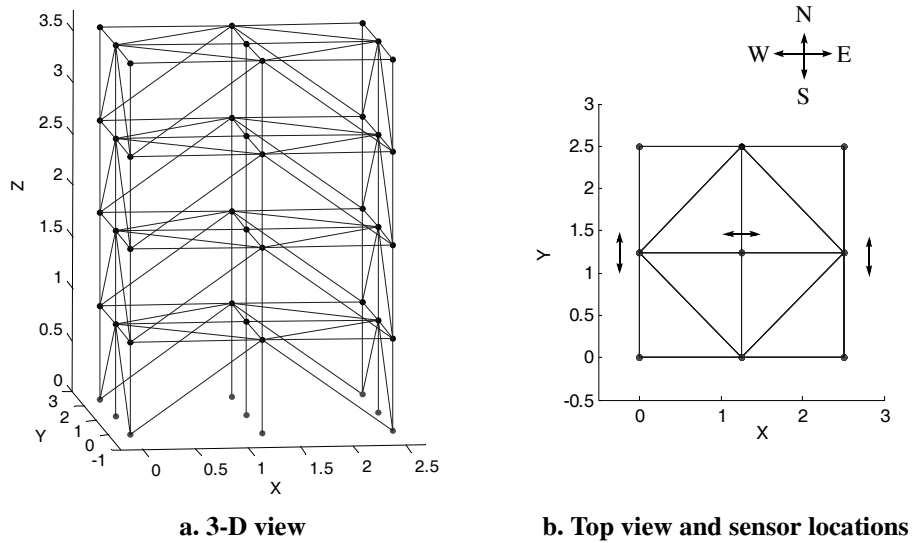


**Figure 2.2 Analytical model of the benchmark problem**

For comparison purposes, the theoretical modal properties of the analytical model were calculated using the stiffness, mass and damping matrices built. These parameters are hereafter referred to as the theoretical properties (see Table 2.2).

**Table 2.2 Theoretical natural frequencies and damping ratios**

<b>Mode number</b>	<b>Description</b>	<b>Frequency Hz.</b>	<b>Damping ratio %</b>
1	E-W motion	7.827	1.0
2	N-S motion	8.397	1.0
3	Torsion	11.115	1.0
4	E-W motion	21.959	1.0
5	N-S motion	23.763	1.0
6	Torsion	31.658	1.0

## 2.4 Analytical Analysis and Results

This section is divided in three subsections. The first one is devoted to the numerical implementation of the free response estimation techniques, including the selection of the parameters necessary to execute them as well as the comparison of the results. In the second subsection, a detailed description of the numerical implementation of all three modal identification techniques is provided. The third and last section is exclusively devoted to the comparison of the techniques.

### 2.4.1 Free Response Estimation

#### Numerical Implementation of NExT

In terms of quality of results obtained by NExT, no major benefits are gained by using data that is sampled at a much higher rate than needed. In contrast, the computational effort increases significantly as higher rates are used. As previously mentioned, the specific objective in the case of the analytical model of the benchmark problem is to capture

the first six modes of vibration, which range approximately between 7 and 31Hz. Thus, data produced with the analytical model is filtered through a low-pass filter, “down-sampling” the data from 200Hz to 100Hz, leaving enough frequency content in the estimated free response to capture the dynamics of the system adequately. Fast Fourier transforms were performed using segments of data with 512 points and averaging in the frequency domain was performed by overlapping the samples by 75% of their length (box windows). As a result, the estimated free responses are 2.56 seconds long. All 300 seconds of the simulated ambient vibration were used.

### **Numerical Implementation of RDD**

As commonly done in the literature, the threshold was expressed in terms of the standard deviation  $\sigma_X^2$  of the reference. Specifically, the threshold was set exactly to this value. Moreover, the range within which signal points were considered triggering points was set to plus or minus 0.5% of the selected threshold. Unlike NExT, where high sampling frequency involves computational expense without much benefit, higher sampling frequency translates in higher chances of points lying within the set range, providing more samples to calculate the RDD signature. Thus, the sampling frequency with which the simulated data from the analytical model of the benchmark structure was kept at 200Hz.

The number of triggering points along the 300 seconds of data used vary slightly depending on the channel selected as reference. In this comparison, these numbers vary randomly between 130 and 160. In addition, segments of 512 points were averaged producing RDD signatures of 2.56 seconds.

### **Comparing NExT and RDD**

The estimated free responses obtained with NExT and RDD are compared in both the time and the frequency domains under the influence of two levels of noise added to the

simulated records. Figure 2.3 shows the decaying responses estimated for one of the sensors that measures north-south vibrations of the top floor. Such estimations were obtained using the acceleration record from the opposite side of the model as reference channel. As clearly shown in Fig. 2.3a, the free responses estimated by both techniques look very similar in the time domain. However, when the frequency content is analyzed, it is clear that the results obtained with NExT concentrate most of the energy in a few frequencies, whereas the random decrement signature distributes the energy more evenly along the entire spectrum.

As expected, the peaks in the spectral density function of the random signature and the cross-correlation function do not contain all the vibrational modes that the structure should exhibit (see Table 2.2). This is due to the fact that the reference channel selected to obtain these free response estimates measures vibrations in the  $y$  axis (north-south) and therefore, the motion of orthogonal modes (east-west) are not captured. This phenomenon occurs despite the non symmetrical distribution of the mass of the model.

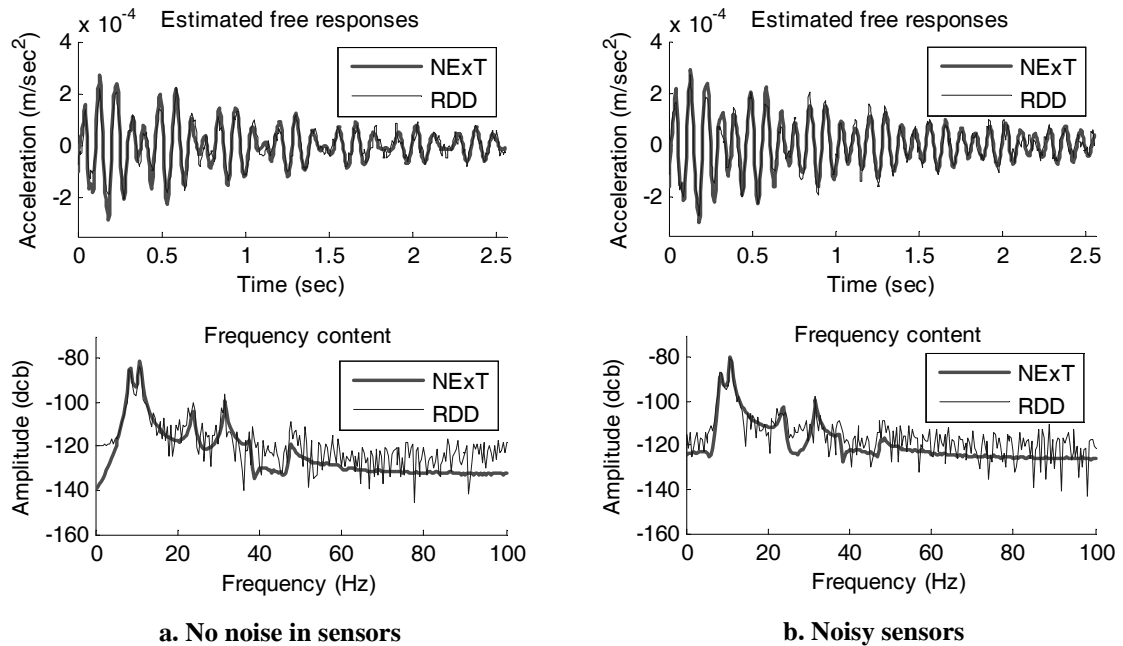


**Figure 2.3 Comparison of estimated free responses by NExT and RDD**

While the free responses of Fig. 2.3a were obtained with noise-free simulated accelerations, those of Fig. 2.3b were obtained from records to which a significant amount of noise was added. In fact, in RMS sense, the signal-to-noise ratio ranged between 0.2 and 0.8 (commonly referred to as 20% and 80% noise). Under these conditions, it is remarkable that the estimated free responses varied only slightly. Yet again, the results obtained with NExT seemed to be more robust, as the peaks remain clear, whereas the third peak of the random decrement result is barely distinguishable. For all these reasons, NExT is used hereafter to estimate free responses of the structure whenever a system identification technique requires it (see ERA-DC later in this chapter).

## 2.4.2 Modal Identification

### Numerical Implementation of ERA/DC

In an attempt to improve the quality of the modal properties identified with ERA/DC, each sensor was used as a reference channel to estimate free responses from NExT. Therefore, a total of 12 sets of results are available for a given set of ambient vibration records. Figure 2.4 shows the complete modal identification process, including the estimation of multiple free responses, the systematic elimination of doubtful modal properties, and the stabilization of modes.

The Hankel matrices used to implement the ERA/DC were composed of 200 columns and 96 rows (8 block rows of 12 sensors each), whereas the block correlation matrices were built with three Hankel matrices as block-columns and two as block-rows. Moreover, as stated in the section devoted to the numerical implementation of NExT, the sampling frequency of the estimated free responses was 100 Hz. As a result, a total of 2.31 seconds of the free response were used to build both  $\mathcal{U}_0$  and  $\mathcal{U}_1$ . The dimensions of these matrices were chosen to make use of the first 2.5 seconds of the decaying response, where, as seen in Fig. 2.3, the signal-to-noise ratio appears to be high. The

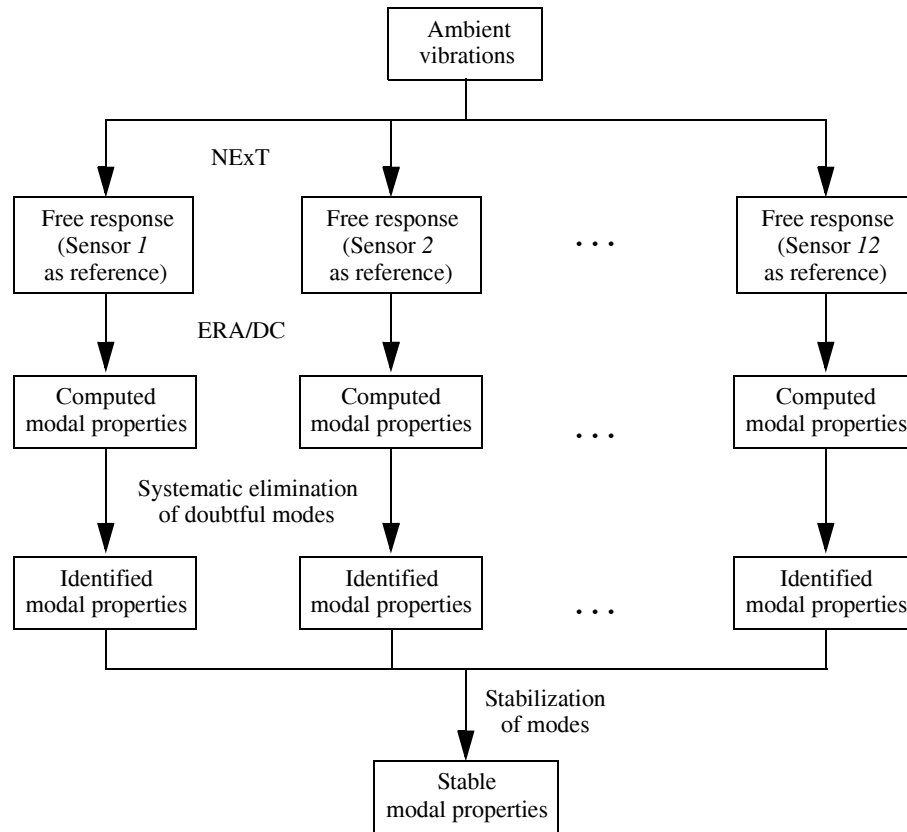


**Figure 2.4 Numerical implementation of ERA/DC**

truncation of matrices  $\Psi$ ,  $\mathbf{R}$  and  $\mathbf{S}$  was carried out using 12 singular values, which means that six vibrational modes were calculated for a given estimated free response.

As previously mentioned, Once ERA/DC has been executed, some of the calculated modes may not be associated with the dynamic system. The systematic elimination of doubtful modal properties is then carried out as follows:

- Modes with unexpectedly high damping ratios are rejected. Since the structure is a steel frame with few non-structural elements, the damping ratios are expected to be very low (perhaps even lower than the 1% introduced into the analytical model). A 10% threshold was used.

- To avoid poorly calculated modes due to the low amplitude of modes at the point of the reference sensor, those modes whose shape vector have an amplitude at the reference point location that is lower than one tenth of the highest value are eliminated.
- Repeated modes are eliminated on the basis of lowest energy content using the associated singular values obtained in the decomposition. The identification of such sets is done as described in the stabilization of modes. However, lower thresholds were used in this case (frequencies within 20% of each other, and MAC values above 0.8). The identification and elimination of modes that are linear combinations of true modes is, on the other hand, more challenging. No action was taken in these cases.
- Because only the first six vibrational modes of the system are targeted (roughly between 7 and 32Hz), only frequencies below 35Hz are taken into account. This practice is common in experimental modal identification, as natural frequencies can easily be identified beforehand with frequency-domain techniques (e.g. spectral density functions).

Once the modal properties for each of the 12 estimated free responses are calculated, the stabilization of modes is executed in order to average all values identified as corresponding to a given vibrational mode. Figure 2.5 shows all frequencies detected from a given free response in the form of a typical stabilization diagram. Here, identified stable vibrational modes are linked with a dotted line. Clearly, for this specific set of simulated ambient vibration records, six modes are considered stable according to the established criteria, with only a few extra modes detected. Only modes detected three or more times with ERA/DC are considered stable in this study.

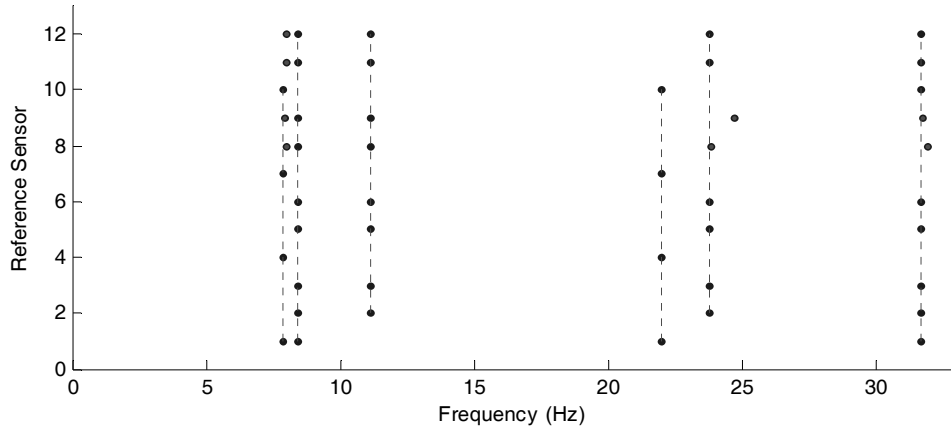


**Figure 2.5 Typical stabilization diagram for ERA/DC**

### Numerical Implementation of PEM/LS

Although not as critical as ERA/DC and its predecessors, the implementation of prediction error methods leaves a number of variables that can be altered and whose correct selection highly depends on the experience of the user. In the case of the two-stage least squares algorithm used in this study, the main variables include the order of both the auto-regressive and the moving average models. In general, an increase in the auto-regressive model order translates not only into more required computational power, but also into a more complex eigensolution of the problem. Therefore, since more eigenvalues and eigenvectors are obtained, the selection of the true vibrational properties of the structure from computational ones becomes more difficult. However, before engaging in a discussion on how to select these values, it is important to understand the effects of the order of the ARMAv models in the accuracy of the modal properties themselves.

Figure 2.6 shows the deviation of the identified fundamental frequency of the benchmark problem from the true analytical value for several ARMAv models. Although somewhat erratic, it can be seen in Fig. 2.6a that a more accurate frequency is obtained as the order of the auto-regressive model is increased. Similarly, the order of the moving

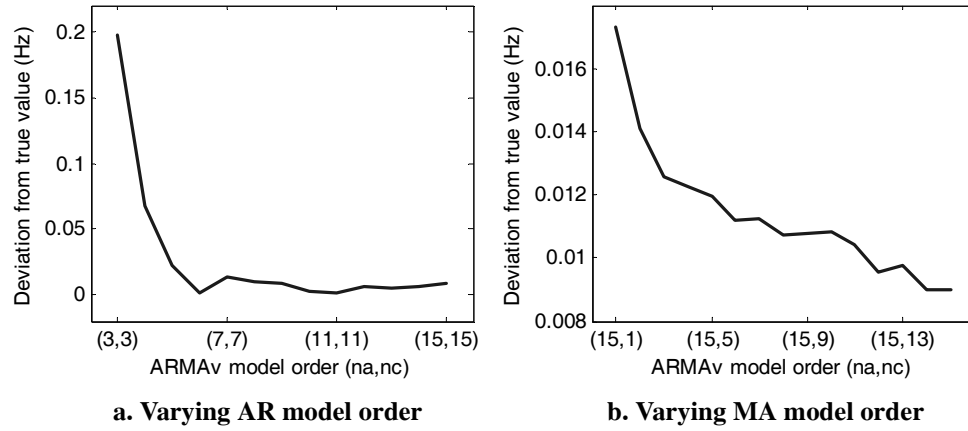


**Figure 2.6 Accuracy of first natural frequency for different ARMAv model orders**

average model affects the identified value in the same manner (see Fig. 2.6b). Higher frequencies, mode shapes and damping ratios are also influenced positively as the order of these models is increased. Since higher order models require more computational power, it could be concluded that the accuracy of the methodology becomes a trade-off with time. However, noise, non-stationary inputs and non-linearities in the system can affect the technique and even make it lose accuracy for excessively high order models.

Figure 2.7 illustrates the implementation of the prediction error method through least squares (PEM/LS) as employed in this study. Note that, unlike the implementation of ERA/DC, the modal properties were not obtained through averaging. The process starts by forming a reliable basis to separate the true vibrational modes of the structure from computational ones, using a series of six low-order ARMAv models. The order of these models were (4,2), (4,3), (5,4), (5,3), (6,4), and (6,5), where the first and second numbers represent the auto-regressive and moving average orders respectively. Moreover, the order of the auto-regressive model estimated in the first step of the algorithm was two times the order of the final ARMAv model. All five minutes of data sampled at 200 Hz were used to identify these models.

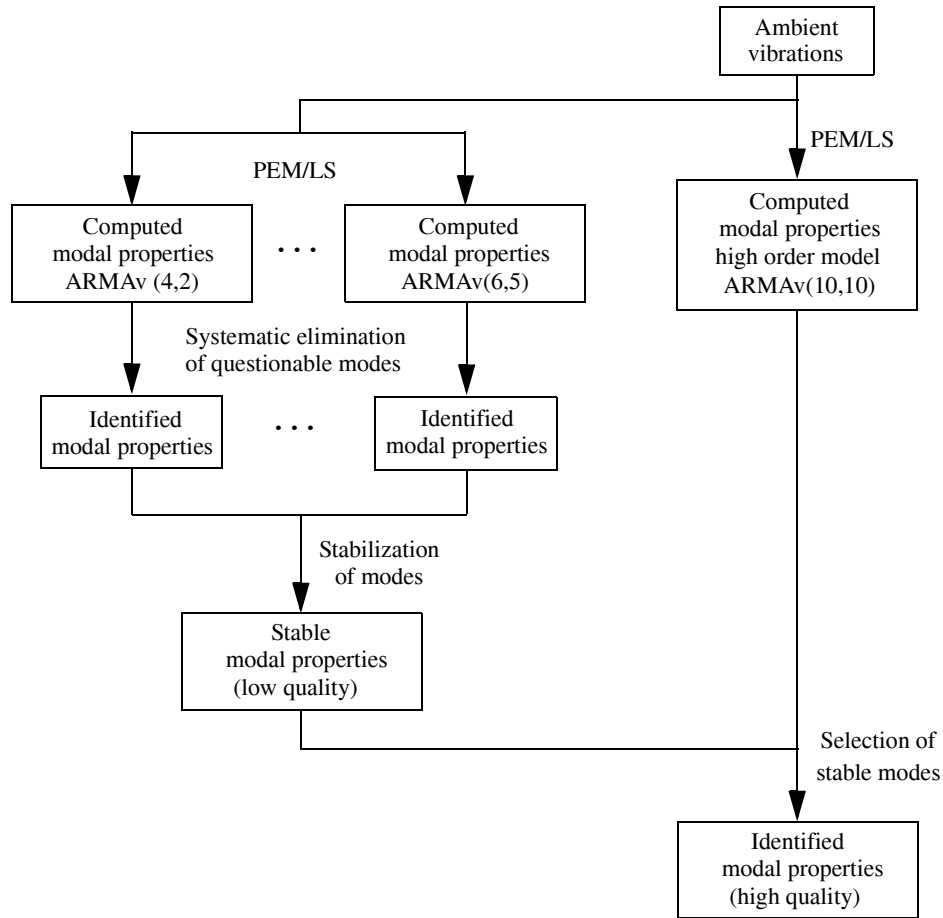


**Figure 2.7 Numerical implementation of PEM/LS**

The systematic elimination of questionable modal properties was carried out using the same criteria used in the implementation of ERA/DC. As expected, this handful of thresholds were particularly useful in the implementation of the PEM/LS algorithm, eliminating most of the computational modes that, by nature, the algorithm estimates with each ARMAv model. Similarly, the stabilization of the identified modes is performed using the same criteria used with ERA/DC. However, this process was carried out with the sole purpose of determining the stable modes of the system. Subsequently, more accurate values were extracted from a high order model with ten auto-regressive and ten moving average matrix coefficients (10,10).

## Numerical Implementation of SSI

Among the algorithms compared in this study, the stochastic subspace identification technique is the most user-friendly as it only requires the selection of the number of singular values to truncate the decomposition. However, depending on the quality of the measurements and the frequency content of the input, it may be necessary to retain a large number of singular values to identify all vibrational modes. Moreover, even for high quality measurements and stationary white noise as input (as in the case of the analytical model employed here), this selection may affect the quality of the results. It can be seen in Fig. 2.8, for instance, that the deviation of the identified first frequency with respect to the true analytical value is decreased for larger truncations. Higher frequencies, mode shapes and damping ratios are influenced similarly.

The identification of modal properties was then carried out using three truncation sizes (20, 22 and 24) and averaging the results by means of stabilization of modes. Systematic elimination of questionable modal properties was executed here using the same criteria exposed previously. However, this procedure was rarely needed. All five minutes of data sampled at 200 Hz were used here. Figure 2.9 summarizes the numerical implementation of the algorithm.

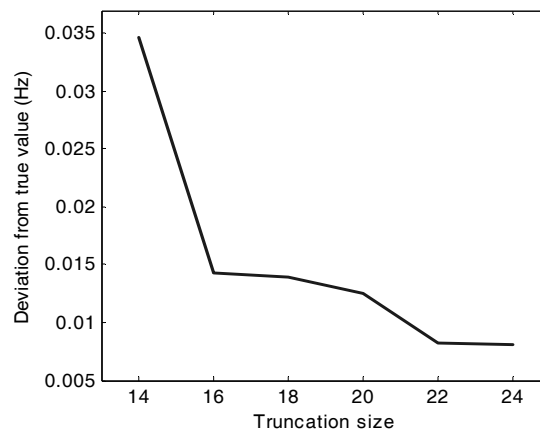


**Figure 2.8 Accuracy of first natural frequency for different truncations**

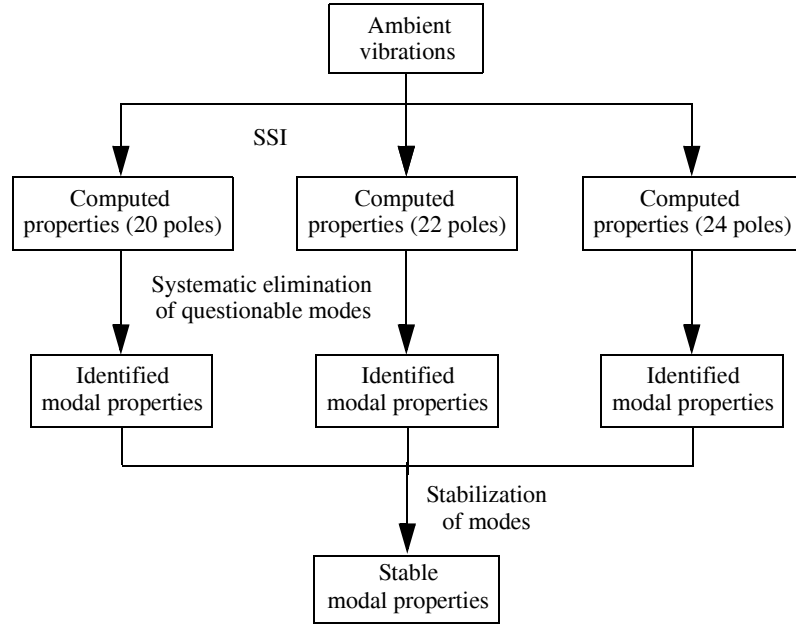


**Figure 2.9 Numerical implementation of SSI**

### 2.4.3 Comparison of Results

Two numerical studies were performed to investigate the capabilities of each algorithm. The goal of the first study is to determine the performance of the different methodologies under the same noise level conditions. The second set of simulations investigates

**Table 2.3 Evaluation criteria**

Criteria	Description	Formula
$J_1$	Accuracy of detected natural frequencies as error percentage	$100 \frac{\omega_{true} - \omega_{id}}{\omega_{true}}$
$J_2$	Accuracy of detected mode shapes through the modal assurance criteria (MAC)	$1 - \text{MAC}(\phi_{true}, \phi_{id})$
$J_3$	Accuracy of detected damping ratios as error percentage	$100 \frac{\zeta_{true} - \zeta_{id}}{\zeta_{true}}$
$J_4$	Number of modes missed	--
$J_5$	Number of extra modes detected	--

the performance of the methodologies under various noise levels. Table 2.3 shows all five evaluation criteria used to carry out the comparison. Here,  $\omega$ ,  $\phi$  and  $\zeta$ , represent the frequencies, mode shapes and damping ratios respectively; whereas the subindices “*true*” and “*id*” stand for analytical and identified.

### Constant Noise

Five hundred simulations were performed to determine the effectiveness of each methodology under the influence of a constant level of noise added to the acceleration records. For each simulation, noise was created as uncorrelated, normally-distributed random signals with zero mean and unit standard deviation. These signals were then multiplied by  $1 \times 10^{-5}$  and added to the measured responses. In an RMS sense, these noise signals range between 3 and 9% of the accelerations used (depending on the sensor location). Running in a Microsoft Windows based Pentium 4 at 2.0 Ghz, each simulation took approximately nine seconds to produce seven minutes of simulated ambient vibration records (from which only the last five were used to avoid using transient responses), and to obtain the theoretical dynamic properties of the 88-DOF model. Subsequently, 10, 30 and 29 seconds were employed to complete the automated ERA/DC, PEM/LS, and SSI algorithms, respectively.

Figures 2.10 and 2.11 show histograms of two of the evaluation criteria used to compare the techniques. All 3000 results (6 frequencies in 500 simulations) are considered equally. Although it is difficult from these plots to compare the efficacy of PEM/LS and SSI with respect to each other, it is clear that both techniques outperform ERA/DC. It is also clear that none of the methodologies were nearly as capable of identifying damping ratios with the same accuracy as they identify natural frequencies. Whereas errors rarely reach 0.5% for the identified frequencies, damping ratios were often off by more than 20 and even 50% (specially when using ERA/DC).

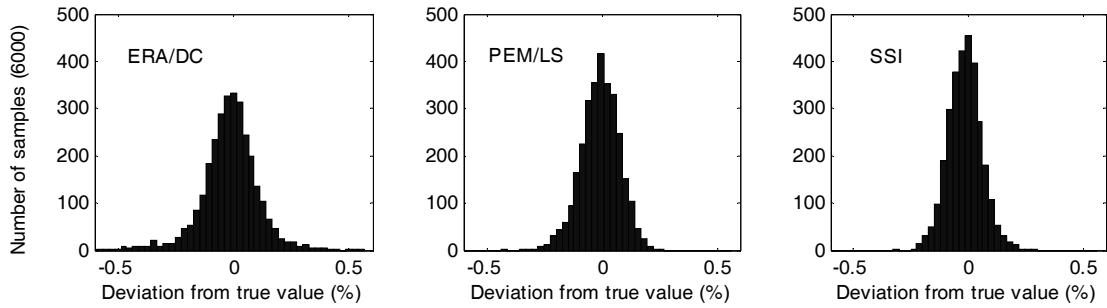


**Figure 2.10 Deviation of identified natural frequencies ( $J_1$ )**

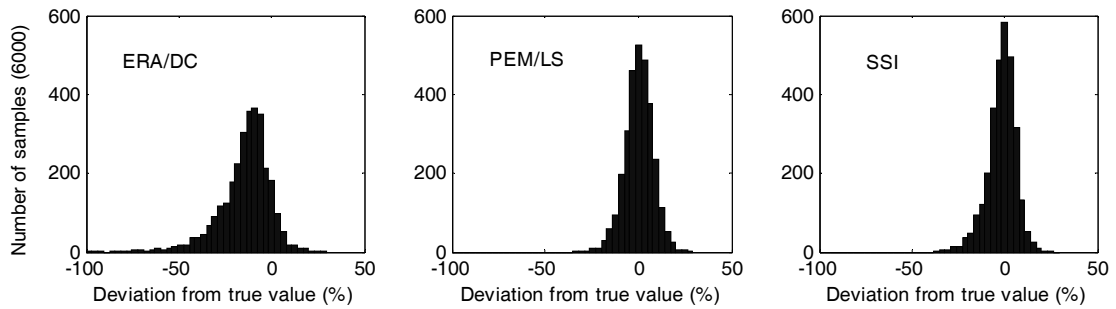


**Figure 2.11 Deviation of identified damping ratios ( $J_3$ )**

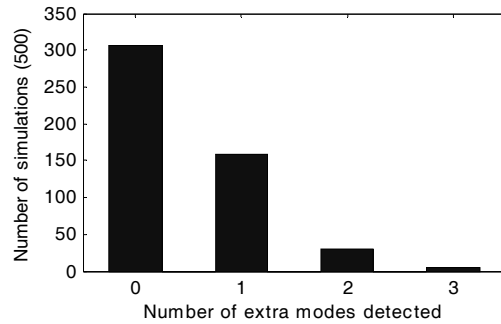


**Figure 2.12 Computational modes detected with ERA/DC ( $J_5$ )**

None of the techniques seemed to be greatly affected by the simulated noise as all three algorithms successfully identified the targeted first six vibrational modes in all 500 simulations (i.e.  $J_4 = 0$  in all cases). In addition, PEM/LS and SSI did not identify any extra modes while ERA/DC identified up to three computational modes. Figure 2.12 shows the histogram of the additional identified by ERA/DC for all 500 simulations.

The mean value and standard deviation of the first three evaluation criteria for the different algorithms are shown in Table 2.4. Again, all 3000 results are employed to calculate the tabulated values. In a mean sense, these results indicate that the PEM/LS algorithm outperforms the other two algorithms in the identification of all modal properties. However, in a standard deviation sense, SSI slightly outperformed PEM/LS in the identification of frequencies and mode shapes. It is difficult to draw conclusions from this first study regarding the relative performances of PEM/LS and SSI. Although slightly better results were obtained with PEM/LS, it can be argued that its numerical implementation is more challenging. Moreover, the computational power required is almost identical.

**Table 2.4 Evaluation criteria for constant noise level**

<b>Algorithm</b>	$\bar{J}_1$	$\sigma_{J_1}$	$\bar{J}_2$	$\sigma_{J_2}$	$\bar{J}_3$	$\sigma_{J_3}$
ERA/DC	$-16.87 \times 10^{-3}$	0.122	$15.45 \times 10^{-4}$	$32.95 \times 10^{-4}$	-14.560	14.529
PEM/LS	$-7.25 \times 10^{-3}$	0.083	$2.91 \times 10^{-4}$	$3.73 \times 10^{-4}$	0.384	7.448
SSI	$-14.38 \times 10^{-3}$	0.071	$3.31 \times 10^{-4}$	$3.52 \times 10^{-4}$	-1.656	7.620

### Variable Noise

The effect of sensor noise in the algorithms was investigated using 1000 simulations with different signal-to-noise ratios. To achieve this goal, the zero mean, unit standard deviation white noise added to the acceleration records of each simulation was multiplied by a different constant. Over all simulations, this constant constitutes a random variable, uniformly distributed between 0 and  $2 \times 10^{-4}$ , which corresponds to a maximum noise level of approximately 80% in average for all acceleration records (in an RMS sense).

Figures 2.13, 2.14 and 2.15 show all 6000 values (6 modes in 1000 simulations) assumed by  $J_1$ ,  $J_2$  and  $J_3$ , respectively. Similar to the constant noise study, but given the high noise level introduced, it is remarkable that all modal properties were detected

by all three evaluated methodologies. It can be observed in Figs. 2.13 and 2.15 that, when identifying natural frequencies and damping ratios, none of the methodologies showed clear signs of sensitivity to noise in the sensors. The identification of mode shapes, however, is affected negatively as the noise level is increased (see Fig. 2.14). In this case, SSI seems to be more robust than ERA/DC and PEM/LS.

As expected, ERA/DC consistently calculated some computational modes. However, no trend was observed as the noise level was increased. Table 2.5 shows the mean value and standard deviation of the first three evaluation criteria. Contrary to the constant noise

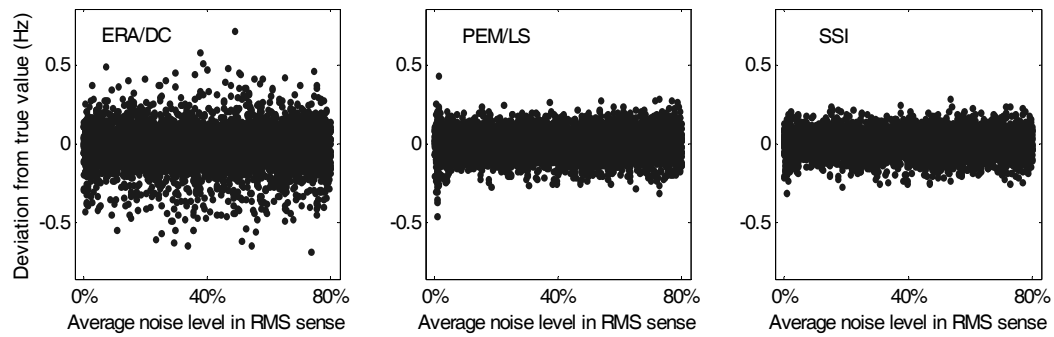


**Figure 2.13 Accuracy of identified natural frequencies ( $J_1$ ) as a function of noise level**

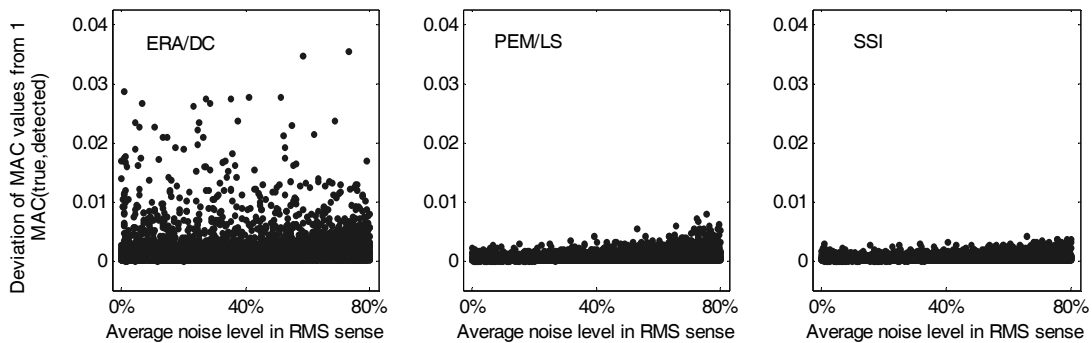


**Figure 2.14 Accuracy of identified mode shapes ( $J_2$ ) as a function of noise level**

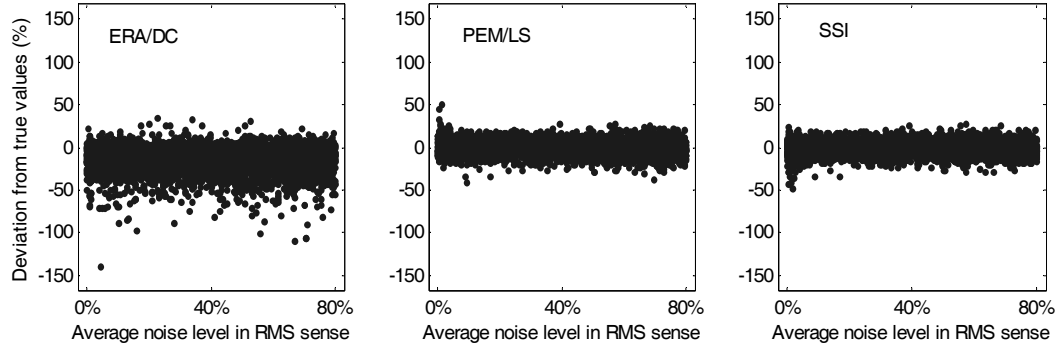


**Figure 2.15 Accuracy of identified damping ratios ( $J_3$ ) as a function of noise level**

study, the results indicate that the SSI algorithm outperforms the other two algorithms in the identification of all modal properties demonstrating its robustness to deal with noisy measurements. Given these results and the fact that subspace identification requires the lowest number of parameters to setup, it is concluded here that, among the algorithms evaluated, SSI is the best choice.

**Table 2.5 Evaluation criteria for variable noise level**

Algorithm	$\bar{J}_1$	$\sigma_{J_1}$	$\bar{J}_2$	$\sigma_{J_2}$	$\bar{J}_3$	$\sigma_{J_3}$
ERA/DC	$-233.7 \times 10^{-4}$	0.121	$16.57 \times 10^{-4}$	$26.44 \times 10^{-4}$	-14.817	13.974
PEM/LS	$-9.15 \times 10^{-4}$	0.079	$5.56 \times 10^{-4}$	$6.92 \times 10^{-4}$	-0.229	7.832
SSI	$2.58 \times 10^{-4}$	0.070	$4.56 \times 10^{-4}$	$4.75 \times 10^{-4}$	-0.157	7.232

## 2.5 Experimental Results

However detailed an analytical study may be, it is never able to reproduce all the characteristics of real systems and particularly those of civil structures. Therefore, despite the effort put into the analytical study, many questions about the viability for modal identification through ambient vibrations remain unsolved. For instance, given the usual low amplitude of ambient vibrations, one might wonder if the measurements are sufficient to

implement any of the methodologies discussed. Moreover, the often overlooked non-linearities of the structure at low amplitudes may play a significant role. Therefore, to investigate the feasibility of ambient modal testing, experimental ambient vibrations from the benchmark structure were analyzed here. Only the stochastic subspace algorithm is implemented for this purpose. It is not intended here to discuss the stationarity of the input loads acting on civil structures and their capability to excite an acceptable amount of vibrational modes. This problem is unique for each case and should be evaluated in the field.

The main problem in evaluating modal properties identified with ambient vibration records, lies in the fact that, unlike analytical studies, the exact dynamic properties are unknown. In the case of the benchmark problem however, these properties can also be obtained from hammer tests, providing a more reliable point of reference. Since ERA/DC was essentially created to deal with free responses, this algorithm was implemented to extract the modal properties of the structure from the impact tests. The implementation of the SSI was identical to that of the analytical study. The following sections describe the evaluation of hammer tests using ERA/DC, and the comparison results.

### **2.5.1 Hammer Testing (Implementation of ERA/DC)**

As mentioned previously, hammer impacts were all located in the southwest corner of the first floor (between first and second stories). Three impacts in the north-south direction and three more in the east-west direction were recorded. Therefore, a total of 6 free responses recorded at a sampling frequency of 1000 Hz are available. Similar to the analytical study, the available data was “down-sampled” to 100 Hz through low pass filters. Figure 2.16 shows, as an example, the response of all 12 sensors taken shortly after one of the impacts. Unlike the estimated free responses obtained with NExT, where only a couple of seconds constituted meaningful data, more than five seconds are part of the decaying response that greatly overpowers the ambient vibration. Thus, larger Hankel

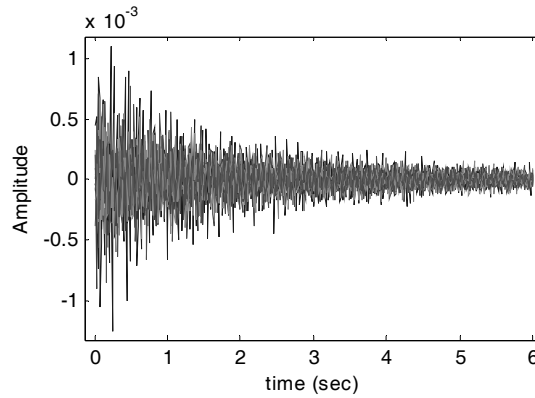


**Figure 2.16 Typical impulse responses**

matrices can be used in this case. These were then composed by 400 columns and 180 rows (15 block-rows of 12 sensors each), whereas the block correlation matrices were built with three Hankel matrices as block-columns and two as block-rows. As a result, a total of 4.18 seconds of the free response were employed to execute the algorithm. Systematic elimination of doubtful modal properties as well as the stabilization of those remaining was carried out using the same criteria applied in the analytical study.

### 2.5.2 Comparison of Results

Table 2.6 contains the modal properties identified with both ambient vibration records (using SSI) and hammer testing (through ERA/DC). Natural frequencies and damping ratios, as well as the MAC correlation between the correspondent mode shapes are tabulated here. Unlike the analytical study, no specific number of vibrational modes were pursued. In fact, a total of seven modes were identifiable from the hammer tests. Note that, perhaps due to a limited bandwidth of the random inputs, the sixth mode was not identified using the ambient vibration records. However, it can be observed that the natural frequencies identified with ambient vibrations are in good agreement with those identified from hammer impacts. In fact, only the second natural frequency differs by more than 1% (1.63%). Damping ratios, on the other hand, poorly agree and the error in these parameters is much larger.

**Table 2.6 Identified modal properties**

Mode	Description	Frequency (Hz)		Damping ratio (%)		Mode shapes $\phi_{ham}, \phi_{amb}$
		Ambient (SSI)	Hammer (ERA)	Ambient (SSI)	Hammer (ERA)	
1	E-W motion	7.466	7.449	1.059	0.796	0.895
2	N-S motion	7.759	7.634	0.973	0.852	0.932
3	Torsion	14.472	14.436	0.805	0.407	0.942
4	E-W motion	19.892	19.832	0.001	0.441	0.995
5	N-S motion	20.989	20.850	0.017	0.493	0.969
6	Torsion	--	22.472	--	0.634	--
7	E-W motion	25.553	25.245	0.828	0.464	0.939

But perhaps the most important parameters in a structural health monitoring context are the mode shapes. Here, only the fourth mode had an excellent agreement between the vectors identified with both tests (i.e. MAC of 0.995). And, although relatively good agreement was observed in most of them, the vectors associated with the first frequency seem to differ significantly (MAC of 0.895). Because relatively long ambient vibration records were analyzed and averages from different estimated free responses were obtained, this phenomenon cannot be attributed to noise in the sensors, but rather to an inconsistent behavior of the structure when vibrating at low and high amplitudes. Although the source of this phenomenon is not precisely known, it is likely that these changes are due to a non-linearity of the structure (e.g. friction in the joints) that affects the behavior of the building mainly when the amplitude of the displacements is small (e.g. ambient vibration). Schematically, Fig. 2.17 helps to visualize the differences between the first three mode shapes of the two tests.

The inconsistencies between the modal properties obtained from ambient vibrations and hammer tests may lead some to argue that, at least in this benchmark problem, ambient vibrations do not suffice to characterize the structure and search for damage. However, once damage was induced to this structure, a mostly successful damage identification

technique was already implemented in 2003 using, exclusively, ambient records (see Giraldo *et al.* [29]). Therefore, the argument of those who do believe in the usability of ambient vibrations is that, as long as the state of the structure is analyzed while vibrating under the same conditions as in the healthy state, the dynamic properties will reflect the changes of its overall stiffness.

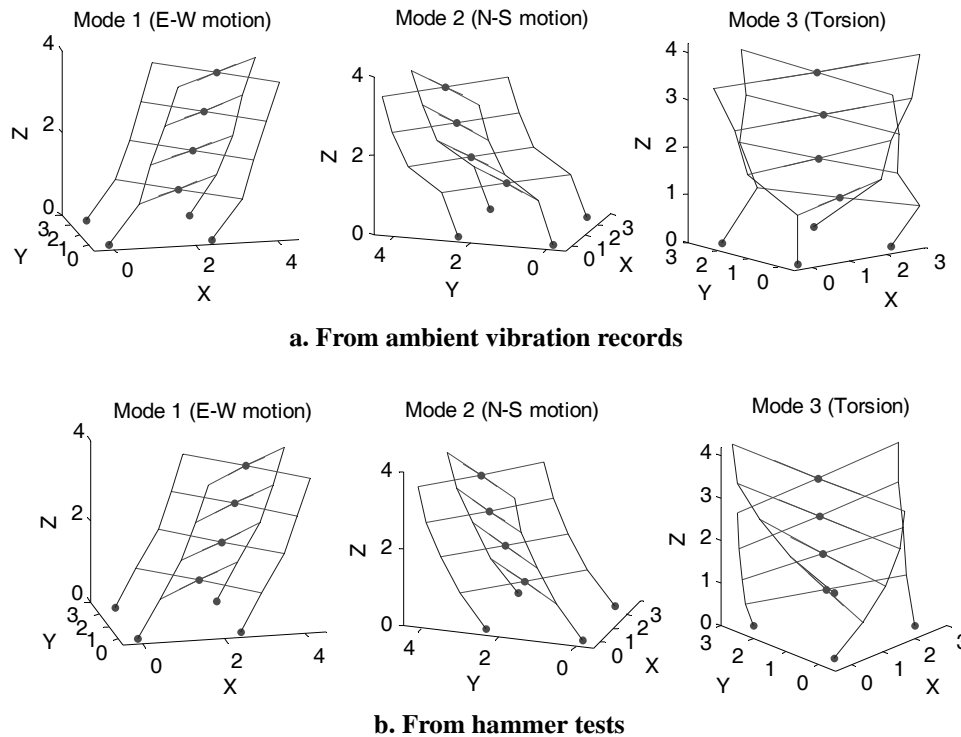


**Figure 2.17 Experimentally identified mode shapes**

## 2.6 Conclusions

This chapter was devoted to the identification of modal properties from civil structures as they vibrate in their natural environment. The three main goals of the study were: 1) to provide a brief introduction to linear systems, their mathematical representations and the physical meaning of their modal properties; 2) the evaluation and comparison of

three of the most popular time-domain modal identification techniques; and 3) the analysis of the performance of the best methodology by comparing it to more traditional ways of testing. An analytical model of a two-bay by two-bay, four-storey building, as well as the actual steel frame were used to accomplish the intended goals.

The three methodologies compared are the eigensystem realization algorithm with data correlations (ERA/DC), the prediction error method through least squares (PEM/LS), and the stochastic subspace algorithm (SSI). Because ERA/DC requires estimation of free responses, the random decrement (RDD) and the natural excitation technique (NExT) were also evaluated and compared. Analytical data from an 88 degree of freedom model that closely represents the actual structure was used to carry out these comparisons. Results indicate that while being the most user-friendly, the SSI algorithm is more robust to noise in sensors. Acceptable results were also obtained with PEM/LS surpassing those obtained from SSI from relatively clean signals. However, as the noise in sensors was increased, its accuracy seemed to be negatively affected. ERA/DC was clearly in disadvantage. Poor results and difficult setup make this algorithm difficult to implement for ambient vibrations.

Experimental data was used to compare the modal properties obtained from real ambient vibrations and the more traditional hammer tests. Although somewhat accurate results were obtained with SSI, results were far from perfect (in terms of the similarity of the results). Limited bandwidth inputs as well as non-linearities of the structure at low amplitude vibrations seem to affect the identification. However, modal properties at low amplitudes seemed to be consistent. Moreover, as demonstrated in past studies of the benchmark problem [29], damage was actually reflected in its modal properties.

## Chapter 3

# Structural Health Monitoring Through Model Updating

Perhaps the most argued issue for researchers of vibration-based health monitoring revolves around the characterization of structures for damage localization. On one hand, some people feel that utilizing a finite element model of the structure introduces modeling errors and decreases the chances of correctly characterizing the structure. On the other hand, there are those who think that by not using a model, valuable information that can be easily obtained from the structure (e.g. mass, geometry) is wasted. Although the most Solomon-like answer to this dilemma is perhaps a combination of both points of view, this research focusses only on the latter by proposing a model updating technique that uses some of the dynamic properties detected from the structures.

Several model updating techniques have been proposed over the years in the fields of mechanical, aerospace and civil engineering for various purposes. Basically, a finite element model known as the identification model (ID-model), is modified in such a way that its dynamic behavior resembles, as closely as possible, that of the structure being analyzed. In 2003, for example, Ching and Beck [18] proposed a two-stage Bayesian approach in which the most probable dynamic properties of the structure are found by reducing the error between the measured response of the structure and a simulated response from a numerical model in the time domain. Mass and stiffness matrices are updated using this probabilistic framework. One year earlier, Caicedo and Dyke [15]

calculated a reduced number of unknowns of the model's stiffness matrix using its characteristic equation and the estimated dynamic properties. Some of the characteristics of the structure, including the mass, were assumed known and invariable in their work. These two schemes are representative of iterative and non-iterative model updating techniques respectively, which, in general, marks a trade-off between the computational effort needed and the precision reached.

Iterative model updating has been performed in the past by using different objective functions that involve natural frequencies and mode shapes. This approach is usually executed by assigning weighting factors to the discrepancy between each of these sets of properties and the desired experimental ones (see Moller and Friberg [57], Bohle and Fritzen [13], and Jaishi and Ren [42]). However, because there are always differences between the structure and the ID-model (regardless of the care taken when constructing it), the optimization usually converges to a set of parameters that sacrifices accuracy to achieve optimal frequencies and the correlation of the mode shapes. Moreover, assigning these weighing factors becomes a task that highly depends on the experience of the engineer in each situation. Unlike control-oriented model updating, in which the accuracy of the frequencies is perhaps the most important issue, the changes in mode shapes are more likely to provide information that can lead to the localization of damage.

The model updating procedure implemented in this research is an iterative algorithm that minimizes an objective function constructed using the correlation between the mode shapes of the structure and the eigenvectors of the ID-model. This correlation is measured using the modal assurance criteria (MAC). Several authors have made use of the MAC for model updating. In 1988 Heylen and Janteer [33] proposed the use of these correlation measurements to update the model of a simple spring-mass, 16-DOF system. To accelerate the updating process, numerical derivatives of the MAC values were obtained in this work. A decade later, Moller and Friberg [57] proposed the use of an objective function that involved both natural frequencies and mode shapes. More

recently, Jaishi and Ren [42] applied the latter work for SHM purposes. The algorithm was further enhanced by using the sensitivities of the mode shapes to changes in the structural parameters. Although the results obtained by all these authors clearly show the potential for using the MAC values in model updating, the algorithms used to optimize the different objective functions are often slow and do not explore all the mathematical possibilities.

Herein a variation of the optimization algorithm known as the conjugate gradients is employed to execute the updating process. The main contribution of the research is the derivation of the needed partial derivatives and Hessian matrix of the selected objective function, using as basis the sensitivities of the mode shapes derived in 1968 by Fox and Kapoor [27]. By providing these tools, the need for time consuming numerical estimations through finite differences is eliminated. Moreover, because the main focus of this research is the applicability of these type of algorithms to civil structures, the robustness of the methodology is tested for the cases of poorly estimated mode shapes as well as their limited availability, both situations common in the field. Section 3.1 discusses the methodology and the mathematical background, whereas a numerical example and the conclusions are provided in sections 3.2 and 3.3 respectively.

### **3.1 Methodology**

The robustness of the methodology proposed in this chapter (as well as that of most model-based SHM techniques) strongly depends on the selection of an appropriate ID-model and its ability to reproduce the dynamic behavior of the structure. The ID-model will determine and limit the range of potential dynamic behaviors that the structure can exhibit. ID-models typically represent the structure in a simplified way, and their level of complexity depends primarily on the measuring capabilities. Therefore, the more degrees of freedom measured, the more complex the ID-model becomes and the better the chances of accurately identifying and localizing structural damage. Unfortunately,

no specific guidelines can be established for the construction of this model, and the experience of the engineer for taking into account both the known characteristics of the structure and the measurements obtained from it plays a fundamental role.

Once the ID-model has been constructed, the first problem that must be resolved is the selection of an appropriate set of updating parameters. Although perhaps not ideally, the use of finite element models limits the search for damage to an element-based search. In other words, changes in the structure have to be reflected exclusively in changes on the elements of the ID-model, leaving connections and boundary conditions unchanged. With this limitation in mind, it is recognized that the updating parameters are reduced to the properties of the elements themselves, including the density and elasticity properties of the material as well as the geometric properties of the cross sectional areas.

One of the main assumptions made in this research is that the mass distribution of the structure does not change with damage. In principle, this assumption is not critical because a significant change in mass, besides being much more evident than stiffness changes, would also have an important impact on the dynamic properties of the structure, and most likely be reported as a change of stiffness by the updating technique. However, the assumption also implies that a characterization of the structure in the pre-damage state is available with the same mass of the damaged state. In structures such as bridges, where the changes in mass are temporary, it is reasonable to argue that periodic characterizations of the structure would accurately describe them under similar mass conditions. However, buildings and their constant change of mass might require special treatment. A statistical analysis such as the one introduced in Chapter 4 may help reduce these effects.

By making the assumption of invariable mass, both the cross sectional area of the elements as well as the density of the material are recognized as constants and the possibilities for updating parameters are reduced to the inertial properties of the elements and

the material's Young's modulus and Poisson's ratio. To keep the number of updating variables small, and recognizing that the Young's modulus of the material has a global effect on the stiffness of the element's principal components, it was decided to assume this property as the only updating parameter. As it will become clear in later sections of this chapter, the selection of the Young's modulus of the elements as updating parameters is also convenient from a mathematical point of view.

The updating process will be described in the following sections. First, the objective function used for updating the identification model is discussed. Consequently, the optimization technique used to find the optimal parameters is described. In the three sections to follow, the mathematical tools needed to carry out the optimization process are derived. Finally, the implementation issues are laid out.

### 3.1.1 The Objective Function

As mentioned previously, the algorithm implemented in this research is an iterative algorithm that maximizes the correlation of the mode shapes of the structure and the eigenvectors of the constructed ID-model. This correlation is measured using the modal assurance criteria (MAC), which, as described in Chapter 2 of this dissertation (and repeated here for convenience), is defined as

$$\text{MAC}(\phi_a, \phi_b) = \frac{\left\{ \sum_{r=1}^N (\phi_{a_r})(\phi_{b_r}^*) \right\}}{\sqrt{\sum_{r=1}^N (\phi_{a_r})^2 \sum_{r=1}^N (\phi_{b_r}^*)^2}}. \quad (3-1)$$

Here, a value close to 1.0 suggests that the two mode shapes  $\phi_a$  and  $\phi_b$  are well correlated. Maximizing this correlation should allow us to accurately characterize the structure at any time and localize damage by comparing the current state with previous

characterizations. An objective function that evaluates the correlation of all identified modes for a given trial  $p$  (i.e. identification model build with a set of selected parameters) will take the form

$$\Omega(p) = \sum_{n=1}^N \left[ 1 - \text{MAC}(\phi_n, \hat{\phi}_n) \right], \quad (3-2)$$

where  $\phi$  and  $\hat{\phi}$  are the corresponding mode shapes from the identification model and the structure respectively, and  $N$  is the number of experimentally detected modes. Therefore, the function  $\Omega(p)$  should be minimized to determine the optimal set of parameters.

### 3.1.2 Optimization Technique

There are numerous algorithms available to optimize linear and nonlinear problems. Researchers in fields such as numerical analysis and statistical computing have filled the literature with studies and alternatives on this topic (see, for instance, Bertsekas [10], Bertsekas and Tsitsiklis [11], and Gill *et al.* [28]). When selecting an algorithm to optimize a nonlinear problem, such as the minimization of Eq. (3-2), it is important to understand first that there is no single technique that works best for all types of nonlinear optimization problems. The selection of an appropriate algorithm strongly depends on several factors such as the number of variables, the presence of constraints and the continuity of the objective function. As described in [36], three general types of algorithms have been found to be effective for most practical purposes:

- For a small number of parameters, stabilized Newton and Gauss-Newton algorithms are efficient. The memory required by these algorithms is proportional to the square of the number of parameters.

- For a moderate number of parameters, various quasi-Newton algorithms are efficient. The memory required is also proportional to the square of the number of parameters.
- For a large number of parameters, various conjugate-gradient algorithms are efficient. The memory required is proportional to the number of parameters.

Because the complexity of ID-models (i.e. the number of parameters to optimize) is different for each case, this research focuses on the more general conjugate gradient algorithm, despite the fact that, for simplistic ID-models, it may not be the most efficient option. However, as long as the objective function of Eq. (3-2) is employed, the mathematical tools derived in later sections can be employed to execute other types of algorithms more suitable for simplistic ID-models with few parameters.

The conjugate gradient algorithm was developed in 1952 by Hestenes and Stiefel [32] as an improvement to the steepest descent method. Despite the vast amount of literature devoted to the method, interested readers are referred to the report written in 1994 by Shewchuk [67], in which a clear summary of the basics is explained. The conjugate gradients method is a mature algorithm that has been extended from linear applications with a number of variations that assume near quadratic objective functions [34]. One of the variations is called conjugate gradients with Newton-Raphson and Fletcher-Reeves which includes special subroutines that deal with line search in any specific conjugated gradient to accelerate its convergence [67]. Details on the algorithm can be found in [26]. Both the gradient vector and the Hessian matrix of the objective function with respect to the optimization parameters (i.e.  $E$  values) are required to perform the optimization. The algorithm can be summarized as shown in Fig. 3.1.

```

 $i = 0$ 
 $k = 0$ 
 $r = -\Omega'(p)$ 
 $d = r$ 
 $\delta_{new} = r^T r$ 
 $\delta_o = \delta_{new}$ 
while  $i < i_{max}$  and  $\delta_{new} > \varepsilon^2 \delta_o$ 
   $j = 0$ 
   $\delta_d = d^T d$ 
  do
     $\alpha = \frac{[\Omega'(p)]^T d}{d^T \Omega''(p) d}$ 
     $p = p + \alpha d$ 
     $j = j + 1$ 
  while  $j < j_{max}$  and  $\alpha^2 \delta_d > \varepsilon^2$ 
     $r = -\Omega'(p)$ 
     $\delta_{old} = \delta_{new}$ 
     $\delta_{new} = r^T r$ 
     $\beta = \frac{\delta_{new}}{\delta_{old}}$ 
     $d = r + \beta d$ 
     $k = k + 1$ 
  if  $k = n$  or  $r^T d \leq 0$ 
     $d = r$ 
     $k = 0$ 
   $i = i + 1$ 

```

**Figure 3.1 Conjugate gradients algorithm with Newton-Ramphson and Fletcher-Reeves (From [67])**

### 3.1.3 Gradients and Hessian of Objective Function

Calculating gradient vectors and Hessian matrices is a computationally expensive process that is often avoided due to large memory requirements and high computational cost. However, as the power of computing tools quickly increases over time, more complex algorithms with large memory requirements can be implemented. Moreover, numerical estimations through finite differences are, in many cases, more time consuming and have poor accuracy. The vector of gradients of the objective function employed in this study can be obtained by differentiating Eq. (3-2) with respect to Young's modulus of each element of the ID-model. In general, the derivative with respect to the elastic modulus of the  $m$ -th element ( $E_m$ ) is

$$\frac{\partial \Omega(p)}{\partial E_m} = \sum_{j=1}^J \left( \frac{\partial MAC(\phi, \hat{\phi})}{\partial E_m} \right). \quad (3-3)$$

It is assumed in this work that the condition of the structure does not change during the time that accelerations are recorded. As a result, when calculating the gradients of the MAC values for Eq. (3-3), the mode shapes of the structure ( $\hat{\phi}$ ) can be treated as constants. Therefore, the expression within the parenthesis of Eq. (3-3) can be written

$$\frac{\partial MAC(\phi, \hat{\phi})}{\partial E_m} = \frac{2(\hat{\phi}^T \phi)(\hat{\phi}^T \phi')}{(\phi^T \phi)(\hat{\phi}^T \hat{\phi})} - \frac{2(\phi^T \phi')(\hat{\phi}^T \phi)^2}{(\phi^T \phi)^2(\hat{\phi}^T \hat{\phi})}, \quad (3-4)$$

where

$$\phi' = \frac{\partial \phi}{\partial E_m}. \quad (3-5)$$

The calculation of the Hessian matrix of the objective function is a more challenging procedure and, certainly, more computationally expensive. It is derived by differentiating the gradients of Eq. (3-3) with respect to each optimization parameter, thus forming a square matrix. In general, each term of the Hessian matrix takes the form

$$\frac{\partial^2 \Omega(p)}{\partial E_m \partial E_n} = \sum_{j=1}^J \left( \frac{\partial^2 MAC(\phi, \hat{\phi})}{\partial E_m \partial E_n} \right), \quad (3-6)$$

which, when combined with Eq. (3-4) yields

$$\frac{\partial^2 \Omega(p)}{\partial E_m \partial E_n} = \frac{\partial}{\partial E_n} \left( \frac{2(\hat{\phi}^T \phi)(\hat{\phi}^T \phi')}{(\phi^T \phi)(\hat{\phi}^T \hat{\phi})} \right) - \frac{\partial}{\partial E_n} \left( \frac{2(\phi^T \phi')(\hat{\phi}^T \phi)^2}{(\phi^T \phi)^2(\hat{\phi}^T \hat{\phi})} \right). \quad (3-7)$$

Again, the detected mode shapes  $\hat{\phi}$  can be treated as constants, and Eq. (3-7) can be expanded to obtain

$$\begin{aligned} \frac{\partial^2 \Omega(p)}{\partial E_m \partial E_n} = \frac{2}{(\hat{\phi}^T \hat{\phi})(\phi^T \phi)^2} \times & \left[ (\phi^T \phi)(\hat{\phi}^T \phi')(\hat{\phi}^T \phi^x) - (\phi'^T \phi^x)(\hat{\phi}^T \phi)^2 + \right. \\ & (\phi^T \phi)(\hat{\phi}^T \phi)(\hat{\phi}^T \phi'^x) - (\phi^T \phi')(\hat{\phi}^T \phi)(\hat{\phi}^T \phi^x) + (\phi^T \phi'^x)(\hat{\phi}^T \phi)^2 - \\ & \left. 2(\phi^T \phi^x)(\hat{\phi}^T \phi')(\hat{\phi}^T \phi) + \frac{(\phi^T \phi')(\hat{\phi}^T \phi^x)(\hat{\phi}^T \phi)^2}{(\phi^T \phi)} \right], \quad (3-8) \end{aligned}$$

where

$$\phi' = \frac{\partial \phi}{\partial E_m} \quad \text{and} \quad \phi^x = \frac{\partial \phi}{\partial E_n} \quad (3-9)$$

are the sensitivities of the mode shapes with respect to the optimization parameters  $E_m$  and  $E_n$ , respectively, and

$$\phi'^x = \frac{\partial^2 \phi}{\partial E_m \partial E_n}. \quad (3-10)$$

### 3.1.4 Sensitivities of Mode Shapes

The sensitivity of mode shapes with respect to changes in structural parameters such as mass and stiffness has been a design tool in both the aerospace and mechanical engineering fields for some years now. Explicit calculation of these sensitivities is a complex task even for simplistic finite element models and the order of the equations needed rapidly increases with the number of elements used. Alternatively, different methods have been proposed over the years. In some of the earliest work, Fox and Kapoor [27] found exact expressions for derivatives of modal properties with respect to any design variable using all eigenvectors of the structure in its current state. Eight years later, Nelson [59]

proposed an approximated method that requires only the eigenvalue and eigenvector under consideration. However, in the context of structural health monitoring of civil structures, only a few researchers have explored the usability of mode sensitivities. Shen and Sharpe [66], for example, use these derivatives to find the extent of already localized damage. Parloo *et al.* [61], on the other hand, developed a non-iterative technique to localize damage using the mode sensitivities and the differential between the mode shapes from the healthy and damaged states. Unfortunately, a large number of mode shapes have to be employed to successfully implement these techniques.

It is important to point out that the derivatives needed to implement the optimization algorithm (i.e. Eqs. (3-9) and (3-10)) are derivatives of the mode shapes of the ID-model. Because all mode shapes of this finite element model can be readily calculated using its mass and stiffness matrices, it makes sense to use the exact expressions proposed by Fox and Kapoor in 1968. Moreover, since the method has shown to quickly converge to the final values by using a limited number of modes, a trade-off can be established here to save computing time.

According to the work by Fox and Kapoor [27], the derivative of the  $j$ -th eigenvalue ( $\lambda_j$ ) with respect to the design variable  $x$  has the form

$$\frac{\partial \lambda_j}{\partial x} = \phi_j^T \left( \frac{\partial \mathbf{K}}{\partial x} - \lambda_j \frac{\partial \mathbf{M}}{\partial x} \right) \phi_j, \quad (3-11)$$

where  $\phi_j$  is the associated eigenvector, and  $\mathbf{M}$  and  $\mathbf{K}$  are, respectively, the mass and stiffness matrices of the model. On the other hand, the derivatives of the eigenvectors are assumed to be a linear combination of all eigenvectors. That is

$$\frac{\partial \phi_j}{\partial x} = \sum_{i=1}^J \beta_j \phi_i \quad (3-12)$$

where  $J$  is the total number of natural frequencies of the system, and

$$\beta_{j_i} = \begin{cases} \phi_j^T \frac{\left(\frac{\partial \mathbf{K}}{\partial x} - \lambda_j \frac{\partial \mathbf{M}}{\partial x}\right)}{(\lambda_j - \lambda_i)}, & i \neq j \\ -\frac{1}{2} \phi_j^T \frac{\partial \mathbf{M}}{\partial x} \phi_j, & i = j \end{cases} \quad (3-13)$$

If the design variable  $x$  is part of the stiffness matrix (i.e. independent of the mass), then the derivative of the mass matrix is equal to zero. Therefore, when differentiating with respect to the modulus of elasticity of the  $m$ -th element ( $E_m$ ), Eqs. (3-11) and (3-12) take the form

$$\frac{\partial \lambda_j}{\partial E_m} = \phi_j^T \mathbf{K}' \phi_j, \quad (3-14)$$

and

$$\frac{\partial \phi_j}{\partial E_m} = \Phi \times \begin{bmatrix} \phi_1^T \mathbf{K}' \phi_j \\ -\frac{\phi_1^T \mathbf{K}' \phi_j}{\lambda_1 - \lambda_j} \\ \phi_2^T \mathbf{K}' \phi_j \\ -\frac{\phi_2^T \mathbf{K}' \phi_j}{\lambda_2 - \lambda_j} \\ \vdots \\ 0 \\ \vdots \\ \phi_J^T \mathbf{K}' \phi_j \\ -\frac{\phi_J^T \mathbf{K}' \phi_j}{\lambda_J - \lambda_j} \end{bmatrix}, \quad (3-15)$$

where the  $j$ -th row of the vector of the right hand side of the equation is equal to zero,  $\Phi$  is a matrix containing all eigenvectors in its columns, and

$$\mathbf{K}' = \frac{\partial \mathbf{K}}{\partial E_m}. \quad (3-16)$$

As suggested by Eqs. (3-8) and (3-10), the implementation of the model updating technique requires not only the derivatives of the mode shapes with respect to the optimization parameters, but also the second derivatives of these parameters. To obtain these second derivatives, Eq. (3-15) is differentiated with respect to the design variable  $E_n$  obtaining

$$\frac{\partial^2 \phi_j}{\partial E_m \partial E_n} = \Phi' \times \begin{bmatrix} -\frac{\phi_1^T \mathbf{K}' \phi_j}{\lambda_1 - \lambda_j} \\ -\frac{\phi_2^T \mathbf{K}' \phi_j}{\lambda_2 - \lambda_j} \\ \vdots \\ 0 \\ \vdots \\ -\frac{\phi_J^T \mathbf{K}' \phi_j}{\lambda_J - \lambda_j} \end{bmatrix} + \Phi \times \begin{bmatrix} \frac{\partial}{\partial E_n} \left( -\frac{\phi_1^T \mathbf{K}' \phi_j}{\lambda_1 - \lambda_j} \right) \\ \frac{\partial}{\partial E_n} \left( -\frac{\phi_2^T \mathbf{K}' \phi_j}{\lambda_2 - \lambda_j} \right) \\ \vdots \\ 0 \\ \vdots \\ \frac{\partial}{\partial E_n} \left( -\frac{\phi_J^T \mathbf{K}' \phi_j}{\lambda_J - \lambda_j} \right) \end{bmatrix}, \quad (3-17)$$

where  $\Phi'$  is a matrix containing all the derivatives of the eigenvectors with respect to  $E_m$  (calculated previously), and the  $j$ -th rows of both vectors multiplying  $\Phi'$  and  $\Phi$  are equal to zero. As explained later in this chapter, the second derivative of the stiffness matrix is equal to zero ( $\mathbf{K}'' = 0$ ). With this in mind, Eq. (3-17) can be further developed and written

$$\frac{\partial^2 \phi_j}{\partial E_m \partial E_n} = \Phi' \times \begin{bmatrix} \frac{\phi_1^T \mathbf{K}' \phi_j}{\lambda_1 - \lambda_j} \\ \frac{\phi_2^T \mathbf{K}' \phi_j}{\lambda_2 - \lambda_j} \\ \vdots \\ 0 \\ \vdots \\ \frac{\phi_j^T \mathbf{K}' \phi_j}{\lambda_j - \lambda_j} \end{bmatrix} + \Phi \times \begin{bmatrix} \frac{(\lambda_1 - \lambda_j)(\phi_1^T \mathbf{K} \phi_j) + (\lambda_1 - \lambda_j)(\phi_1^T \mathbf{K}^x \phi_j') - (\lambda'_1 - \lambda'_j)(\phi_1^T \mathbf{K}^x \phi_j)}{(\lambda_1 - \lambda_j)^2} \\ \frac{(\lambda_2 - \lambda_j)(\phi_2^T \mathbf{K} \phi_j) + (\lambda_2 - \lambda_j)(\phi_2^T \mathbf{K}^x \phi_j') - (\lambda'_2 - \lambda'_j)(\phi_2^T \mathbf{K}^x \phi_j)}{(\lambda_2 - \lambda_j)^2} \\ \vdots \\ 0 \\ \vdots \\ \frac{(\lambda_j - \lambda_j)(\phi_j^T \mathbf{K} \phi_j) + (\lambda_j - \lambda_j)(\phi_j^T \mathbf{K}^x \phi_j') - (\lambda'_j - \lambda'_j)(\phi_j^T \mathbf{K}^x \phi_j)}{(\lambda_j - \lambda_j)^2} \end{bmatrix}, \quad (3-18)$$

where  $\lambda'_j$  is the derivative of the eigenvalue with respect to  $E_m$ , and  $\mathbf{K}'$  and  $\mathbf{K}^x$  are the derivatives of the stiffness matrix with respect to  $E_m$  and  $E_n$ , respectively.

### 3.1.5 Derivatives of the Stiffness Matrix

The derivative of the stiffness matrix of a finite element model with respect to the Young's modulus of any of the elements can be easily obtained. Moreover, because it is assumed in this research that the rest of the components of the stiffness matrix remain unchanged, the derivative  $\mathbf{K}'$  is constant and can be calculated only once and stored in memory. To explain the differentiation of this matrix let us consider the 3-element, 3-DOF, shear model shown in Fig. 3.2.

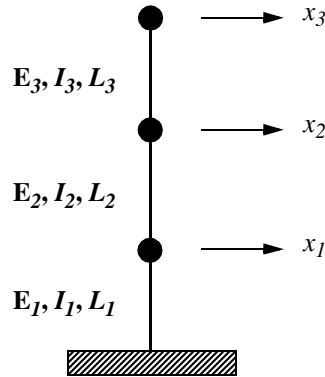


**Figure 3.2 Shear model with 3 DOF**

Assuming that no rotations of the nodes are allowed, the stiffness matrix of the model is given by

$$\mathbf{K} = \begin{bmatrix} E_1 \frac{12I_1}{L_1^3} + E_2 \frac{12I_2}{L_2^3} & -E_2 \frac{12I_2}{L_2^3} & 0 \\ -E_2 \frac{12I_2}{L_2^3} & E_2 \frac{12I_2}{L_2^3} + E_3 \frac{12I_3}{L_3^3} & -E_3 \frac{12I_3}{L_3^3} \\ 0 & -E_3 \frac{12I_3}{L_3^3} & E_3 \frac{12I_3}{L_3^3} \end{bmatrix}. \quad (3-19)$$

The derivative of  $\mathbf{K}$  with respect to  $E_2$  is easily obtained by differentiating the matrix (in an element-by-element basis) with respect to this parameter, obtaining

$$\frac{\partial \mathbf{K}}{\partial E_2} = \begin{bmatrix} \frac{12I_2}{L_2^3} & -\frac{12I_2}{L_2^3} & 0 \\ -\frac{12I_2}{L_2^3} & \frac{12I_2}{L_2^3} & 0 \\ 0 & 0 & 0 \end{bmatrix}. \quad (3-20)$$

In other words, the derivative of the stiffness matrix with respect to the parameter  $E_m$  can be obtained by setting  $E_m = 1$  and  $E_n = 0$  for all  $n \neq m$ . Because this derivative becomes independent of the variable itself, its second derivative is equal to a zero matrix.

### 3.1.6 Implementation Issues

When performing a comparison between a mode shape of a structure and its counterpart from an ID-model, the former has to be extended to the DOF's of the ID-model, or the latter has to be restricted to the sensor locations. There are several methodologies for the

expansion of experimental mode shapes to cover unmeasured DOF's. However, because the extension of these modes is computationally expensive it was decided that the eigenvectors of the ID-model would be truncated. This approach seems to be the preferred one among researchers in model updating.

A drawback of the methodology is the fact that the expressions found by Fox and Kapoor [27] require the mode shapes be mass-normalized. To perform this normalization, the Guyan reduced mass technique is used (see Guyan, [31]). Thus, the  $r$ -th element of the non-normalized  $j$ -th mode  $\bar{\phi}_{j_r}$  is

$$\phi_{j_r} = \frac{\bar{\phi}_{j_r}}{\sqrt{\bar{\phi}_j^T \mathbf{M} \bar{\phi}_j}} \quad (3-21)$$

where  $\mathbf{M}$  is the model's mass matrix, reduced to the measured degrees of freedom. This method assumes that the inertial forces at the eliminated degrees of freedom are negligible, which is usually valid for low frequency modes. All equations of this chapter are calculated using mass-normalized modes. The normalization of the experimental modes was performed using the analytical modes in the denominator of Eq. (3-21).

In theory, the exact derivatives of the mode shapes with respect to the optimization parameters are obtained by using all the eigenvectors of the model. However, as Moller and Friberg [57] demonstrated, sufficiently accurate approximations for model updating can be obtained with a limited number of vectors. The number selected highly affects the efficacy of the optimization algorithm, especially in the present case, where the derivatives and the Hessian matrices of the mode shapes are required. Unfortunately, the selection of an appropriate number of eigenvectors depends on the type of model being updated and no general rule can be established. Perhaps a useful method to select this number is by looking at the convergence of the mode shape derivatives, as the number increases.

A critical problem that could lead to an unstable optimization algorithm is the pairing of non-corresponding mode shapes. This problem is not so difficult to avoid with certain types of continuous structures such as beams, in which mode shapes can always be associated with increasing frequencies. However, for other types of structures, the nearness of two frequencies is certainly not informative enough to pair two modes. To solve this problem, the modal assurance criteria (MAC) was also used here, always retaining the order of the structure's modes and changing those of the ID-model if needed. It is also important to emphasize that Eqs. (3-4) and (3-8) are sensitive to the sign of paired modes.

Perhaps the biggest concern when implementing an optimization algorithm on a nonlinear problem is the possibility of convergence to a local minimum without achieving the pursued global minimum. However, given the characteristics of civil structures, it is known that the variation of their modal properties when damage exists is typically relatively low. Therefore, if the optimization of the parameters in the healthy state is guaranteed to be a global minimum, the optimization process in the damage state should quickly find its way to a global minimum also (i.e. using the optimized healthy parameters as starting point). The problem is then reduced to assuring that the optimization in the healthy state has explored all the possibilities. Although costly, one way to overcome this problem is applying the optimization algorithm with different and random starting points. Genetic algorithms also constitute an alternative to address this issue.

### **3.2 Validation through Analytical Model**

To test the potential of the technique an analytical model of a 32m long beam was created. The beam is simply supported at both ends with a third support located 12m from the left end (see Fig. 3.3). Although intuitively simple, this type of continuous structures pose a challenge to dynamic-based SHM techniques for various reasons. For instance, the global effect that any kind of damage has on the modal properties of the structure

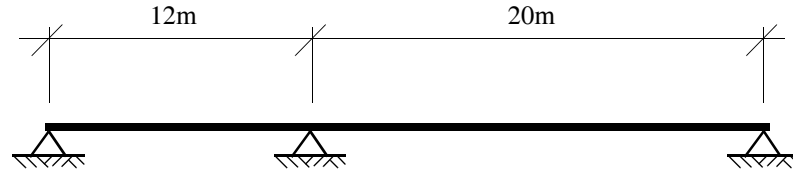


**Figure 3.3 Finite element model of the continuous beam with three supports (512 elements)**

makes it difficult to localize the weakness. Moreover, the continuous distribution of the mass and stiffness causes that discretized and lumped ID-models introduce significant modeling errors.

The finite element model of this continuous beam was created using 512 Euler-Bernoulli elements whose properties can be summarized as:  $I_x = 6 \times 10^{-5} \text{ m}^4$ ,  $A = 0.05 \text{ m}^2$ ,  $E = 2 \times 10^{11} \text{ N/m}^2$ , and  $\rho = 8000 \text{ Kg/m}^3$ . Only inplane motion of the nodes was allowed (vertical motion and rotation), for a total of 1023 degrees of freedom. Four damage scenarios (including the healthy case) were simulated by reducing the stiffness of certain elements as indicated in Table 3.1.

**Table 3.1 Damage scenarios**

Damage scenario	Damaged elements	Stiffness reduction
1	--	--
2	153	20%
	154	40%
	155	40%
	156	20%
3	375	50%
	376	50%
4	(Scenarios 2 and 3 combined)	

To isolate the problem of model updating and characterization of the structure from the issues involved with modal identification, rather than using time history responses to calculate the modal properties of the finite element models, these were calculated using their mass and stiffness matrices. However, to demonstrate that the methodology can be reasonably robust to noise in the sensors, once the efficacy of the methodology is proven to update models using these theoretical mode shapes, a random noise vector is added to the modal information made available. This noise is a uniformly distributed random signal with zero mean and a standard deviation equal to  $2e-5$ , equivalent to approximately 0.2% of the values of the mass-normalized modes (in an RMS sense). From the 1023 DOF in the analytical model, only 30 uniformly distributed points of information were made available (vertical motion), simulating sensors placed every meter within the span of the bridge. Moreover, only the first six frequencies and mass-normalized mode shapes were employed in the optimization algorithm (see Fig. 3.4).

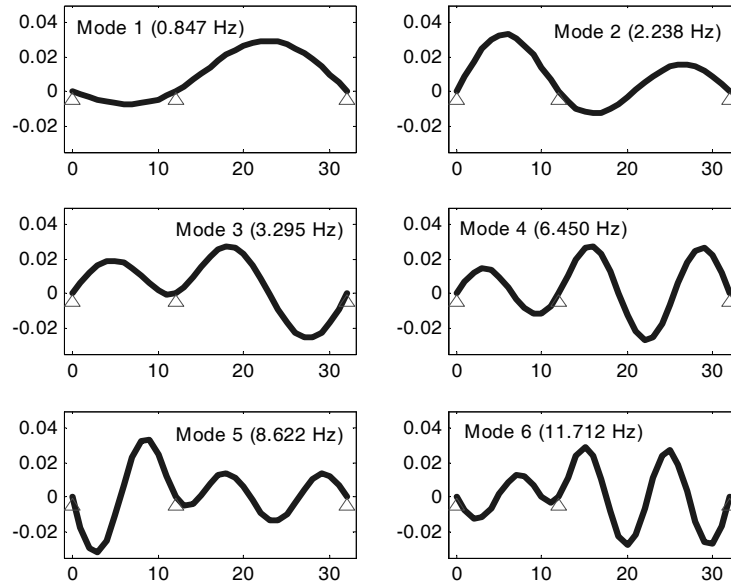


**Figure 3.4 Mass-normalized mode shapes of the healthy model**

### 3.2.1 The Identification Model

To take advantage of all modal information made available, the identification model was constructed with 32 elements and 33 nodes including the supports (see Fig. 3.5). Similarly to the analytical model, only in plane motion of the nodes was allowed, thus obtaining 30 vertical displacements and 33 rotations (63 DOF). Both the mass and the geometric properties of the original finite element model were used to build the simplified ID-model.

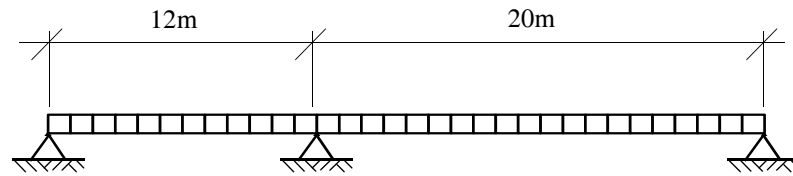


**Figure 3.5 ID-model with three supports (32 elements)**

When updating the ID-model, the evaluation of the objective function for any given trial of optimization parameters (32 Young's moduli) is performed by removing the rotational degrees of freedom from the eigenvectors of the model. With this truncation, the mode shapes of the ID-model are described by 30 points of information located at the simulated sensor positions in the analytical model. Given the geometry of both models, each element of the ID-model can be associated with 16 elements of the analytical model. For the damage scenarios shown in Table 3.1, the expected stiffness reductions in the ID-model are displayed in Table 3.2.

**Table 3.2 Expected stiffness reduction on ID-model**

Damage scenario	Element of ID-model
1	--
2	10
3	24
4	10 and 24

### 3.2.2 Convergence of Mode Shape Sensitivities

As mentioned previously, the number of eigenvectors used to calculate their sensitivities to changes in structural parameters has an important impact on the computational power required to execute the optimization algorithm. Therefore, understanding the convergence of these sensitivities as the number of eigenvectors used is increased allows the designer to truncate this calculation and accelerate the minimization process without risking the stability of the algorithm. Unfortunately, the convergence of this values is highly dependent on the model and no general guidelines can be provided. In the case of the continuous beam, for instance, 85% of all sensitivities of the first six modes reach values that are within 10% of their exact values when using as few as 20 eigenvectors. As an example, Fig. 3.6 shows how the calculated derivatives of the first and sixth modes approach their exact values as the number of eigenvectors used to calculate them is increased. 20 eigenvectors were used to execute the optimization algorithm in this numerical example.

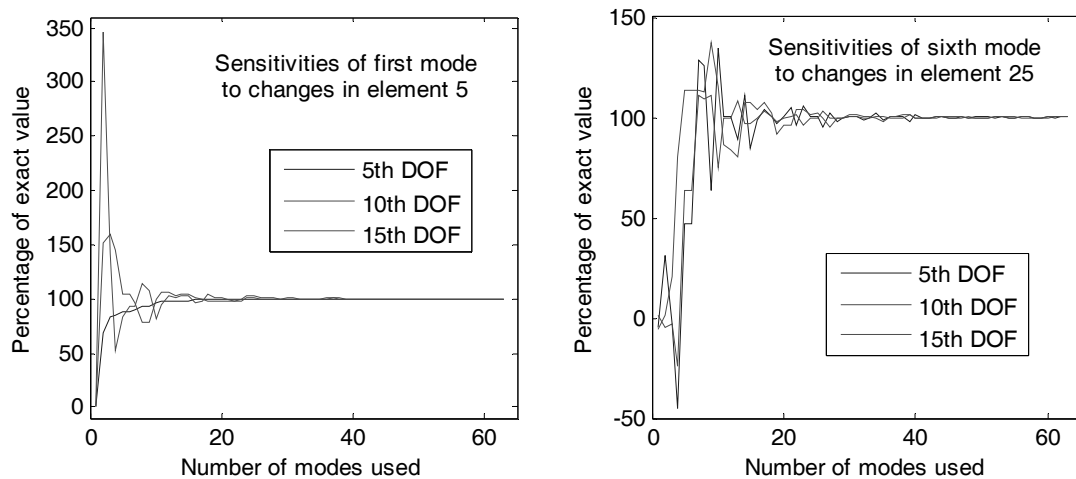


**Figure 3.6 Convergence of mode shape sensitivities**

### 3.2.3 Optimization Results

Figure 3.7 shows the optimized Young's modulus of the elements of the ID-model for all damage scenarios. These values are shown as the remaining stiffness of the elements with respect to the undamaged case (in percentage). It is clear from the diagrams that, for the second and third damage scenarios, weaknesses are present in the 10th and 24th elements of the ID-model, respectively. These indications of damage correspond to those expected from the reductions of stiffness induced in the finite element model (see Table 3.1). It is also clear from the fourth damage scenario that the optimization algorithm was capable of detecting multiple stiffness reductions throughout the model. Although the mode shapes used for these cases are the exact values from the 512-element analytical model, it is remarkable that the weaknesses are localized with the use of a limited number of truncated mode shapes (i.e. only 30 points of information from six mode shapes), which makes the methodology very attractive for civil applications.

It should be noted that, since the ID-model is a simpler representation of the structure, the detected reductions of stiffness are not equal to those reductions induced to the finite

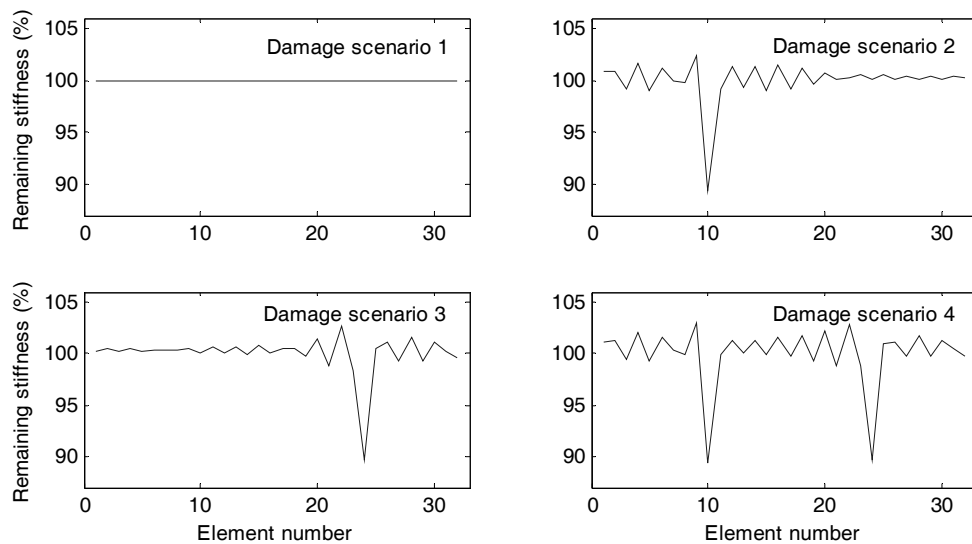


**Figure 3.7 Optimization results (ideal conditions)**

element model. This outcome is due to the fact that each element of the ID-model represents 16 elements in the original model. However, identified stiffness losses should reflect the overall status of the spanned portion of the structure and can be used to alert for possible damage. Also linked to modeling differences, is the fact that in addition to the correctly identified weaknesses, other elements of the ID-model reflect non-existent changes in all damage scenarios. This variation is especially clear in the vicinity of the damaged elements, whose identified modulus of elasticity becomes somewhat erratic. This problem becomes even more critical in cases where the damage induced is near the end of the element spanned. In general, a higher number of sensors and a more detailed ID-model as well as the use of more mode shapes in the optimization process should minimize this problem.

Figure 3.8 shows the results obtained once the available mode shapes are corrupted with noise as described previously. Although the stiffness detected for all undamaged elements becomes more erratic, those elements whose stiffness is expectably reduced are still clearly identifiable.

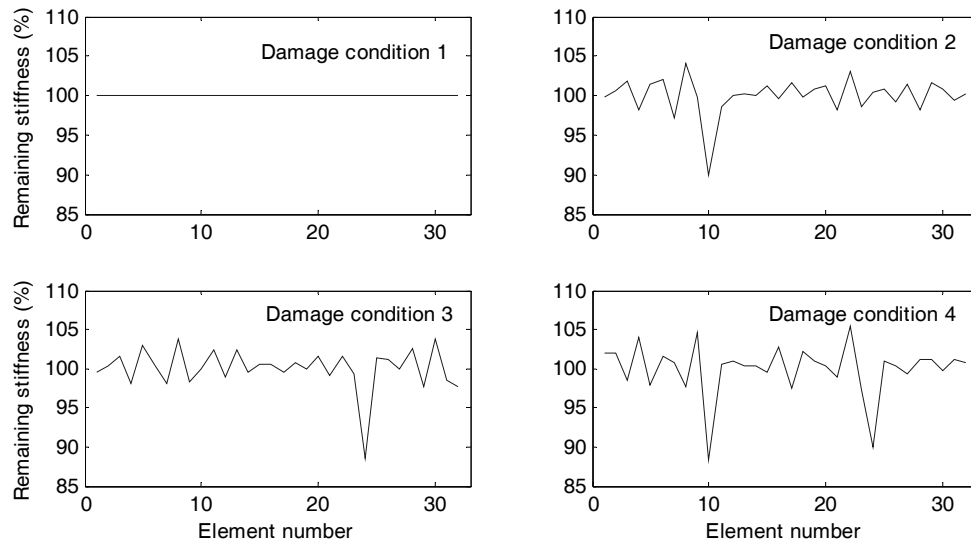


**Figure 3.8 Optimization results (noisy mode shapes)**

### 3.2.4 Convergence Rate

To evaluate the efficacy of the proposed technique its convergence rate is tested and compared with other types of optimization algorithms under the same circumstances. One of the algorithms employed in this comparison is the nonlinear minimization developed by Nelder and Mead [58]. Also known as the Simplex method, this algorithm uses a triangulation process to find local minima of multivariate functions. In addition, the method of conjugate gradients is tested providing only the gradients of the objective function. In this case the algorithm estimates the Hessian matrix numerically. Both of these algorithms are included in the optimization toolbox of Matlab [55]. The convergence rate of all algorithms is shown in Fig. 3.9, which clearly demonstrates the advantage of analytically calculating the Hessian matrix of the objective function. Running times shown are the times employed by a Microsoft Windows based Pentium 4 at 2.0 GHz.

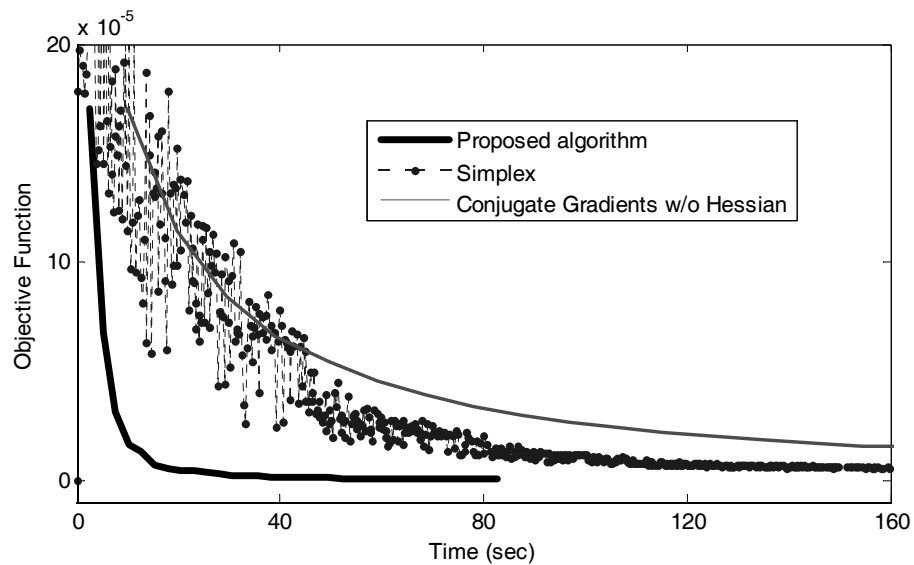


**Figure 3.9 Convergence rate of three optimization algorithms**

### 3.3 Conclusions

Model updating for structural health monitoring purposes was carried out using a mature optimization algorithm known as Conjugate Gradients with Newton-Raphson and Fletcher-Reeves. The optimization is based on the correlation between the mode shapes of the structure and the eigenvectors of an analytical model referred to as the identification model. Young's moduli of all elements of this model are selected as the optimization parameters, whereas the modal assurance criterion (MAC) is used to measure the correlation of the modes. A two-dimensional finite element model of a beam with three simple supports is used to test the performance of the proposed methodology. Results indicate that stiffness changes can be detected with a reasonable number of sensors and a limited amount of mode shapes. In addition, the robustness of the methodology to mildly corrupted modal properties was successfully evaluated. As with any other vibration-based SHM technique, detection depends on the capacity of the damage to change the modal properties of the structure.

Although promising results are shown in this chapter, the robustness of the proposed model updating technique for structural health monitoring purposes is still to be tested for a wider range of structures. Given the global changes produced by local damage, continuous structures, such as the beam with three supports, are possibly more suited to this sensitivity based technique. Similar results were obtained for a simply supported beam evaluated under the same circumstances. However, structures with a more lumped distribution of their mass (e.g. buildings) may not take full advantage of the mode shape sensitivities employed in the optimization process.

To carry out the proposed characterization of a structure through updating of an identification model, only an estimate of the mass matrix (or relative quantities) is required. These types of estimates are readily obtainable from construction plans and detailed studies of the current status of the structures. This approach is sufficient for most of the

existing parameter identification procedures. Variability of the mass, however, is a more challenging issue that can manifest itself in different ways for different structures and should be investigated in future studies. Buildings, for instance, do not usually have sudden changes of mass, but rather, live loads that tend to increase very slowly with time. It is also important to point out, however, that every damage detection technique is not necessarily appropriate for all types of structures. Each technique has capabilities and limitations that must be explored and delineated. Systems that employ combinations of the individual techniques may ultimately be necessary to realize a structural health monitoring system, taking advantage of the capabilities of each technique while minimizing the limitations.

Although the discrepancy of the natural frequencies has not been used in this study, this does not mean that this information is not useful in health monitoring. In fact, in some cases where the symmetry of structures may play an important role, this variation could be used to ensure that no local minimum has been reached with the optimization process (as opposed to a global minimum). However, these cases are not considered in this research and should be considered in the future. The variation of the frequencies has been successfully used in SHM to identify the existence of damage, without specifying the location or the extent (Level 1 as classified by Rytter [65]). Sohn *et al.* [69], for instance, has developed important conclusions in this area.

## Chapter 4

### Accommodating Varying Environmental Conditions

Although many algorithms have been developed in the last two decades to detect damage in civil structures using dynamic properties, few studies have considered the challenge imposed by the variability of these properties due to changing and uncontrollable environmental conditions such as temperature, temperature gradients, and humidity. Among the few, Sohn *et al.* [69] proposed an effective method based on outlier analyses used by several researchers in different fields (see, for instance, Worden *et al.* [74] and Tarassenko *et al.* [71]). The method uses a neural network trained with results of a non-linear principal component analysis that determines the distribution of certain identified structural parameters over an undetermined number of environmental factors that affect its behavior. The method effectively eliminates the effects of the surrounding conditions to accurately detect the existence of damage. Kullaa [50] and Yan *et al.* [76,77] both took further steps with similar methodologies, the former applying it to civil structures, and the latter doing some experimental work with scaled models. These techniques only detect the existence of damage but are unable to locate it within the structure (i.e. level I as classified by Rytter [65]).

The analysis proposed in this research extends those previously developed approaches to achieve accurate localization of damage in the structure regardless of the environmental conditions that affect its dynamic behavior. The proposed scheme can be divided in three

main steps: (1) identification of modal properties of the structure under the influence of multiple environmental conditions; (2) characterization of the structure as a function of the detected dynamic properties and an identification model (ID-model) representative of the system; and (3) reduction of influence of the external conditions by means of a statistically-based analysis. The latter goal, and focus of this chapter, is achieved by accomodating the influence using a principal component analysis (PCA) to map the distribution of the numeric characterizations over an unknown number of external factors. Direct measurement of the factors influencing the behavior is not required with this approach. The statistical nature of the methodology also minimizes effects of noise in the sensors, which is often a concern whenever a deterministic analysis is performed [30].

The analytical model of the benchmark problem on SHM used in Chapter 2 for modal identification is also used herein to demonstrate the effectiveness of the analysis proposed. The robustness of the technique is tested by considering modeling errors as well as a considerable amount of sensor noise. Environmental conditions are simulated with changes in temperature as well as temperature gradients across the dimensions of the structure. These variations affect the stiffness of the elements and, therefore, the global modal properties. Although some structures, due to redundancies present, may also experience a stress stiffening resulting from thermal expansion of the members, these effects are expected to be minimal in the free-standing benchmark structure and are neglected herein. Local damage is modeled as a reduction of the Young's modulus of certain combinations of elements in the structural model. Nine structural configurations are investigated.

The chapter is unfolded in two main sections. In the first section, the basic steps of the methodology are discussed, whereas the second section is devoted to the analytical analysis of the SHM benchmark problem. Multiple dynamic simulations of ambient vibrations with random simulated environmental conditions are executed in order to perform

a reliable analysis. Results indicate that the methodology proposed is very effective for reducing the effects of the unknown external conditions. However, the actual localization of weaknesses depends on the technique used to characterize the structure and is not the main concern of this chapter.

## 4.1 Methodology

The identification of modal properties is performed in this chapter using a combination of the natural excitation technique (NExT) and the eigensystem realization algorithm with data correlations (ERA/DC). Both techniques were introduced in Chapter 2 of this thesis. This task is performed with simulated ambient response data when the structure is influenced by a variety of random environmental conditions. It is assumed herein that the external conditions are invariant during the brief period of time while the acceleration measurements are recorded. Subsequently, characterizations of the structure for each set of detected modal properties is carried out using the non-iterative technique developed by Caicedo *et al.* [15]. Although not in detail, this technique is introduced later in this chapter. Interested readers are referred to the original paper as well as the more explanatory main author's doctoral dissertation [14].

Once the stiffness values of the healthy structure are identified, a principal component analysis (PCA) is performed. This type of analysis reveals the trend present in the identified parameters when influenced by external conditions and can be used to accommodate this influence. The analysis proposed has the potential to be combined with other types of numerical characterizations of structures such as the iterative model updating technique introduced in Chapter 3. However, to demonstrate the potential of the analysis to adjust to other types of characterizations, it was decided to implement it here with a more mature technique. The complete SHM framework including the modal identification with stochastic subspace identification (rated best in Chapter 2) and the stiffness

characterization of the structure with the model updating technique introduced in Chapter 3, will be tested in the fifth chapter of this dissertation.

#### 4.1.1 Stiffness Characterization Through Least Squares

In 2002, Caicedo and Dyke [15] proposed a non-iterative technique that uses the characteristic equation of an identification model and the identified modal properties of the structure to determine the elemental stiffness values (Young's modulus) of the members of the ID-model. This technique assumes that the mass matrix of the structure (or a reasonably good estimation of the relative quantities) is known. Consider the characteristic equation

$$\mathbf{K}\phi_i = \mathbf{M}\lambda_i\phi_i \quad (4-1)$$

where  $\lambda_i$  is the  $i$ -th eigenvalue (square value of the  $i$ -th natural frequency of the structure), and  $\phi_i$  is the  $i$ -th eigenvector (corresponding to the  $i$ -th mode shape). In their work, the left-hand-side of Eq. (4-1) is reorganized as

$$\delta_i \mathbf{k} = \mathbf{M}\lambda_i\phi_i, \quad (4-2)$$

where  $\mathbf{k}$  is a vector containing only the unknown stiffness values corresponding to specific elements in the identification model, and  $\delta_i$  is a matrix built using the eigenvector  $\phi_i$  and the known portions of the stiffness matrix  $\mathbf{K}$  of the ID-model (i.e. geometry and boundary conditions). Using all  $m$  identified mode shapes and natural frequencies, Eq. (4-2) becomes

$$\Delta \mathbf{k} = \Gamma, \quad (4-3)$$

where

$$\Delta = \begin{bmatrix} \delta_1 \\ \delta_2 \\ \vdots \\ \delta_m \end{bmatrix} \quad \text{and} \quad \Gamma = \begin{bmatrix} \mathbf{M}\lambda_1\phi_1 \\ \mathbf{M}\lambda_2\phi_2 \\ \vdots \\ \mathbf{M}\lambda_m\phi_m \end{bmatrix}. \quad (4-4)$$

The unknown stiffness values can be estimated as

$$\mathbf{k} = \Delta^+ \Gamma, \quad (4-5)$$

where  $^+$  denotes the pseudo-inverse. One of the advantages of this methodology is that only the non-zero elements of the stiffness matrix of the ID-model are identified using the geometry of the structural elements. The procedure to obtain the matrix  $\Delta$  can be automated using a finite element mesh. A complete description of the technique for Euler-Bernoulli beam elements can be found in [14].

#### 4.1.2 Principal Component Analysis

PCA is a multi-variate statistical method also known as proper orthogonal decomposition or Karhunen-Loeve transform. It is a mathematical procedure that transforms a number of (possibly) correlated variables into a smaller number of linearly uncorrelated variables called *principal components*. PCA has been applied in structural vibrations for a variety of purposes, including modal analysis and parameter identification [76]. In 2005, Yan *et al.* [76] used this approach to identify the existence of damage while accommodating the influence of those environmental conditions that have a linear affect (or nearly linear) on the natural frequencies of the system. Perhaps the main advantage of this technique is that measuring the environmental factors becomes unnecessary. The methodology was further developed by the same authors, applying it to civil structures and accounting for nonlinear variations [77]. However, the focus on statistical variations

of natural frequencies restricts the technique to detecting only the existence of damage, without knowing its location or extent.

It is widely known that environmental conditions such as temperature, temperature gradients, and humidity have a noticeable impact on the modal properties of a structure. As a direct consequence, characterizations obtained using detected modal properties are also affected. When PCA is performed using identified stiffness values of the healthy structure over a wide range of environmental conditions, the distribution of those identified values across the unknown external factors can be mapped. The associated singular value decomposition reveals not only a group of vectors that each sample (i.e. stiffness values identified with a set of environmental conditions) can be expressed in terms of, but also the level of influence of each vector. By using the components with the highest level of influence (associated with the most influencing environmental conditions), one can create a transformation matrix with which the data is mapped into the hyper-space spanned by these components and back into the original axes. The residual error after such transformation is independent of the vectors selected to create it. In other words, the error does not depend on the external factors influencing the changes of the structure and can be used as a reliable indicator of damage. A more detailed discussion is provided in the following paragraphs.

Let us first consider the matrix  $\mathbf{Y} \in \mathbb{R}^{J \times K}$  whose column vectors  $\mathbf{y}_k$  are the identified stiffness values of the elements of the ID-model at time  $t_k$ , and whose row vectors contain all the identified stiffness values of the  $j$ -th element. In this case  $J$  and  $K$  are the number of elements and samples respectively. A singular value decomposition of the covariance matrix of  $\mathbf{Y}$  is [76]

$$\mathbf{Y}\mathbf{Y}^T = \mathbf{U}\mathbf{\Sigma}^2\mathbf{U}^T, \quad (4-6)$$

where  $\mathbf{U} \in \Re^{J \times J}$  is an orthonormal matrix (i.e.  $\mathbf{U}\mathbf{U}^T = \mathbf{I}$ ) whose columns  $\mathbf{u}_m$  define the principal components forming a subspace spanning the data, and  $\Sigma$  is a diagonal matrix with the singular values in descending order representing the level of influence of the principal components. The fact that the matrix containing the singular values is pre- and post-multiplied by  $\mathbf{U}$  and  $\mathbf{U}^T$ , respectively, in this equation is due to the symmetry of  $\mathbf{Y}\mathbf{Y}^T$ . Whereas some of the principal components may be associated with one particular environmental factor (e.g. temperature changes), some others, may be associated with a combination of two or even more. However, in addition to these highly influencing principal components, a remaining set of vectors that have less influence over the identified values result from the decomposition. These additional vectors may be due to noise in sensors, incorrect measurements as a result of non-stationary input, or occasional mass variations. Thus, these vectors can be discarded. As discussed later in this chapter (section 4.2.2), the selection of an appropriate number of principal components is not critical.

To project the stiffnesses values of a given sample  $\mathbf{y}$  into the environmental-factor characterized space  $\mathbf{x}$ , a transformation matrix  $\mathbf{T}$  (known as the loading matrix) is built using the first  $M$  columns of  $\mathbf{U}$  (associated with the most influencing factors). That is

$$\mathbf{x} = \mathbf{T}^T \mathbf{y}, \quad (4-7)$$

with  $\mathbf{T} \in \Re^{J \times M}$ ,  $\mathbf{y} \in \Re^{J \times 1}$ , and  $\mathbf{x} \in \Re^{M \times 1}$  (known as the scores vector). The new data can be re-mapped into the original axes using the reverse transformation

$$\hat{\mathbf{y}} = \mathbf{T} \mathbf{x}, \quad (4-8)$$

and the residual error  $\mathbf{e}_w$  due to the loss of information while performing the two way projection can be calculated as

$$\mathbf{e}_w = \mathbf{y} - \mathbf{y} . \quad (4-9)$$

$\mathbf{e}_w$  is then a function of those principal components ignored when creating the matrix  $\mathbf{T}$ , and, because of the orthonormal properties of all principal components, is independent of those vectors selected to create it and the environmental conditions associated with them.

Although in classical PCA the collected data is standardized so that the mean and standard deviation of each row vector is zero and unity, respectively, the standardization of the data is slightly different in this study. The matrix  $\mathbf{Y}$ , as used in Eq. (4-6), is formed with the elements

$$y_{jk} = \frac{y_{jk} - \mu_j}{\mu_j} \times 100 , \quad (4-10)$$

where  $y_{jk}$  is the non-normalized parameter identified for the  $j$ -th element (in this case Young's modulus) at time  $k$ , and  $\mu_j$  is the mean of the row vector  $\mathbf{y}_j$ . This standardization allows us to analyze the residual error as a percentile reduction in the stiffness detected in the elements of the identification model with respect to their original values.

As damage is introduced in the system, the value of the residual error (rather than the absolute value of this quantity) due to the two-way projection should decrease for those structurally defective elements. This change is an indication of damage that is independent of the environmental factors. However, because the principal components that span the hyper-space that contain the healthy data do not correctly describe the new damaged system, the extent of the damage may not be identified correctly. Moreover, as will become clear in the simple example provided later in this chapter, some undamaged elements may indicate a non-physical gain of stiffness, or in the worst case, lightly damaged elements may be masked by heavily damaged ones. To overcome this difficulty, the

technique is divided in three steps. First, by setting a strict threshold, the residual error is used to separate damaged elements from those that appear healthy.  $\mathbf{T}$  is then modified to build a prediction model that calculates the most likely stiffness values of all elements of the identification model using the identified values of those elements with no apparent damage. Finally, the residual error is recalculated and used to localize and quantify damage.

To better understand the methodology, a simple, two-dimensional example is provided to help visualize how the principal components describe the variation of the identified stiffness values when affected by external factors, and how this knowledge can be used to discard their effect. Suppose then that we are trying to identify damage in a simple structure by identifying the Young's moduli of a two-element identification model.

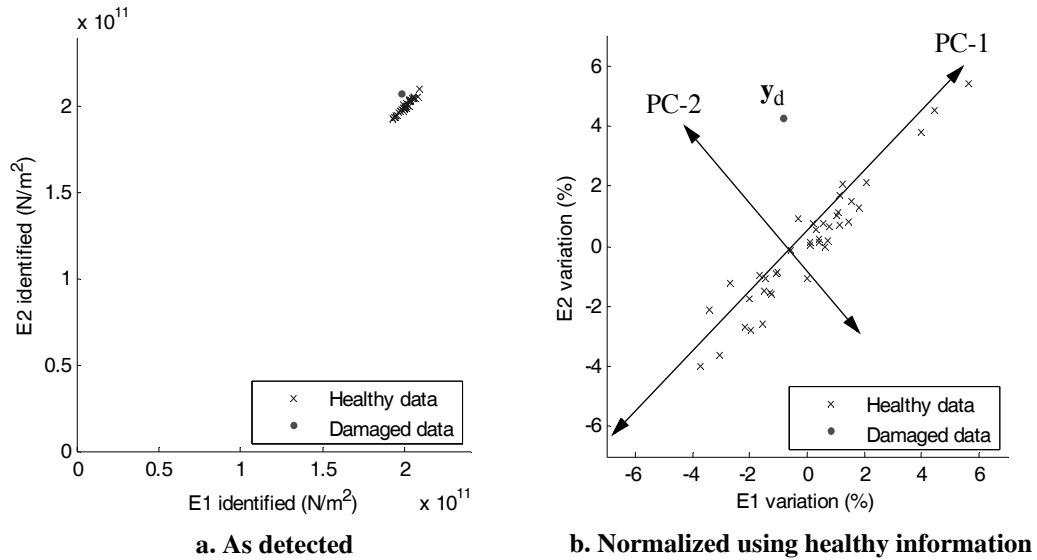


**Figure 4.1 Identified stiffness values of the two dimensional example ( $E_1$  and  $E_2$ )**

Assume also that the structure is affected by multiple factors such as changes in temperature and humidity. Fig. 4.1a shows 40 identified points ( $E_1$  and  $E_2$ ) of the healthy

structure and a single point identified in a damaged state of the structure in which the first element lost 5% of its initial stiffness.

Using data collected in the healthy state we can standardize the identified values so that percentile points of variation with respect to the mean can be observed ( $x$  and  $y$  axes in Fig. 4.1b). From this figure, it can be observed that an environmental factor exists that makes the identified stiffness values vary along what appears to be a straight line, whereas other factors make these values slightly vary in other directions. A principal component analysis of the standardized healthy information determines the two principal components (denoted in Fig. 4.1b as PC-1 and PC-2) in terms of which the data can be expressed.

Let us now focus on the damaged data point shown in Fig. 4.1a as identified, which is denoted as  $\mathbf{y}_d$  after the normalization process has been performed with healthy data (see Fig. 4.1b). This point can be expressed in terms of the principal components using the projection given in Eq. (4-7), obtaining a set of new coordinates  $y_{d1}$  and  $y_{d2}$  (see Fig. 4.2). By using only the first principal component (PC-1) to project the data point into the line spanned by this component, and back in to the original axes the point  $\hat{\mathbf{y}}_d$  is obtained. The error left by the transformation can then be expressed in terms of the original axes and tells us that a variation with respect to both  $E_1$  and  $E_2$  has occurred. In fact the projected point lies farther to the right of the original point revealing a positive variation of  $E_1$  (loss of stiffness). Similarly, the projected point is further down from the original data point revealing a negative variation of  $E_2$  (gain of stiffness). Obviously, it is not possible for an element to gain stiffness. Therefore, we can say with confidence that the stiffness of the first element ( $E_1$ ) has decreased, whereas the second element appears to remain healthy. However, the magnitude of those changes cannot be found using the residual error as calculated.

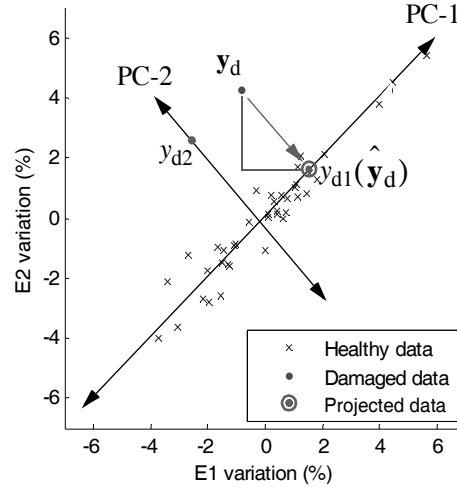


**Figure 4.2 Residual error after projection**

As a second step, the most likely stiffness values of all elements is calculated using those identified values that appear to remain healthy (only  $E_2$  in this case), and the principal components selected for the transformation (in this case PC-1). From Eqs. (4-7) and (4-8) we learned that there exists a linear combination of the selected principal components (i.e. scores vector) that can be used to re-map the stiffness values detected. This linear combination can be redefined using only the stiffness of the seemingly healthy elements. That is

$$\mathbf{T}_u \mathbf{x}_u = \mathbf{y}_u, \quad (4-11)$$

where  $\mathbf{y}_u$  is the incomplete sample and  $\mathbf{T}_u$  is the transformation matrix  $\mathbf{T}$  whose rows have been removed accordingly with  $\mathbf{y}_u$ . The vector of coefficients  $\mathbf{x}_u$  can be calculated as

$$\mathbf{x}_u = (\mathbf{T}_u)^+ \mathbf{y}_u, \quad (4-12)$$

where  $^+$  indicates the pseudo-inverse. Therefore, the most likely set of stiffness values of all elements of the ID-model  $\mathbf{y}_p$ , given the values of those apparently healthy elements, are

$$\mathbf{y}_p = \mathbf{T}\mathbf{x}_u, \quad (4-13)$$

and the residual error becomes

$$\mathbf{e}_p = \mathbf{y} - \mathbf{y}_p. \quad (4-14)$$

In the two-dimensional case, for instance, the predicted data point is shown in Fig. 4.3 and is denoted as  $\mathbf{y}_p$ . In this case  $\mathbf{e}_p$  reveals a reduction of stiffness of the first element  $E_1$  of 5% (as indicated in Fig. 4.3) while  $E_2$  does not indicate any change. Similar to Eq. (4-9), the residual error is a function of those principal components ignored to create the prediction model and independent of the vectors selected to create it.

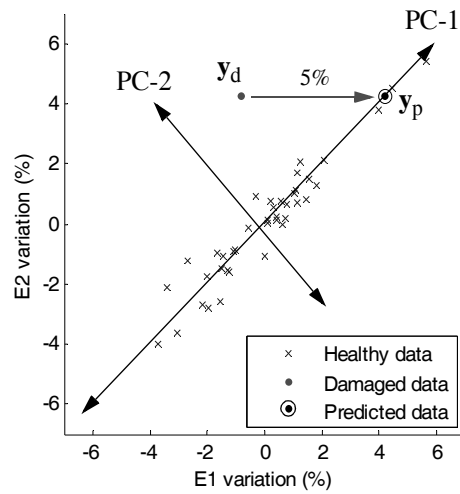


**Figure 4.3 Prediction model based on healthy elements**

To apply this methodology, it is assumed that periodic measurements are being acquired from the structure and therefore the variation of the identified stiffness values of the identification model with respect to changes in environmental conditions can be mapped accurately. However, as the unavoidable noise in sensors and temporary variations of the structure's dynamics can alter the identification process, it seems somewhat inadvisable to alert for damage once a single sample shows some possible loss of stiffness. The criterion for damage is then based on an outlier analysis in which a maximum variation of stiffness is defined to separate the admissible error from that with apparent influence of damage. To do this, an X-bar control chart [68] is constructed for each element by drawing two lines: a centerline ( $C_L$ ) and an additional horizontal line corresponding to the lower limit ( $L_L$ ). In this case, these are

$$C_{L_j} = E(e_{p_j}) \quad , \text{ and } \quad L_{L_j} = E(e_{p_j}) - \alpha \quad (4-15)$$

where  $E(e_{p_j})$  is the expected value of the residual error for all samples of the  $j$ -th element before damage is introduced, and  $\alpha$  is the admissible damage in percentile points. The construction of this chart allows us to count the number of times the error lies outside of the admissible range adopted (*i.e.* points below  $L_L$ ). A damage warning is then issued if three consecutive points lie outside the admissible range or if the residual error is unusually large.

The most important advantage of this PCA-based approach is that it does not require measuring the environmental factors that influence the behavior of the structure. This ability relies on the assumption that damage does not change the dynamic properties in the same way that environmental factors do (an unlikely case in which the PCA would not be applicable). Moreover, the effect of noise in sensors is mitigated when a large number of samples is employed, and the criterion to issue damage alerts does not rely on a single sample. It is also important to point out that this type of analysis is not limited to the stiffness identification method employed in this chapter. In fact, most vibration-

based parameter identification methods that exist in the literature are influenced by the variability of structures and could be complemented with PCA to discard the effects of the external conditions. However, the assumption that the environmental conditions have a linear (or weakly nonlinear) effect on the identified parameters does impose a constraint on such implementations. For example, the variability of concrete's Young modulus for temperature changes is a case in which the external factors' influence may be too nonlinear for this approach to be useful.

## 4.2 Validation Through Analytical Model

To test the efficacy of the proposed technique, the finite element model developed for the benchmark problem on structural health monitoring was used. This 88-DOF FE-model as well as its simulated ambient vibrations were described in detail in section

**Table 4.1 Damage patterns investigated in this study**

Case	Elements	Reduction of stiffness (%)	Expected damaged elements on ID-model
1	Undamaged structure.	--	None
2	Brace on the first floor of the south half of the east side.	10	4
3	Both braces on the second floor of the west side	10	6 and 8
	Both braces on the second floor of the east side	30	
4	All braces on the south half of the east side	10	4, 8, 12, and 16
5	Brace on the first floor of the north half of the east side	30	4, 8, and 15
	Brace on the second floor of the south half of the east side	10	
	Brace on the fourth floor of the west half of the north side	10	
6	Central column on the third floor of the east side	50	12
7	Beam on the first floor of the north half of the east side	100 (removed)	4 and 8
8	Column on the second floor of the south-east corner	50	5 and 8
9	Central column on the second floor of the north side	50	7, 9, and 13
	Beam on the third floor of the east half of the south side	50	

2.3.2 of this dissertation. Modal identification was carried out using the natural excitation technique (NExT) in combination with the eigensystem realization algorithm with data correlations (ERA/DC) and their implementation was also performed as indicated in Chapter 2. Nine case scenarios are considered in this study including the undamaged state of the structure. Damage was induced using reductions of stiffness of the elements of the finite element model as indicated in Table 4.1.

To simulate varying environmental conditions, changes in temperature were introduced as well as two independent temperature gradients. The overall temperature was assumed to be a random variable distributed uniformly between 0°C and 40°C (32°F and 104°F). Both temperature gradients, were assumed to be normally distributed random variables with zero mean and standard deviation  $\sigma = 4$ . The first gradient case is such that, for a given gradient  $x$ , there is a difference in temperature equal to  $x$  between the top and bottom elements of the structure which is linearly distributed over the height of the building. Similarly, the second temperature gradient introduces a spatial difference in temperature between the east and west faces of the structure. The variability of steel's Young's modulus for temperature changes is shown in Fig. 4.4 [76].

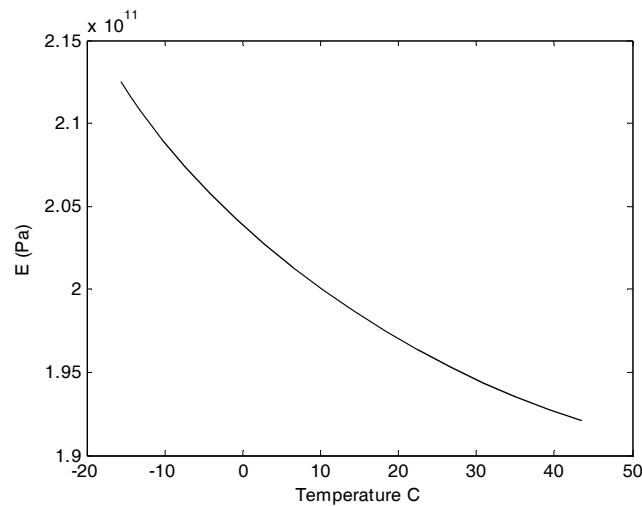


**Figure 4.4 Young's modulus of steel vs. temperature (after [76])**

### 4.2.1 Identification Model

As mentioned previously, the selection of an appropriate identification model is closely related to the success of any model-based SHM technique. Because a limited number of sensors were used (12), some assumptions were needed to select an identification model that took full advantage of the information available. For instance, since no measurements of vertical displacements are available from the analytical model, all degrees of freedom of the ID-model in this direction were constrained. Moreover, none of the recorded accelerations provide any information of the in-plane deformation of the floors. Given all these limitations, a rather simplistic all-column identification model with 16 elements was utilized (see Fig. 4.5b). Geometric properties of the ID-model and its elements, as well as the mass distribution are based on the properties of the analytical model used to produce acceleration records.

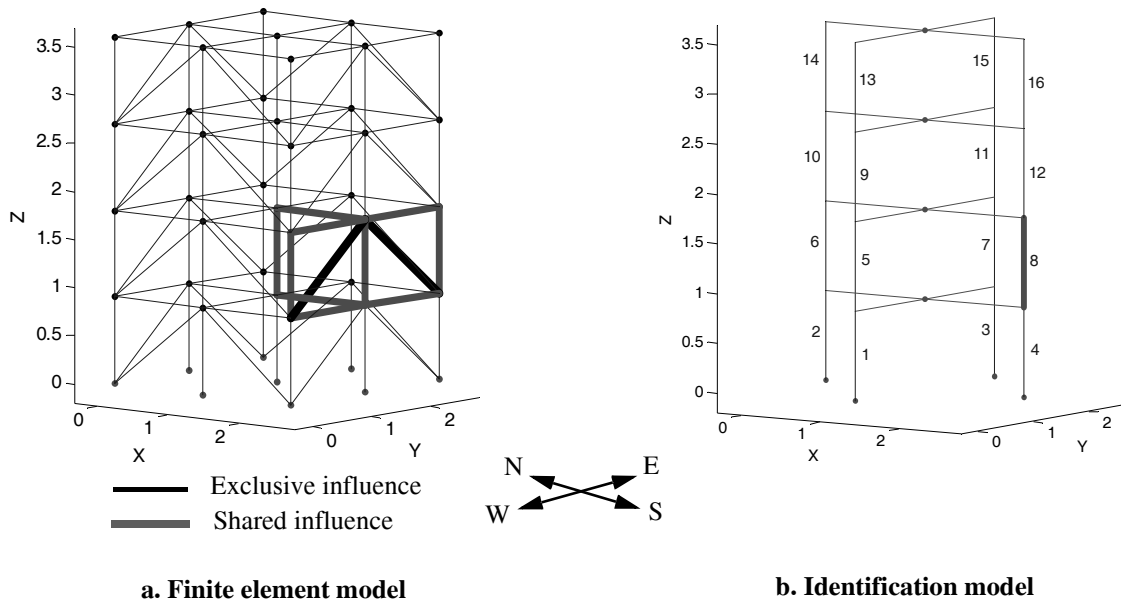


**Figure 4.5 Association between members of the finite element model and elements of the identification model**

All columns adjacent to any particular floor, are rigidly linked to a central node that is allowed to displace in-plane only (both translational directions and rotation). This reduces the number of DOF's of the model to three per floor, for a total of 12. As a result of such condensation, each element of the ID-model has contributions from a portion of the structure, and the identified damage cannot be attributed to a single member but to that particular group of elements. Fig. 4.5a shows how the members of the analytical model influence a single element of the ID-model. Note that some members of the finite element model affect only one corresponding element of the ID-model, while some others contribute stiffness to several elements of the model.

#### 4.2.2 Applying PCA

As explained in previous sections, the identification of stiffness values of the elements of the ID-model is affected by environmental conditions and noise in sensors, both of which are changed randomly for every simulation performed in this study. Fig. 4.6a, for instance, shows the identified stiffness values under two different and random environmental conditions and noise. Although different values were obtained, both simulations were performed with the healthy model of the structure. Thus, a deterministic analysis of

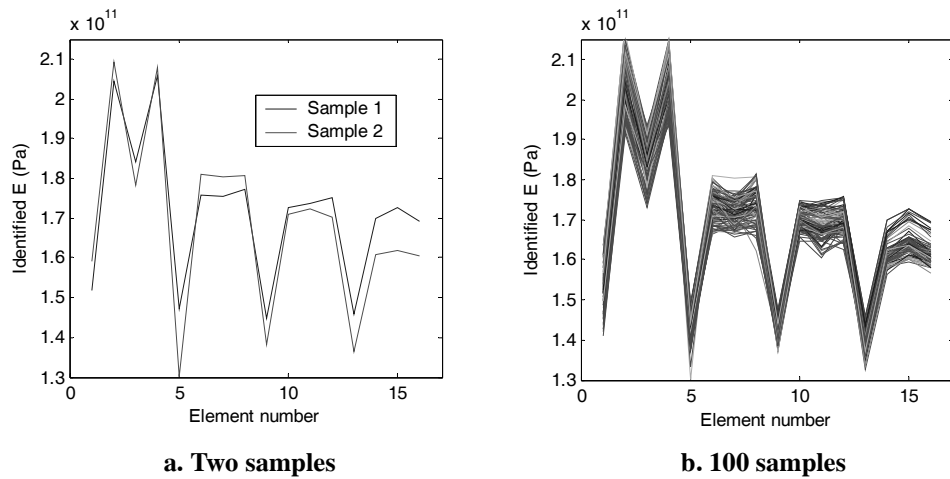


**Figure 4.6 Identified stiffnesses in the healthy state**

these two samples could mistakenly conclude that, when performing the second simulation, some of the elements experienced a significant loss in stiffness as compared to the first simulation. All samples obtained from the healthy model are shown in Fig. 4.6b. The need for a statistical analysis is clear from this example.

If the effect of the external factors over the stiffnesses of the elements is linear, the identified values should remain in the hyperplane defined by the  $m$  principal components with high energy content. Therefore, the residual error due to the projection increases as  $m$  is reduced and decreases for a higher  $m$  value. In real applications the number of environmental factors is not known and could be difficult to find by observing the singular values [76]. It may be intuitive to select a higher number of principal components in order to obtain a small residual error. However, since the residual error itself is the indicator of damage, its amplitude is not so important for the outlier analysis. Thus, the selection of an exact dimension  $m$  is not very critical. In some cases, it may be useful to select several values of  $m$  for verification. In this study,  $m$  was chosen as 3.

It is important to emphasize the importance of having sufficient samples of the healthy structure for a wide range of environmental conditions. This ensures that the distribution of the identified stiffnesses over these factors is well known and can be mapped accurately when performing the singular value decomposition. In this study, a total of 100 simulations of the healthy state of the analytical model were performed to apply the PCA analysis. When damage is present, however, only 50 simulations were used.

To separate those elements with apparent damage from those that seem unchanged a limit of 1% was set. This means that those elements whose identified stiffness have decreased by at least 1% when performing the two-way projection (i.e.  $e_w > -1\%$ ) are excluded to build the prediction model using Eqs. (4-12) and (4-13). In addition, the coefficient of admissibility  $\alpha$  in the outlier analysis (see Eq. (4-15)) was selected as 2. In other words, the outlier analysis is set so that those elements whose stiffness seem to

have decreased by more than 2% according to the prediction model (i.e.  $e_p > -2\%$ ) are considered outliers. A warning shall then be issued in case three consecutive samples report the same (or greater) loss of stiffness.

Figure 4.7 provides the residual error  $e_p$  of the elements of the first floor of the ID-model as calculated using the values obtained with the prediction model. The first 100 samples correspond to the healthy data points and are expected to vary randomly around the mean but remain close to this value. The last 50 samples correspond to case 2, in which a single brace from the east side of the first floor has lost 10% of its stiffness. As indicated in Table 4.1, element 4 of the ID-model is expected to show a reduction of the identified stiffness. Clearly, the residual error of this element decreases significantly (in a magnitude sense), to the point that only a few data points remain within the threshold prescribed. In this case, 49 out of all 50 damaged samples showed that element 4 had a stiffness reduction of more than 1% when performing the initial two-way projection (i.e.  $e_w < -1\%$ ). This means that 49 of the prediction models were built without using the identified stiffness value associated with this element. Similarly, a few other elements had to be excluded to form some of the prediction models due to the resultant initial error. However, only two prediction models were built excluding a maximum of three identified values.

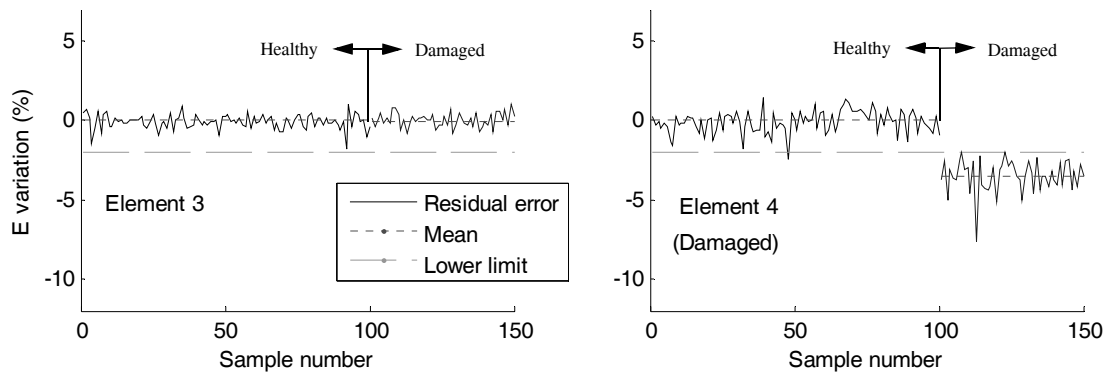


**Figure 4.7 Residual error ( $e_p$ ) of two elements of the first floor before and after damage (case 2)**

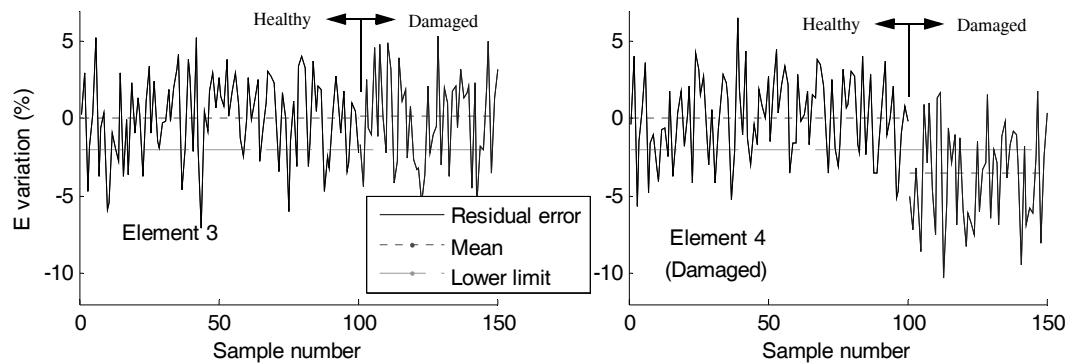


**Figure 4.8 Variation of stiffness values detected of two elements of the first floor before and after damage (case 2)**

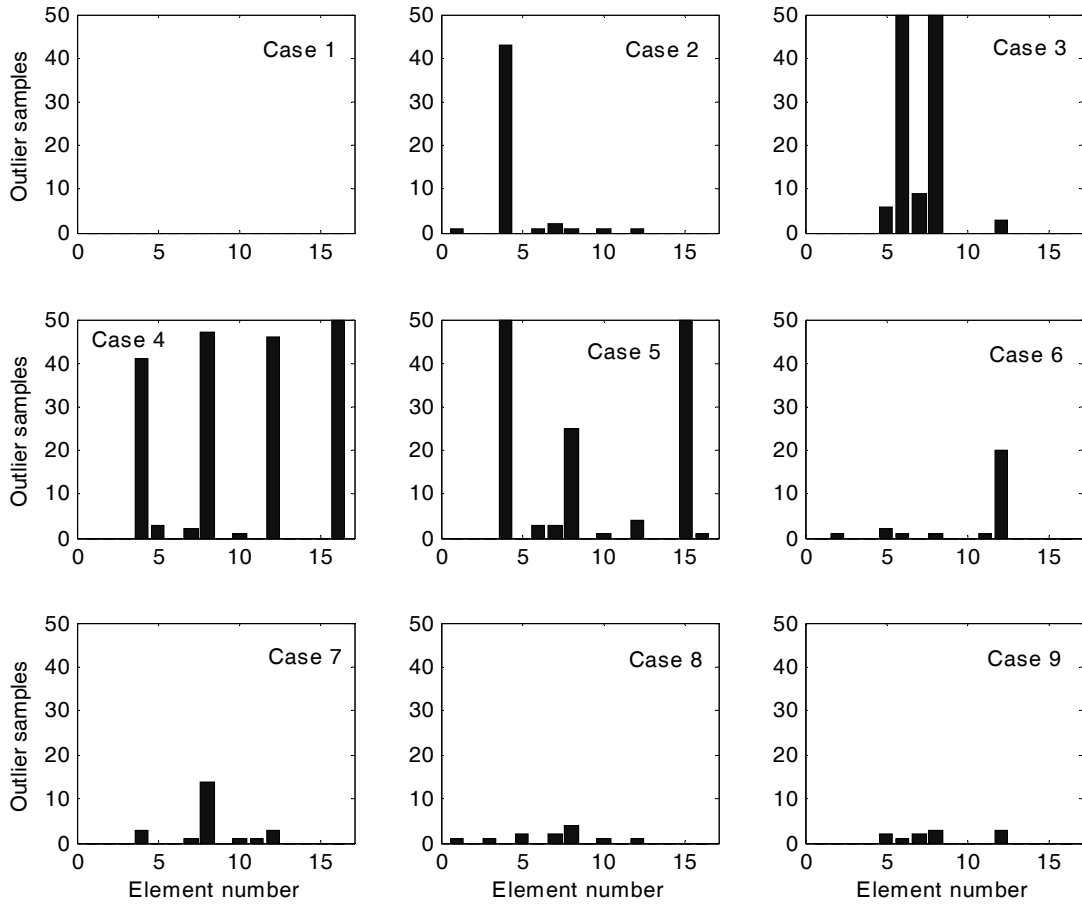
The benefits of the PCA analysis proposed in this chapter can be clearly seen when the variability of the Young's moduli detected are analyzed directly. As an example, Fig. 4.8 shows this variability for the same two elements whose residual error was shown in Fig. 4.7. Notice that, in the mean sense, the detected loss of stiffness of element 4 is the same (about 3.5% of its initial value). However, the deviation of these distributions is much higher, making it more difficult to reliably determine the state of the structure or issue warnings alerting for possible damage.

Table 4.2 shows the warnings issued for each damage case, indicating the element involved and the number of samples required to obtain three consecutive outlier points. Notice that the first three damaged scenarios (cases 2, 3, and 4) are detected very accurately and the first three samples are sufficient to issue the corresponding warnings. Although not as quickly, damage in cases 5 and 6 are also detected accurately. In case 5, for instance, warnings are issued promptly for elements 4 and 15, but 14 samples are needed to issue a damage warning for element 8.

**Table 4.2 Warnings issued**

<b>Case</b>	<b>Warning issued for element</b>	<b>Samples needed</b>	<b>Status</b>
1	--	--	--
2	4	3	Correct
3	6	3	Correct
	8	3	Correct
4	4	3	Correct
	8	3	Correct
	12	3	Correct
	16	3	Correct
5	4	3	Correct
	8	14	Correct
	15	3	Correct
6	12	8	Correct
7	4	--	False negative
	8	17	Correct
	12	19	False positive
8	5	--	False negative
	8	--	False negative
9	7	--	False negative
	9	--	False negative
	13	--	False negative

The number of outlier data points of all 16 elements for all case scenarios are shown in Fig. 4.9. Contrary to the already mentioned cases 2 through 6, in which accurate warnings were issued once damage was induced, very few outlier points were detected for cases 7, 8, and 9, resulting in inaccurate warnings or none at all. In these cases the damage induced did not have the same impact on the dynamic properties of the structure, and as a result, the damage identification was not successful. For instance, when the damage described in case 7 was induced on the healthy structure, the natural frequency that suffered the maximum variation was decreased by 0.37% (for fixed environmental variables and no noise present). The reason for this low variation of the structure is the



**Figure 4.9** Outlier samples of residual error ( $e_p > 2\%$ )

high stiffness added by the diagonal elements. This can easily be seen in the first damaged scenarios (cases 2 through 5) where even small variations of the diagonal elements can be detected promptly. However, high variations in the stiffness of the column and beam elements have little impact on the structure's dynamic properties, and thus are challenging to detect.

To demonstrate the capabilities of the proposed technique to detect various types of damage whenever the dynamic properties of the structure are altered, cases 7, 8, and 9 were analyzed with the unbraced structure as the reference (i.e. healthy state). Under this new configuration, the damaged induced in these cases had a significant impact on the

dynamic properties allowing us to detect and localize the changes imposed to the healthy structure. Table 4.3 shows the warnings issued for these cases. Damage is correctly identified in all cases with a few samples.

**Table 4.3 Warnings issued for unbraced cases**

Case	Warning issued for element	Samples needed	Status
1 (unbraced)	--	--	--
7 (unbraced)	4	3	Correct
	8	3	Correct
8 (unbraced)	5	3	Correct
	8	6	Correct
9 (unbraced)	7	3	Correct
	9	3	Correct
	13	3	Correct

### 4.3 Conclusions

A statistically based analysis that helps reducing the effects of changing environmental conditions has been developed and combined with an established parameter identification method. The efficacy of the method was demonstrated using an analytical model of the SHM benchmark structure. Both modeling errors and sensor noise were considered in this numerical example. Forced responses simulating ambient vibration were used to determine structural properties. Numerous samples were obtained for a variety of simulated environmental conditions. The distribution of these properties over the unknown external effects was obtained through PCA, mapping the data into the hyper-space defined by the principal components, and back into the original axes. The residual error due to this projection was successfully used as a indicator of damage and a prediction model was used to quantify its extension. This approach, as well as most vibration-based techniques that use global dynamic properties of the structure, is limited to scenarios in

which damage results in a loss of stiffness in the structure that is significant enough to change the dynamic properties.

Herein the effect of temperature is modeled as a variation of the Young's Modulus of the elements of the finite element model. However, real structures with certain constraints also experience stress stiffening of the members due to thermal expansion. When the structure cannot expand freely, this effect has also an impact on the global modal properties. Due to the design of this free-standing test specimen, and the uniformity of the material, these effects are neglected in this study.

## **Chapter 5**

### **SHM Framework Definition and Validation**

The conclusions of the comparative study of Chapter 2 as well as the techniques introduced in Chapters 3 and 4 are combined herein to create a structural health monitoring framework that aims for the identification and localization of damage within a structure regardless of the environmental conditions that affect its dynamic behavior. This framework is analytically tested using a finite element model of a typical highway bridge which was loaded with non-white random inputs to simulate ambient vibrations. Several uncertainties typically found in real-world applications are considered in this numerical example in order to add some realism to the study and to test the robustness of the technique. Various configurations of structural integrity and environmental conditions are also considered.

To categorize the framework as a whole we have to look at some of its characteristics (see classification of SHM techniques in Chapter 1). For instance, according to the information provided to the user, the framework can be categorized as a level 2 technique (as classified by Rytter [65]), provided that it successfully identifies and localizes damage within the structure. Moreover, because dynamic responses are utilized in the time domain, the scheme can be considered to be both a vibration-based and a time-domain technique. Lastly, because a finite element model of the structure is updated, then the framework qualifies as a model-based technique.

The four sections in which the present chapter is divided attempt to achieve each of the defined main objectives, namely: 1) the definition of the framework as a succession of steps that should be taken for its successful implementation; 2) the introduction of a realistic numerical model; 3) the validation of the premises of the SHM scheme using simulated responses; and 4) the stipulation of its capabilities and limitations. It is important to emphasize that, although civil engineering structures are the main target of this dissertation, the framework as a whole (or in part) is likely to perform well in other engineering fields. However, its viability, requirements and limitations may differ significantly and should be investigated for specific cases.

## **5.1 The Structural Health Monitoring Framework**

The proposed framework can be divided in six basic steps which are described in the sections below. Unfortunately, no specific guidelines can be established for the execution of these steps and the experience of the engineer for taking into account all the variables that influence the final results is essential. However, based on the experience obtained while performing the research involved in this dissertation, several pieces of advice are offered to the reader for the realization of each step. Some of these discussions will become clear as the numerical problem is introduced later in this chapter.

### **5.1.1 Identification of Dynamic Properties**

An accurate identification and numerical description of the mode shapes of the structure is key for the success of the proposed scheme. This task, however, is much more complex than simply selecting a method to analyze the dynamic records (for which Chapter 2 provides some insights). In fact, problems such as the selection of the number of sensors, their optimal placement, and the characteristics of the recorded data should be addressed beforehand. In general, previous knowledge of the structure is very important and a detailed finite element model should help in solving some of these issues. It is

important to emphasize that the number of modes shapes identified should be as high as possible as each provides some information about the state of the structure. The following sections discuss some of the most important issues to be addressed while carrying out the identification of modal properties.

### **Number of Sensors**

Rather than a technical question, the number of sensors to be employed should be a budgetary issue. In general, the higher the number of sensors, the better the description of the structures's mode shapes is, and a more detailed identification model can be constructed. Some might argue that a high number of sensors also means that more difficulties arise, such as the collection of large amounts of data, energy supply and even communication issues. However, with the tools that are commercially available today, these are all issues that can be resolved with a generous budget.

### **Sensor Placement**

Once the number of sensors is defined, their placement throughout the structure should be determined considering two main factors, namely: 1) the amount and shape of the modes expected to be identified; and 2) the ID-model that will be used to characterize the structure at any given time. To analyze this problem and find an effective solution, a detailed finite element model of the structure is recommended. Such model can roughly reveal in advance the frequencies and shapes of the modes to be identified and therefore, provide information for the engineer to strategically place sensors and obtain an ample description of all mode shapes. This type of analysis can replace the simplistic concept of observability, which uses the system and output matrices of the model ( $\mathbf{A}$  and  $\mathbf{C}$ , respectively) to determine whether a vibrational mode can be detected but does not provide information on the obtained description of the associated shape. However, it is important to keep in mind that, ultimately, the ambient loads are the ones that limit the

modal information that we can detect. Preliminary records of the structure's dynamic response to ambient loads should help determine the excited modes.

It is also important to place sensors so that the degrees of freedom of the ID-model can be directly associated with the measurements taken. By assuring this direct relationship we can avoid the problem of linearly transforming mode shapes or expanding them, a procedure that is time consuming and widely criticized by several researchers because it adds unnecessary errors to the calculations.

### **Data Acquisition**

Acquiring useful vibration records from structures is usually more complicated than intuition indicates. The main decisions to be made concern the sampling rate, signal filtering, length of records, and the times of day at which data should be recorded. Although a high sampling rate ensures that all excited modes of the structure are recorded, as stated in Chapter 2, an increasing amount of data points not only requires more computational power, but may also have a negative impact on the identification results. Therefore, the sampling rate should be decided upon using previous knowledge of the maximum natural frequency expected from the structure, which can easily be found by analyzing the frequency content of preliminary records of the structure at various points. According to the Nyquist theorem, sampling rate should be at least twice the highest natural frequency expected in order to avoid aliasing signals. A factor of 3 to 5 is recommended. Moreover, filters can be used to optimize the information obtained within a defined frequency range and minimize the negative effects of unexpected high frequency signals. The basics on signal conditioning can be found in [56].

To make decisions regarding the length of the records and the most suitable times, it is important to understand the nature of the service and ambient loads that excite the structure on a regular basis. In buildings, for instance, service loads provided by occupants

are highly dependant on the time of the day and the identification should highly benefit from those loads. A very different approach should be taken when trying to identify the modal properties of bridges. In this type of structures traffic usually provides vibrations with enough amplitude and frequency content to carry out the identification. However, the mass added to the structure may be significant and perhaps have a non-negligible influence on the modal properties of the bridge. A good understanding of these issues is very important to make an educated judgment.

### **Data Processing**

Herein, data processing refers to the actual analysis of the recorded vibrations and the identification of the natural frequencies, mode shapes and damping ratios of the structure. Although this identification can be carried out with multiple techniques, the comparison performed in Chapter 2 showed that the subspace identification (SSI) method is the most robust and reliable among some of the most popular time domain techniques. However, even if this method is selected to analyze the data, there are a few parameters that must be selected in order to execute it. Among these parameters we can find the size of the Hankel matrices and the realization order. Although several tips for the successful implementation of the SSI method were provided in Chapter 2, the experience of the user with the algorithm is fundamental.

#### **5.1.2 Building an Identification Model**

As stated in Chapter 3, the robustness of most model-based SHM techniques strongly depends on the selection of an appropriate ID-model and its ability to reproduce the dynamic behavior of the structure. Therefore, their construction should be tightly linked to the physical properties of the structure. For instance, both mass and stiffness quantities should be obtained and meticulously distributed throughout the nodes and elements of the ID-model. However, to take full advantage of the model updating technique of

Chapter 3, some other factors such as the placement of the sensors must be taken into consideration. The following paragraphs should help understand these issues and perhaps ease the construction of this model.

The bottom line is that the ID-model must exhibit mode shapes that can be distinctively associated with those identified from the structure. Although ID-models typically represent the structure in a simplified way, their simplicity should not compromise this direct association. It is worth noting that, because the natural frequencies are not employed in the optimization process, their order or their proximity is irrelevant. However, a well constructed ID-model is expected to have similar natural frequencies and in the same order as those displayed by the structure.

Unlike some non-iterative techniques (see, for instance, Caicedo [14]), the model updating scheme introduced in Chapter 3 allows the use of ID-models with more degrees of freedom than those associated with measurements recorded from the structure. This means that the expansion of the detected mode shapes becomes unnecessary allowing the use of more elaborate ID-models. However, it is important to keep in mind that the efficiency of the model updating technique is highly dependent on both the number of updating parameters and the number of DOF of the ID-model. In fact, the computational requirements grow exponentially as either of these two factors is increased.

### **5.1.3 Forming an Accurate Baseline**

Because the characterization of the structure is achieved through optimization process of a nonlinear problem, the initial set of parameters plays a fundamental role both in terms of efficiency as well as accuracy. This initial set of parameters is referred to as the baseline of the updating process and should be optimal in the sense that, when the objective function is evaluated with modal properties of the healthy system, it is guaranteed to represent a global minimum. Much like later characterizations of the structure, this set of

parameters is calculated by updating the ID-model with identified modal properties. However, given the importance of this set, and the fact that they are calculated only once, special attention should be given not only to the identification of the structural mode shapes, but also to the updating process. For instance, if more traditional identification methods are available (e.g. forced vibrations) and within budget, then this possibility should be considered.

However, even if very accurate modal properties are available to calculate a baseline, the optimization algorithm is not guaranteed to reach a global minimum (given that a random set of initial parameters is provided). There are a number of ways to deal with this difficulty such as the use of multiple and random initial sets or even genetic algorithms. However, these processes are time consuming and decisions should be made taking into account the computational capabilities and the time constraints.

An important factor that must be determined prior to the implementation of the SHM scheme is the number of modes to be used for later characterizations of the structure. It is recommended that all identified mode shapes be used as each provides distinctive information. However, it is necessary to use the same mode shapes for each characterization, regardless of the structural condition, as well as the initial search for the baseline. It is important to recognize that the framework uses the changes in the mode shapes as the fundamental source of information. Therefore, characterizations obtained with a different set of mode shapes, even when a single mode shape is associated with a different frequency, cannot be used.

#### **5.1.4 Setting up the Optimization Algorithm**

A number of variables must be selected prior to the execution of the updating algorithm. Among these variables are the parameters of the ID-model subjected to change, the number of modes used in the calculation of the sensitivities, and those associated

directly with the conjugate gradients algorithm. The following paragraphs provide some insights into these issues.

It was shown in Chapter 3 that the selection of the Young's modulus of the elements as updating parameters is mathematically convenient for the model updating process. Both the gradients as well as the Hessian matrix can be obtained when utilizing these parameters. However, the model updating methodology also allows the user to update a limited number of these parameters. Whether all moduli or a limited number should be updated is a decision that must be made upon knowledge of the identified structural mode shapes. For instance, in some cases (as will be shown in the numerical example presented later in this chapter) the identified mode shapes do not provide sufficient information regarding the status of certain members of the structure. As a consequence, the associated elements of the ID-model tend to be highly sensitive to small changes in the dynamic properties and are likely to indicate nonexistent losses or even gains of stiffness. In such cases, the Young's modulus of those elements should be updated only to create a baseline for all elements of the ID-model (see section 5.1.3), but should not be updated to characterize the structure once the framework is in place.

One of the parameters that has the largest influence on the efficiency of the optimization algorithm is the number of vibrational modes used to calculate the sensitivities of the mode shapes of the ID-model. As stated in Chapter 3, when using the method proposed by Fox and Kapoor [27], exact values are obtained when all eigenvalues and eigenvectors of the ID-model are employed in the calculation. However, the computational power and the memory required to compute these values rapidly increase as the number of mode shapes and their associated frequencies are increased. To select a number of vibrational modes that results in a computationally efficient algorithm without sacrificing much accuracy, the convergence of the sensitivities has to be analyzed as suggested in Chapter 3.

Lastly, the conjugate gradients algorithm with Newton-Raphson and Fletcher-Reeves must be setup with some parameters, the most influential one being the maximum number of iterations allowed when updating the ID-model. For a linear optimization problem, the algorithm is guaranteed to find the global minimum in a maximum number of iterations equal to the number of parameters being updated. For nonlinear problems, however, this statement is no longer true and the convergence depends on the characteristics of the ID-model. Although the selection of this parameter should be based upon experience with the algorithm, it is recommended that the optimization be allowed to run several times with an unlimited number of iterations and for different sets of identified modal properties. The number of iterations required to converge and the convergence rate of the objective function for these cases should provide useful feedback for the selection of a limit.

### **5.1.5 Multiple Characterizations of the Healthy Structure**

It is important for the healthy structure to be characterized multiple times under the influence of a wide range of environmental conditions. By doing this multiple characterization, the effects of these factors over the identified parameters (i.e. optimized moduli of elasticity) can be mapped accurately and accommodated at later times once the framework is fully functioning. To achieve this goal in regions with seasons and high variations of temperature, characterizations should be obtained through all these changes. However, because there is a need to characterize the structure over a relatively long period of time, it is important to point out that the structure is assumed to remain healthy during this time.

### **5.1.6 Outlier Analysis and Issuing Warnings**

As shown in Chapter 4, two thresholds are established when implementing the outlier analysis proposed. The first threshold is used to reject identified  $E$  values outside the

normal variations (and construct a prediction model using those that are seemingly healthy), whereas the second one is used to define which elements are damaged (i.e. outlier points). Defining the first threshold is a task that should depend on the uniformity of the optimized parameters, which, ultimately, depends on the quality of the identified modal properties as well as the ability of the optimization algorithm to reach global minima. For instance, if the identified sets of  $E$  values are usually sets with high deviations from the healthy values (even after the environmental conditions have been accommodated) then this threshold should be set to a higher value. In such a case, a low threshold would translate into building the prediction model with too few elements, likely deteriorating the results. On the other hand, the second threshold should be set at whatever value is considered by the engineer as a damage indicator. Also left to the criterion of the system designer is the required number of consecutive outliers to issue a damage warning and take the needed action.

The model updating algorithm employed in the proposed framework becomes useless in those cases in which damage introduces radical changes to the dynamics of the structure, be it introducing new modes or changing the existing ones to the extent that they become difficult to recognize in an automated environment (as indicated by the modal assurance criteria, MAC). It is obvious that, in such cases, the condition of the structure has been altered considerably and damage is almost certain. Therefore, and even though no characterization of the structure (i.e. set of updated parameters) can be obtained through the optimization algorithm, the sample should be considered as an overall outlier. As explained before, damage warnings should be issued when a predefined number of consecutive outliers are detected. In such cases, the technique drops to a level 1 technique (as classified by Rytter [65]), detecting only the existence of damage but being unable to localize it.

## 5.2 Numerical Example

The numerical model selected to test the proposed SHM framework is representative of a highway bridge (see Fig. 5.1). With 12 meters of width, the bridge has two spans of 20 and 32 meters, respectively. Three simple supports provide the boundary conditions. As shown in Fig. 5.1b, the bridge is composed of five steel girders supporting a 10cm thick concrete slab which is assumed to be continuously connected to the girders. Diagonal elements provide lateral support to the girders every 4 meters. The girders are regular W16x89 sections as described in [4], whereas the diagonal elements have a combined area  $3e-3\text{ m}^2$ . Girders and connecting elements have a modulus of elasticity of  $E=2e11\text{ N/m}^2$ .

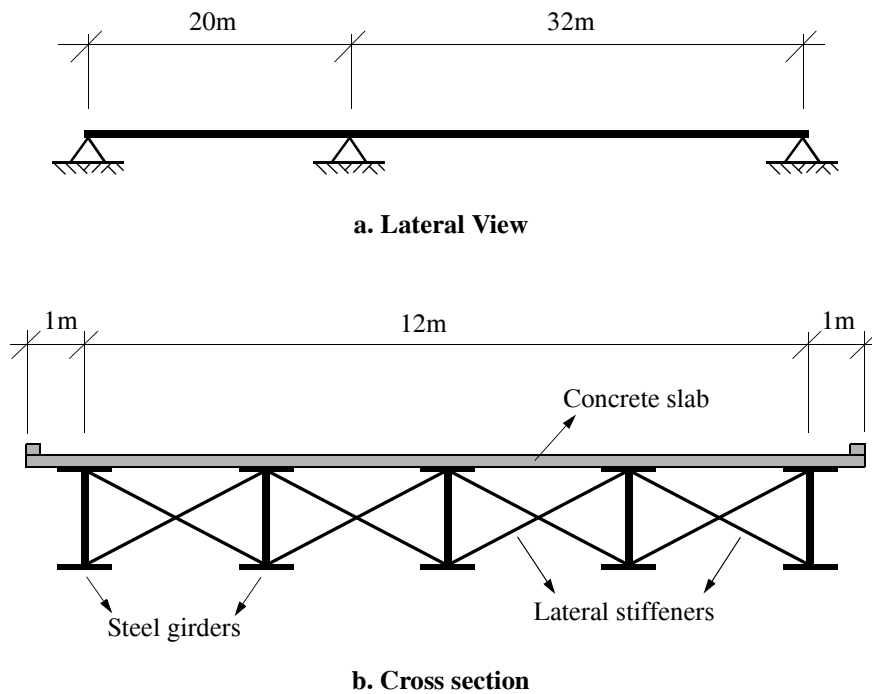


**Figure 5.1** Typical highway bridge with three simple supports

### 5.2.1 The Finite Element Model

To simulate dynamic responses of the bridge as well as environmental changes and a variety of structural conditions, a finite element model was created with 174 Euler-Bernoulli elements connecting 135 nodes (see Fig. 5.2). This model is often referred to simply as “the structure” throughout this chapter. It has a total of 750 degrees of freedom, with the only restrictions being the displacements in all directions of the 15 supported nodes as well as their rotations with respect to the  $x$  axis. The main issues associated with the construction of this FE-model are discussed in the following sections.

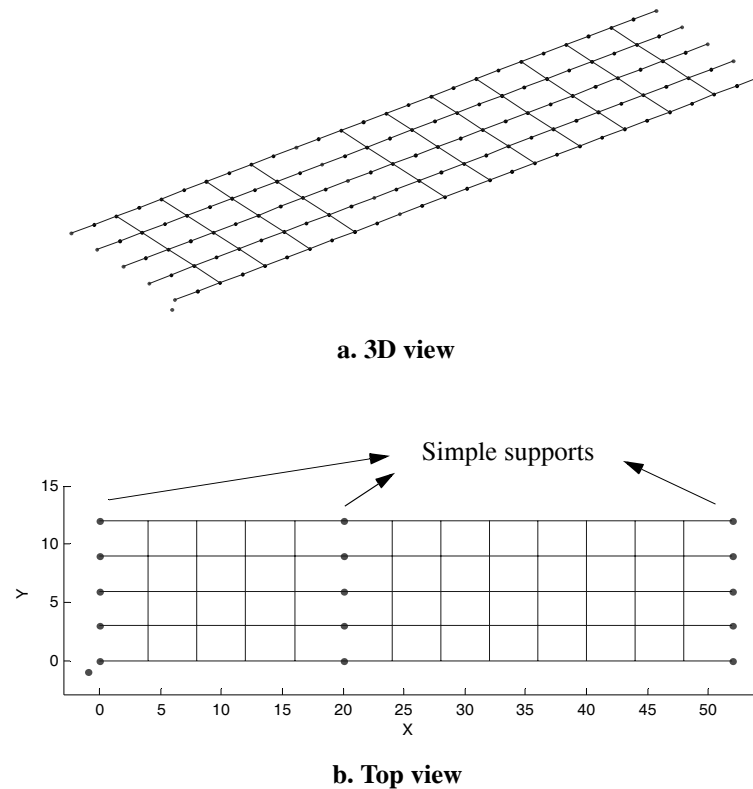


**Figure 5.2** Finite element model

### Stiffness and Mass Distribution

The cross sectional properties of all elements were carefully selected based on the properties of the structural members of the bridge and their most likely behavior as composite elements. For instance, because the concrete slab is assumed to be continuously connected to the steel girders, the inertia of the longitudinal elements was calculated as a combination of the two. The properties of these elements are  $I_x = 6.285e - 4 \text{ m}^4$ ,  $I_y = 2.887e - 2 \text{ m}^4$ ,  $J = 5e - 5 \text{ m}^4$ , and  $A = 4.7e - 2 \text{ m}^2$ . Similarly, the properties of the connecting elements were calculated as a combination of the two diagonals and the concrete slab resulting in the properties  $I_x = 1.225e - 3 \text{ m}^4$ ,  $I_y = 0$ ,  $J = 0$ , and  $A = 1e - 2 \text{ m}^2$ . All elements have the mass of the associated steel material uniformly distributed over their length. In addition, the mass of the concrete slab was added as lumped masses at the nodes of influence in a simple tributary distribution.

To add some realism to the problem, it was decided to consider the uncertainties associated with the actual strength of the structure as constructed. It is well known that, regardless of the quality of the materials employed and the construction practices, the final strength of the elements is always unknown and most likely different from those values for which they were designed. These uncertainties were simulated by multiplying the Young's modulus of all 174 elements of the FE-model by random numbers that were uniformly distributed between 0.9 and 1.1. In other words, and similar to real scenarios, the actual stiffness of the healthy structure is unknown and only expected values are provided (i.e.  $E = 2e11 \text{ N/m}^2$ ).

### Varying Environmental Conditions

Regardless of the condition of the structure, each characterization is performed with a different set of environmental conditions that surrounds it. Similar to Chapter 4, these conditions are simulated here using changes in temperature as well as three temperature

gradients across the dimensions of the FE-model. The overall temperature is assumed to be a random variable distributed uniformly between 0°C and 40°C (32°F and 104°F), whereas the temperature gradients, were assumed to be normally distributed random variables with zero mean and standard deviation  $\sigma = 4$ . The first gradient is used to simulate differences in temperature between both sides of the structure (e.g. sun hitting one side only). This difference in temperature is then linearly distributed over the width of the bridge. Similarly, the second and third gradients introduce spatial difference in temperatures between the end supports and the central support. Note that these conditions are assumed to remain stable during the short period of time during which ambient responses are simulated. The variability of steel's Young's modulus for temperature changes is shown in Fig. 4.4 [76].

The FE-model fails to take into consideration the residual stresses originated by differential expansion of the materials and the restrictions imposed by the boundary conditions. Unlike the example provided in Chapter 4, in which these effects were considered negligible due to the uniformity of the material and the free standing conditions, a more noticeable effect is expected for the type of structure analyzed in this chapter. The consequences of this omission will be analyzed when the results are presented in later sections.

### **5.2.2 Damage Scenarios**

Similar to the numerical examples provided in Chapters 3 and 4, local damage is simulated here as a reduction of the Young's modulus of certain combinations of elements in the FE-model. As summarized in Table 5.1 and displayed in Fig. 5.3, twelve structural configurations are investigated. The first configuration corresponds to the undamaged structure, whereas configurations two through nine correspond to multiple scenarios in which the girders of the bridge have partially lost their stiffness. Cases ten and eleven are also simulated with the reduction of stiffness of longitudinal elements. However,

these cases are being analyzed to explore the capabilities of the technique when the boundary conditions are altered. Case ten, for instance is formed by reducing the stiffness of both elements adjacent to one of the middle supports by 20%. Case eleven, on the other hand, is simulated by completely removing the element next to one of the left supports of the bridge, causing the same effect as the removal of the support itself. Lastly, case twelve targets the connecting members of the bridge by reducing the stiffness of one of these elements by 40%.

**Table 5.1 Damage scenarios**

<b>Case</b>	<b>Elements</b>	<b>Reduction of stiffness (%)</b>
1	--	--
2	17, 18	20
3	69, 70	50
4	29, 30	30
5	55, 56	30
6	60	40
7	7, 8	20
	123, 124	20
8	3, 4	15
	23, 24	20
9	19, 20	20
	21, 22	20
	23, 24	20
10	10, 11	20
11	1	100
12	150	40

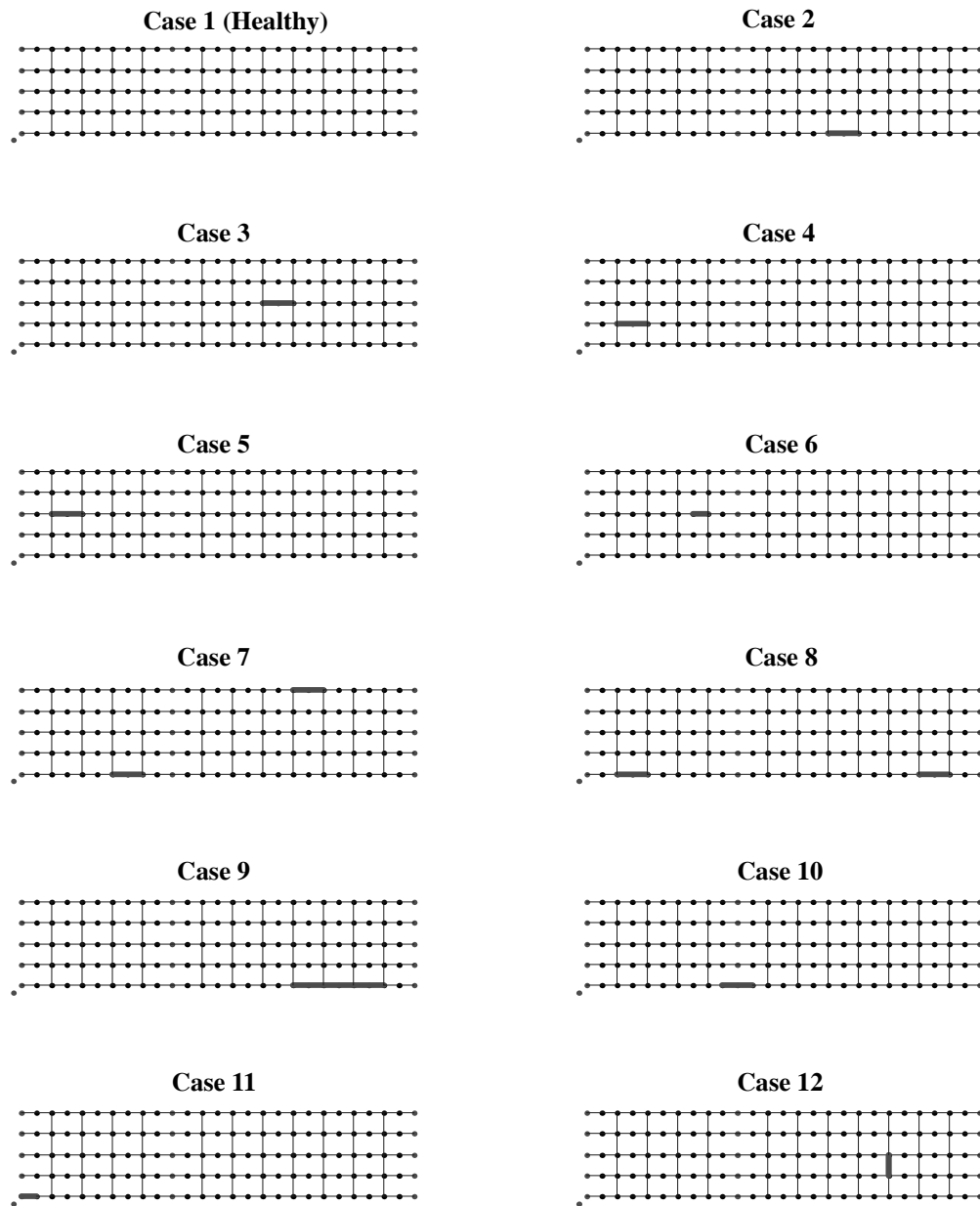


**Figure 5.3** Damage scenarios

### 5.2.3 Simulating Dynamic Responses

Simulating ambient vibrations of civil structures using FE-models and mathematically created loads has always been criticized by researchers. Our inability to measure ambient and service loads has forced engineers to presume their statistical properties and reproduced them using customized random signals. Moreover, using a finite element model, it is difficult to reproduce the exact localization and distribution of these loads. Although simulated ambient vibrations are used in this analytical study, a few extra steps have been taken in order to attenuate these flaws. For instance, instead of the band limited white noises used in various studies, the random signals used to load the FE-model have a non-flat frequency content (as shown in Fig. 5.4). These signals were obtained by applying a linear filter to Gaussian white noise, and will be used to test the SSI method to achieve the premises of Andersen [5] and Ibrahim *et al.* [39], whom, as mentioned in Chapter 2, showed that correct modal identification can be achieved under these circumstances.

Uncorrelated random forces were applied to the central nodes of the FE-model every four meters (for a total of 11 nodes). Each node was loaded with three forces including a

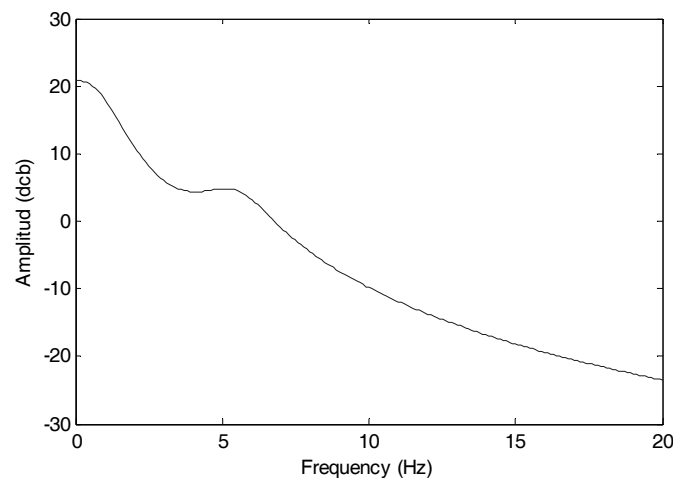


**Figure 5.4** Frequency content of random inputs

vertical force, a horizontal force (transverse to the bridge) and a torque. All 33 forces have zero mean and a standard deviation of 0.39 and 0.12N for the vertical and horizontal forces, respectively, and 3.85Nm for the torques. Similar to the numerical example provided in Chapter 2, the disturbances are independent of the structural response. In addition, to ensure that no transient responses of the FE-model are used in the modal identification process, the first 60 seconds of all simulations were systematically discarded.

### **5.3 Implementation of the SHM Framework**

In the following sections the SHM framework is executed in six steps as suggested earlier in this chapter. The discussions provided focus on the implementation issues and should be helpful for applying the technique to other cases.

#### **5.3.1 Identification of Dynamic Properties**

The first challenge is the accurate identification of the modal properties of the bridge as it vibrates under the influence of the simulated ambient forces. Although no budgetary limitations are present in an analytical study, it was important to keep the number of sensors low in order to show the viability of the technique. Similarly, the length of the records needed to be reasonably short. For this reason, only 33 sensors recording 10 minutes of data were employed. Recall that each dynamic simulation is inherently affected by a random set of simulated environmental conditions.

It was suggested earlier in this chapter that a detailed FE-model of the structure is particularly helpful for making decisions such as the placing of sensors and the sampling frequency. Although the model described in Section 5.2.1 is partially unknown (stiffness values were randomly modified to consider material and construction uncertainties), the author has an unrealistic advantage here as the structure itself is an analytical model.

However, given the characteristics of the bridge, such decisions are not difficult. For instance, it is somewhat obvious that the mode shapes will include those corresponding to vertical and horizontal bending motions as well as torsion of the deck. Therefore, vertical sensors will be placed symmetrically and uniformly along the sides of the bridge to capture vertical and torsional modes, whereas horizontal sensors will be placed along the center of the deck to capture horizontal motions. Figure 5.5 shows the final placement of all 33 sensors.

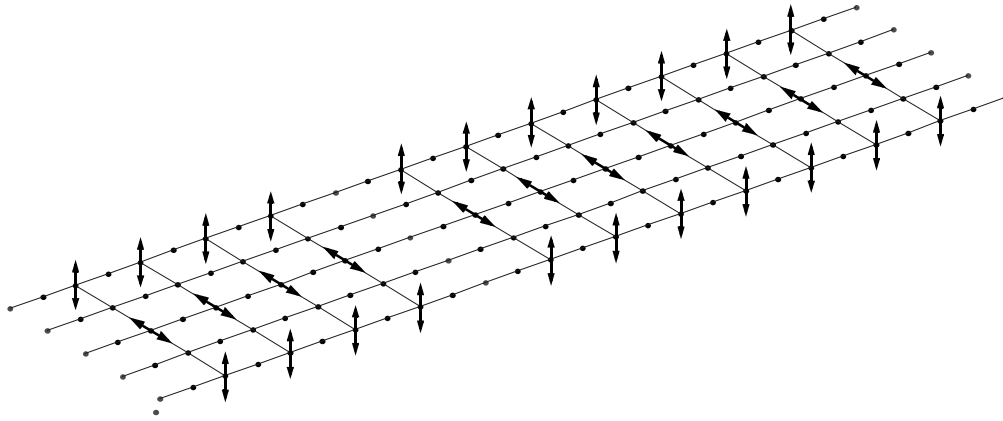


**Figure 5.5 Sensor placement**

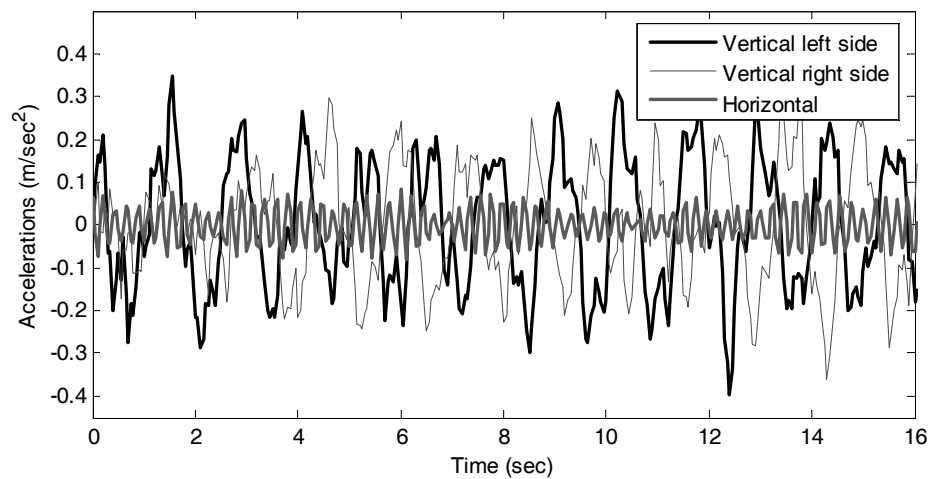


**Figure 5.6 Accelerations recorded from three sensors**

To simulate realistic data acquisition conditions, the accelerations recorded from the FE-model were contaminated with uncorrelated Gaussian white noise signals. All 33 signals have zero mean and a standard deviation of  $\sigma = 3e - 3$ . However, there are some differences in terms of the RMS ratio between the noise signals and the acceleration records they contaminate. On average, the noise added to the vertical acceleration is only 3%, whereas the average for the horizontal accelerations is 20%. Figure 5.6 shows, as an example, 16 seconds of three contaminated signals from those sensors that produce the highest accelerations.

After analyzing a few data sets obtained from simulations performed at relatively high frequencies, it became clear that only the first ten modes of the structure were being excited with enough energy to be identified consistently with the SSI algorithm. These modes vibrate at frequencies that range from 0.67 to 6.29Hz. Thus, to reduce the computational power and improve the accuracy of the identification, ambient vibration simulations were performed at 20Hz. According to the Nyquist theorem, this sampling frequency allows the correct identification of all ten excited modes.

The implementation of the SSI algorithm was carried out as suggested in Chapter 2 (see Fig. 2.9). After analyzing the stability of the results, it was decided to use Hankel matrices with eight block rows of data. Moreover, each data record (i.e. 10 minutes of 33 sensors at 20Hz) was decomposed four times to estimate realizations of the system with 30, 32, 34, and 36 poles. The modal properties of all four realizations were calculated and stabilized using the same evaluation criteria used in Chapter 2 (frequencies within 2% and mode shapes with MAC values of 0.9 minimum). Figure 5.7 shows the identified natural frequencies as well as their associated mode shapes for a random set of environmental conditions.

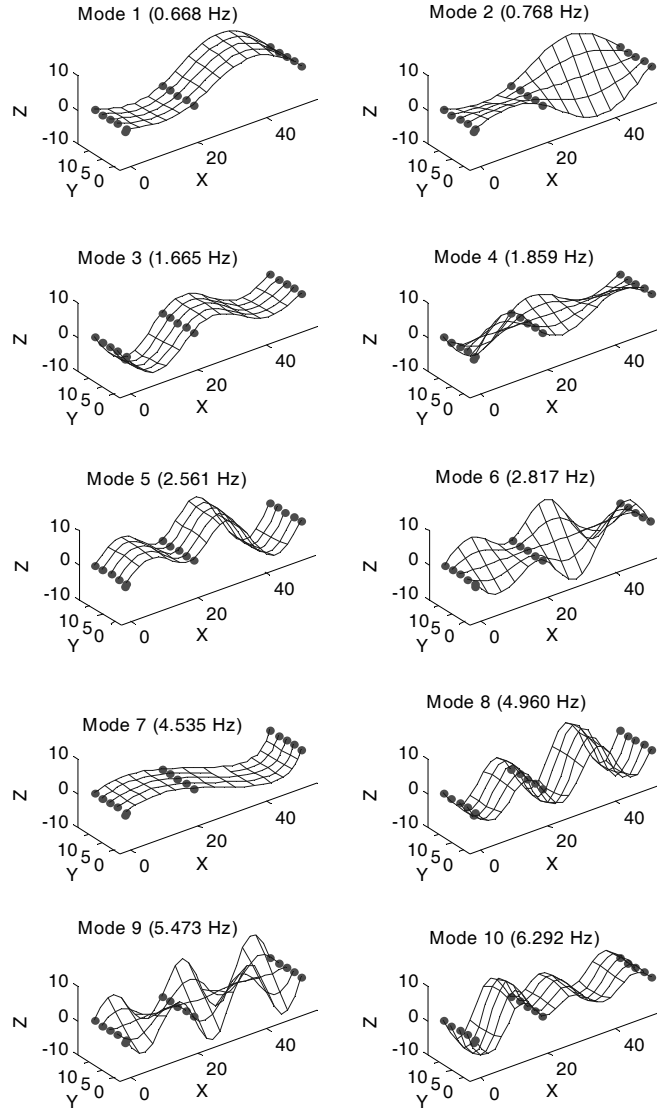


**Figure 5.7 Identified modal properties of the healthy structure**

### 5.3.2 The Identification Model

As mentioned previously, the computational power required to update the ID-model is highly dependent on its complexity. For this reason a rather simplistic model was built with only 61 elements connecting 42 nodes and boundary conditions similar to those of the bridge (see Fig. 5.8). The following paragraphs provide discussions on some of the many considerations that were accounted for while building this model.

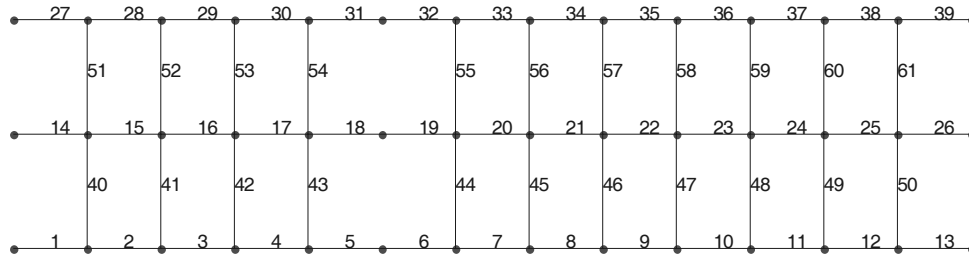


**Figure 5.8 Identification model**

Given the properties of the bridge and the nature of the loads that these type of structures receive, no significant motions are expected in the longitudinal direction (axial modes). In fact, no measurements are even taken in this direction. For this reason, all displacements in the  $x$  axis were eliminated from the ID-model, thus reducing the amount of degrees of freedom by 33. Similarly, because axial deformation of connecting beams should be minimal, the displacements in the  $y$  axis of all lateral nodes were constrained to displace with the central node, further reducing the amount of DOF by 22. An additional group of 22 DOF can be condensed by linking the rotations of the lateral nodes with respect to the  $z$  axis to those of the corresponding central nodes. As a result of these condensations, the ID-model is reduced to only 139 DOF. Note that this number is a small fraction of the 750 DOF of the FE-model, revealing that modeling errors are significant, as expected in real-world applications.

The cross sectional properties of the three longitudinal elements were selected in such a way that the overall stiffness of the ID-model matches the expected values of the bridge in all directions. For instance, it was assumed that the central longitudinal elements of the ID-model entirely represent the central girder of the bridge as well as half the stiffness of the adjacent girders. Thus the properties  $I_x$ ,  $I_y$ ,  $J$ , and  $A$  of the central elements are equal to those of the bridge girders multiplied by two. With a similar reasoning, the properties of the lateral longitudinal elements are equal to those of the girders of the

bridge multiplied by 1.5. The connecting beams, on the other hand, have a direct correspondence to elements in the structure and their properties are set accordingly.

The mass of the elements of the ID-model was uniformly distributed across their length, whereas the mass of the concrete deck was distributed among the nodes of the model in a simple tributary distribution. Moreover, the initial Young's modulus of all 61 elements is set equal to the expected values of the structural members of the bridge (i.e.  $E=2e11\text{N/m}^2$ ). However, in the search for a baseline (see section 5.3.3), these values will be updated and used as a starting basis for all characterizations of the structure once the scheme is fully implemented. Note that all the sensors placed on the structure can be directly associated with degrees of freedom of the ID-model greatly facilitating the evaluation of the objective function in the updating process. Based on the correspondence of

**Table 5.2 Expected damaged elements of ID-model**

<b>Case</b>	<b>Elements of FE-model</b>	<b>Reduction of stiffness (%)</b>	<b>Expected damaged elements of ID-model</b>
1	--	--	None
2	17, 18	20	9
3	69, 70	50	22
4	29, 30	30	2 and 15
5	55, 56	30	15
6	60	40	17
7	7, 8	20	4
	123, 124	20	36
8	3, 4	15	2
	23, 24	20	12
9	19, 20	20	10
	21, 22	20	11
	23, 24	20	12
10	10, 11	20	5 and 6
11	1	100	1
12	150	40	48

the elements of the ID-model with the structural members of the bridge, the SHM framework should yield damage warnings for the elements indicated in Table 5.2, if implemented successfully.

### 5.3.3 The Search for a Baseline

To ensure high accuracy of the baseline, and considering that this calculation is performed once, a number of special measures were taken. For instance, the modal properties of the structure were estimated using 15 minutes of ambient vibrations, five more than those used in subsequent characterizations of the structure. The following paragraphs explain in detail how the ID-model was updated in the search for this baseline.

To ensure that a global minimum is reached, a total of 21 updating processes were carried out with different sets of initial conditions, including that in which all elements start with the expected modulus of elasticity (i.e.  $E = 2e11\text{N/m}^2$ ). The additional 20 processes had random initial conditions that uniformly varied within 10% of the expected values. The baseline was then selected from the process that reached the lowest objective function. These processes were carried out with no limit in the number of iterations of the conjugate gradients algorithm (i.e. until convergence is reached).

All 61 Young's moduli were updated in this search for a baseline. Moreover, 100 eigenvalues of the FE-model and their corresponding eigenvectors were used to find the sensitivities of the mode shapes. It is worth noting that the computational power required to perform all these calculations was significant, perhaps to the point that, if later characterizations had been performed with the same setup, this study would have been impractical. Figure 5.9 shows the identified Young's moduli, whereas Fig. 5.10 shows the modal properties of the ID-model built with these values.

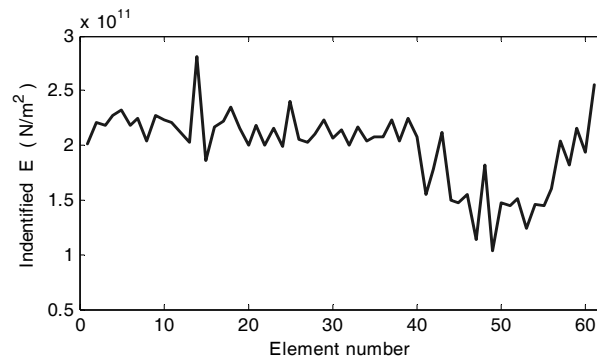


**Figure 5.9 Identified baseline for the optimization process**

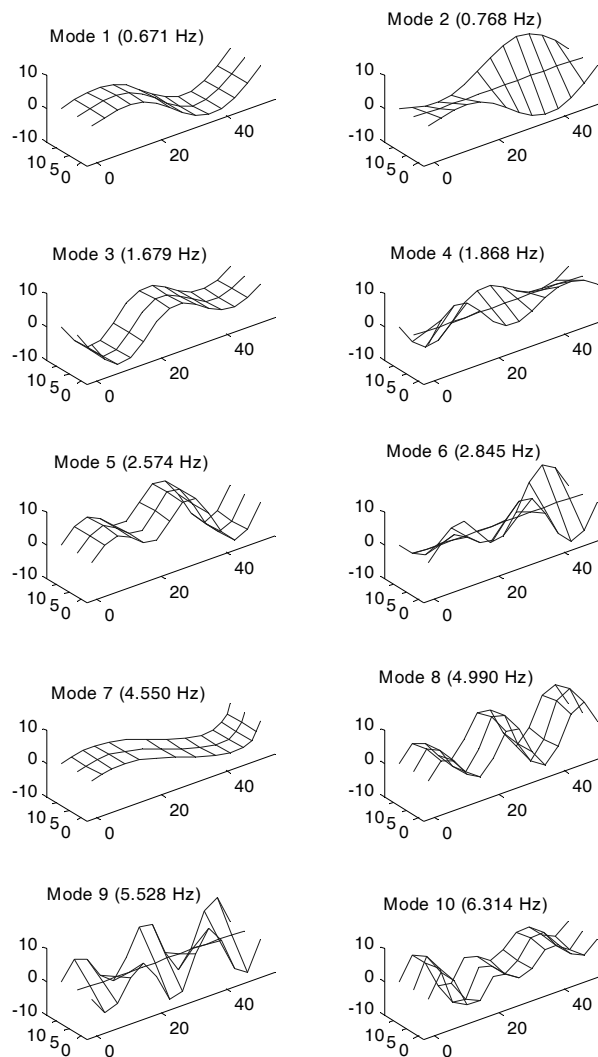


**Figure 5.10 Modal properties of the updated ID-model**

### 5.3.4 Setting up the Optimization Algorithm

The first issue that must be resolved is the selection of the parameters of the ID-model that will be updated. Note that, with the measurements recorded, the bending of the deck in the transversal direction cannot be determined. This type of deformation constitutes the main source of information about the condition of the connecting beams that provide lateral support to the girders. Note also that nine of the ten vibrational modes identified from the structure (see Fig. 5.7) are different configurations of bending in the longitudinal direction and torsional deformation of the deck, which mostly depend on the stiffness of the main girders. Therefore, given the limited amount of information, updating the Young's moduli of the connecting elements becomes difficult and even minor changes in the structure can result in high variations in their identified values. Therefore, it was decided not to update the elements of the ID-model associated with these structural members. As a result, only 39 elements are updated.

40 modes were used in the calculation of eigenvector sensitivities of the ID-model. By using this relatively low number of modes, 89.9% of the 12,870 calculated sensitivities (39 elements and 10 modes described by 33 points) reach values that are within 10% of the exact sensitivities. As an example, Fig. 5.11 shows how some of the calculated sensitivities of the first and sixth eigenvectors approach their exact values as the number of

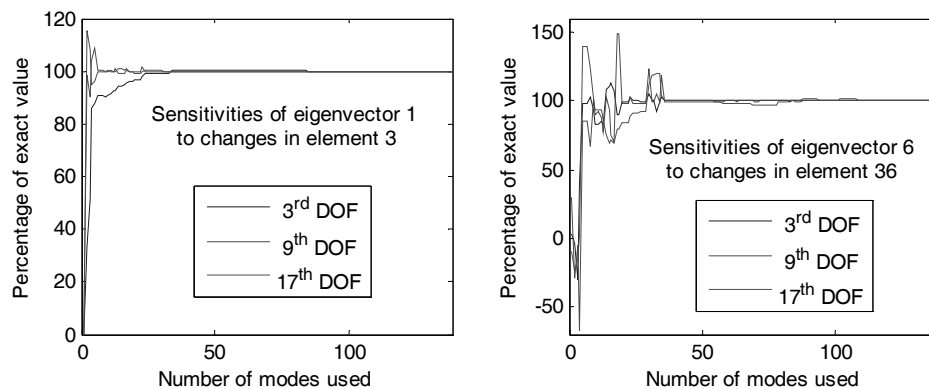


**Figure 5.11** Convergence of mode shape sensitivities

modes used to calculate them is increased. In addition, a maximum of 78 iterations (with 6 Fletcher-Reeves line-search iterations) were allowed for the conjugate gradients algorithm to search for a global minimum. This limit was set after observing that approximately two thirds of all processes reached convergence with less than 78 iterations.

### 5.3.5 Multiple Characterizations of the Healthy Structure

To properly map the influence of the environmental conditions over the identified stiffness values, the structure, in its healthy state, was characterized 100 times. Each characterization was performed using different identified modal properties of the FE-model under the influence of random environmental conditions and noisy sensors. Figure 5.12 shows all identified values as well as the normalized values, which show the deviation with respect to the mean values in percentile points (see Eq. 4-10).

### 5.3.6 Outlier Analysis and Issuing Warnings

As seen in Fig. 5.12b the normalized parameters deviate from the mean values significantly. Therefore, to set the first threshold required in the proposed PCA analysis and thus select the elements used in the prediction model, a relatively high limit of 3% was

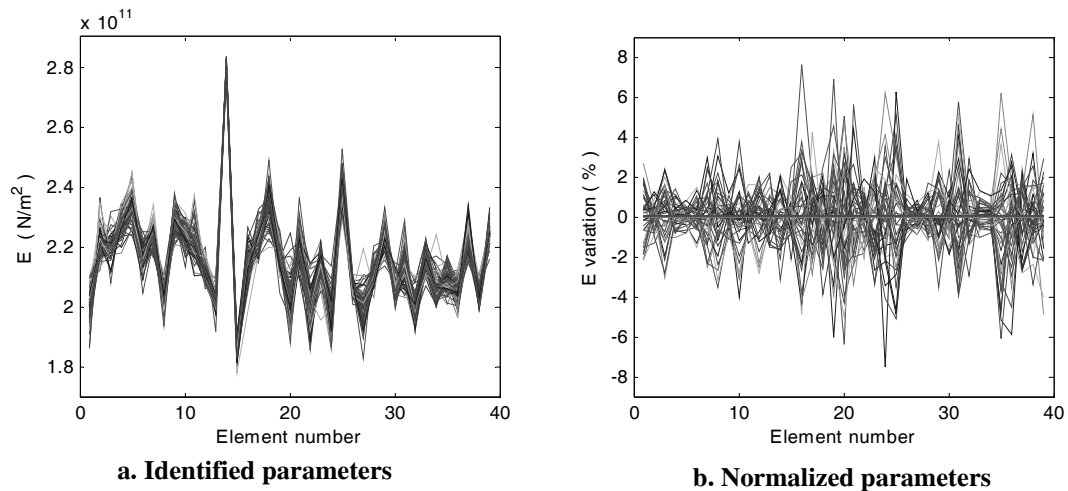


**Figure 5.12 100 characterizations of the healthy structure**

used. In addition, the coefficient of admissibility  $\alpha$  in the outlier analysis (see Eq. (4-15)) was selected as 5. In other words, those elements whose stiffness seem to have decreased by more than 5% according to the prediction model (i.e.  $e_p > -5\%$ ) are considered outliers. A warning shall then be issued in case three consecutive samples report the same (or greater) loss of stiffness.

Once damage is induced to the FE-model, 20 simulations and subsequent characterizations are performed. Figure 5.13 shows the outlier samples for each of the 39 updated elements in all 12 damage scenarios. Table 5.3 shows all warnings issued, indicating the element and the number of samples required to obtain three consecutive outliers.

**Table 5.3 Warnings issued**

Case	Warning issued for element	Samples needed	Status
1	--	--	--
2	9	3	Correct
3	22	3	Correct
4	1	10	Vicinity
	2	6	Correct
	15	7	Correct
5	15	3	Correct
6	17	5	Correct
7	4	3	Correct
	36	3	Correct
8	2	4	Correct
	12	3	Correct
9	10	4	Correct
	11	4	Correct
	12	4	Correct
10	5	3	Correct
	6	4	Correct
11	All	3	Correct (level 1)
12	--	--	False Negative

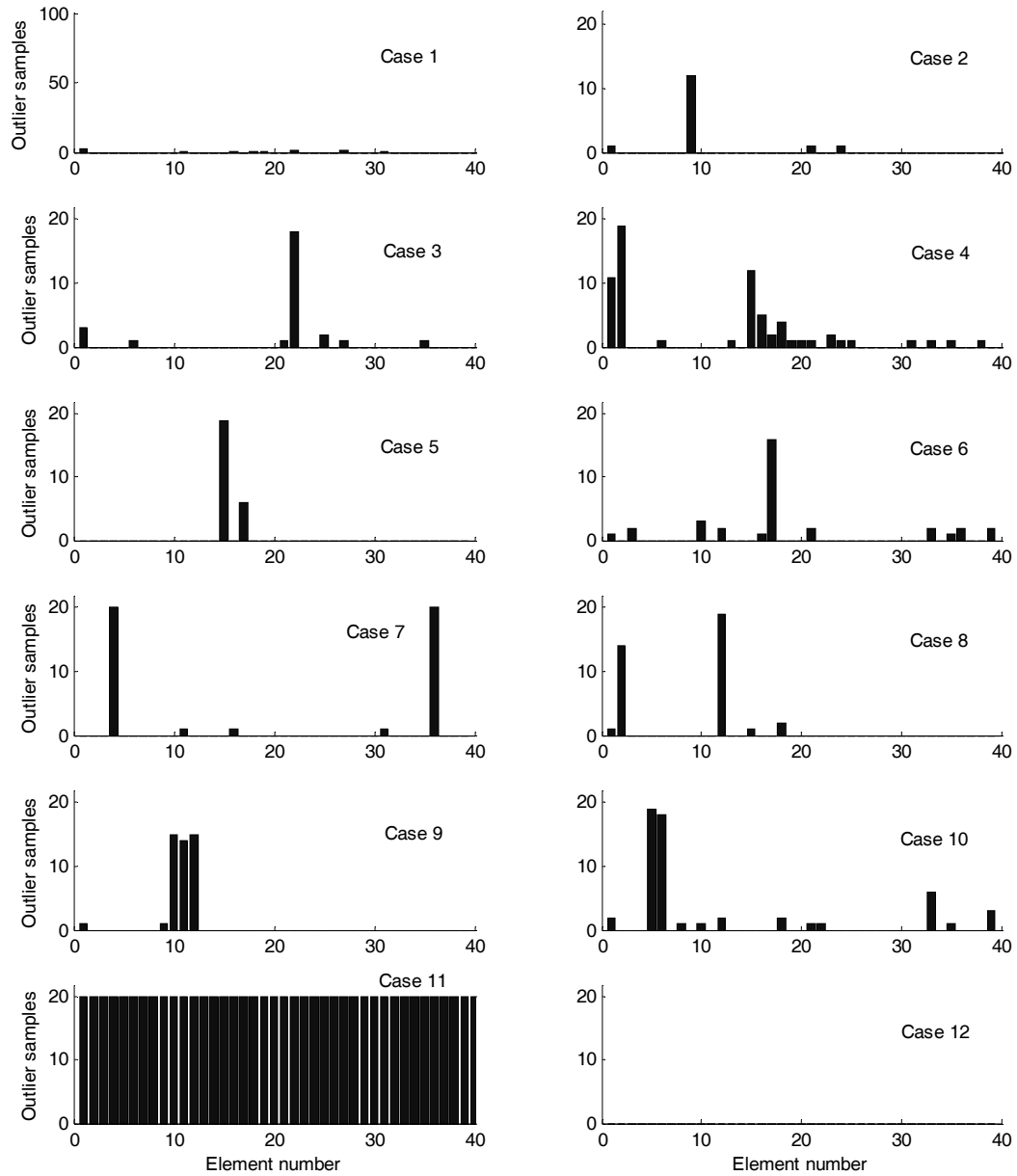


**Figure 5.13 Outlier samples of residual error ( $e_p > 5\%$ )**

Note that, with the exception of cases 11 and 12, all damage scenarios are detected and localized promptly by the framework. Among these ten cases, Case 4 was perhaps the most difficult to identify. As simply deduced from Figs. 5.3 and 5.8, the damaged elements of this case cannot be associated with a single element of the ID-model but with a

group of them (elements 2 and 15). With the characterizations obtained from this damaged model, six and seven samples were needed to count three consecutive outliers and issue warnings for elements 2 and 15 respectively. Moreover, after 10 characterizations of this damage case, a warning was issued for element 1, which is not directly associated with the damaged elements of the FE-model but with those in the immediate neighborhood.

Note also that in Case 11 all samples are considered as outliers and, therefore, warnings are issued for all elements of the ID-model. As it turns out, the removal of the support of one of the beams introduced radical changes in the dynamics of the bridge, to the point that the automated framework does not recognize the new mode shapes of the structure in order to couple them with mode shapes of the ID-model and carry out the optimization process. As explained previously in this chapter, such cases should be treated as outlier samples, provided that unrecognizable changes in the dynamics of the structure are most likely indicators of heavy damage. The framework issues a warning for case 11 indicating the existence of damage, but is unable to localize it within the structure.

The only false negative (damage going undetected) obtained from the cases analyzed was obtained in case 12. The damage in this case was induced in one of the connecting beams that provide lateral support to the main girders. Although, one might expect the damage to be reflected as changes in the longitudinal elements in the vicinity of the weakness, the changes to the dynamic properties were not sufficient to issue warnings for any element. This case is representative of all cases in which the connecting beams lose some of their initial stiffness. Perhaps a more dense distribution of sensors throughout the structure could allow the framework to localize such weaknesses. However, as demonstrated in this case, the limited amount of sensors employed in this example does not allow us to identify all types of damage.

### The Effects of the PCA Analysis

The overall temperature surrounding a structure has, in general, a relatively large influence over its modal properties. The natural frequencies of a steel structure, for instance, can differ by more than 2% between a cold day of winter at 0°C (32°F) and a hot day of summer at 40°C (104°F). However, the influence of this variable on the mode shapes is expected to be small unless residual stresses generated by differential expansion of the materials or restricting boundary conditions play a significant role. As a result, characterizations of a structure obtained with model updating techniques that use both natural frequencies and mode shapes are sensitive to temperature changes. For this reason, when the PCA analysis was combined with the non-iterative technique proposed by Caicedo *et al.* [14] in Chapter 4, the advantages of this type of analysis became evident.

The analytical results obtained in this chapter, however, do not show the same kind of positive impact the PCA analysis had in the numerical example presented in Chapter 4. The two main reasons for this deficiency are, namely: 1) the fact that the model updating technique used in the framework only uses the mode shapes as the source of information; and 2) the fact that this study fails to take into account residual stresses in the structure. As a result of this combination, the overall temperature has absolutely no impact on the mode shapes of the FE-model and, therefore, no impact on the characterizations of the structure. The PCA analysis is only useful in this example to reduce the influence of simulated temperature gradients, which, have little impact on the mode shapes of the FE-model.

In averaged values over the 20 damaged samples, Fig. 5.14 shows the residual error calculated with the PCA analysis as well as the variability of the Young's moduli identified with respect to the mean of the undamaged cases. Note that not much benefit is gained from the PCA analysis in this numerical example. In fact, advantages are only noticeable when verifying the slightly lower standard deviation of the residual errors, revealing the

reduction of some unknown effects (the temperature gradients, for instance). However, more meaningful and positive effects are expected in real scenarios, where variations of temperature can influence the mode shapes.

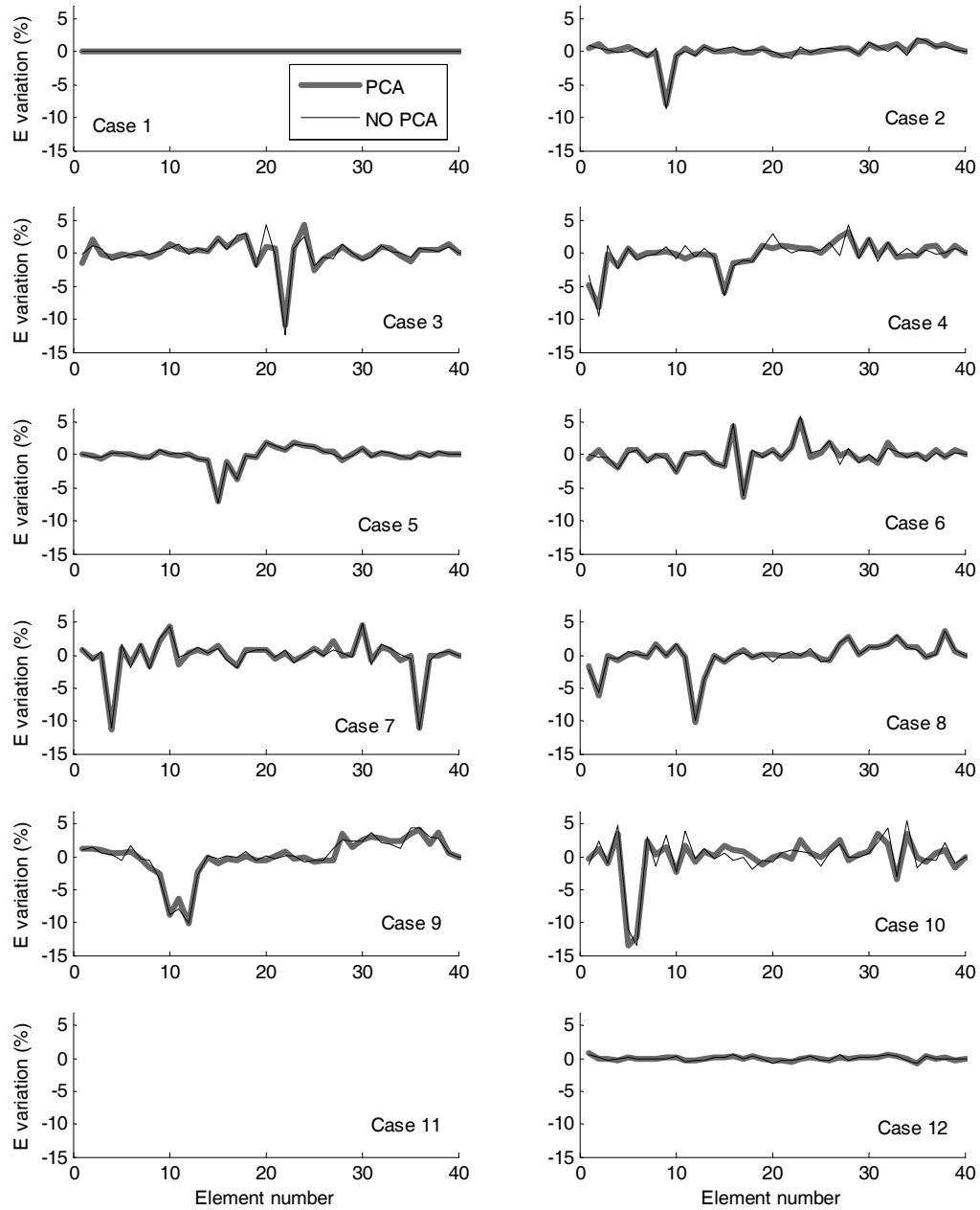


**Figure 5.14 Residual error (PCA) and Young's moduli reduction (no-PCA)  
(Averaged values over 20 samples)**

## 5.4 Conclusions

A structural health monitoring framework that uses the ambient vibrations of civil structures as the source of information was proposed in this chapter and broken down in six basic steps. This framework facilitates the identification and localization of damage regardless of the environmental conditions that affect the structure's dynamic behavior. The capabilities of the methodology were clearly demonstrated with simulated dynamic responses of a finite element model that represents a typical highway bridge. To add some realism to the study and test the robustness of the technique, several uncertainties and modeling errors typically found in real applications were considered in this numerical example. The main advantages and limitations of the proposed framework are discussed in the following paragraphs. The author acknowledges that these pros and cons are the result of the experience gained with the research involved in this dissertation, and that the implementation of the framework in other cases or engineering fields may disclose more useful information.

Although no specific minimum limit can be defined in general, the model updating methodology requires a considerable number of highly accurate mode shapes to characterize the structure. For instance, the correct localization of the all damage scenarios analyzed in this chapter, would not have been possible if only 8 mode shapes were available. But perhaps even more critical is the fact that these identified mode shapes were almost identical to the true eigenvectors (analytically calculated from the FE-model) and that their quality was barely sufficient. In terms of the modal assurance criterion, the identified mode shapes had a MAC average of 0.9996 when compared to the corresponding true values. As demonstrated by the numerical example of this chapter and the comparative study in Chapter 2, the stochastic subspace identification algorithm, aside from being highly accurate, is notably insensitive to the unavoidable measurement noise. However, the question on whether ambient loads are able to excite a significant

amount of vibrational modes with sufficient energy to be properly identified remains unsolved and should be investigated for specific applications.

Perhaps one of the most significant advantages of the model updating technique proposed as part of the framework is the fact that the construction of the identification model is not limited by the number of sensors used to identify the modal properties of the structure. This allows the user to construct more complex ID-models that better represent the structure, greatly improving the characterization of the structure. As indicated before, however, there is a trade-off as the complexity of the ID-model highly compromises the computational power required to implement the technique.

Because the evaluation of the objective function does not impose a pre-defined number of mode shape points, the number of sensors can be altered during the implementation of the technique with no major consequences. This feature constitutes a very attractive characteristic of the framework as the reliability of centralized sensor networks are not always perfect and the temporary loss of one or more sensors is relatively common. A further investigation should be conducted to analyze the numerical consequences.

The framework is a time consuming method and requires plenty of computational power and memory. To give the reader an idea of this issue, it can be mentioned that a personal computer with an Intel Pentium 4 microprocessor, 1GB of memory, and running at 2.4MHz, took an average of 29 minutes to obtain a single set of optimized Young's moduli. This time can be broken down into three specific tasks: 1) four minutes performing the dynamic simulation to obtain ten minutes of acceleration records, 2) one minute identifying the modal properties using the stochastic subspace algorithm, and 3) 24 minutes in the optimization of the parameters of the ID-model.

Although not much benefit was gained from the principal component analysis in the numerical example used in this chapter, this type of analysis provides a powerful tool to

reduce the effects of the environmental conditions for many SHM techniques (as clearly shown in Chapter 4). However, when combined with the model updating technique discussed in Chapter 3, a more positive outcome can be realized in real scenarios where the variations of temperature may have an influence on the relative values of the mode shapes of the structure.

The robustness of the framework has yet to be tested on a wider range of structures and its performance will vary with different applications. For instance, structures with a more lumped distribution of their mass (e.g. buildings) will likely not take full advantage of the mode shape sensitivities employed in the optimization process. Moreover, in some cases in which the symmetry of the structures may play an important role, the information provided by the variability of the mode shapes might not be sufficient to reach a global minimum of the evaluation function. An example that combines both of these difficulties is the SHM benchmark problem employed in Chapter 2. Although not shown here, characterizations of this structure obtained with the proposed framework tend to mask the damage losses as these are distributed between reductions and gains of geometrically opposite elements.

## Chapter 6

### Conclusions

The ultimate goal of this dissertation was to create a structural health monitoring framework for civil structures that aims the identification and localization of damage within a structure regardless of the environmental conditions that affect its dynamic behavior. After providing a general background on dynamic-based SHM and the existing techniques, the research focussed on three of the most critical steps in a chapter by chapter basis, namely: 1) the identification of the modal properties using ambient vibrations; 2) the characterization of the structure's stiffness at any given time; and 3) the reduction of the influence of the environmental conditions. The conclusions reached and developments proposed were combined in a six-step methodology that was tested with a finite element model of a typical highway bridge. The main findings of the research can be summarized as follows:

- A statistical comparison of three of the most popular modal identification techniques indicated that the stochastic subspace identification (SSI) method is a reliable way to estimate modal properties of structures as they vibrate in their natural environment. This comparison was carried out in the second chapter with both simulated as well as experimental data obtained from a four-storey steel building known as the SHM benchmark problem.

- The use of a mature optimization algorithm such as the conjugate gradients provides a powerful tool to characterize the stiffness of a structure and localize damage by observing the changes of the identified values. Characterizations are obtained by updating a representative finite element model such that the correlation of its mode shapes with those estimated from the structure is optimized. The evaluation criterion and the mathematical tools required to implement the optimization algorithm were derived in Chapter 3.
- When the unknown and always varying environmental conditions have a linear (or nearly linear) influence on numerical characterizations of a structure (e.g. identified Young's moduli), these effects can be accommodated by applying a principal component analysis to the identified parameters. This type of analysis was proposed in Chapter 4 and requires multiple characterizations of the healthy structure under a wide range of environmental conditions in order to accurately map the influence and reduce it in post-damage characterizations.
- The six-step structural health monitoring framework, as defined in Chapter 5, is capable of detecting and localizing the damage induced to a realistic finite element model of a typical highway bridge. These encouraging results were obtained despite a limited amount of sensors and a considerable number of realistic conditions considered in the study (e.g. modeling uncertainties, noisy sensors, non-white excitation). However, it became clear that a relatively high number of highly accurate mode shapes are required to successfully implement the methodology.

Depending on their nature, SHM techniques target specific types of damage. The dynamic-based framework developed in this dissertation, for instance, targets the localization of structurally deficient members capable of changing the global dynamic properties. On the other hand, other researchers have focussed their work on developing techniques to detect other forms of damage such as corrosion, fatigue and cracking,

which, may or may not affect the dynamic behavior of the structure. Therefore, to become more attractive to the industry and become a reality in our infrastructure, SHM systems must combine various techniques with different capabilities. Moreover, it is clear that, to stimulate the industry into applying the developed methodologies, studies of the cost-benefit ratio need to be carried out in the research community.

Although civil engineering structures are the main target of this dissertation, it is important to emphasize that the proposed SHM framework as a whole (or in part) is likely to perform well in other engineering fields. However, its viability, requirements and limitations may differ significantly and should be investigated for specific cases.

## 6.1 Future Work

One of the limitations of this study is associated with the fact that all finite element models employed were built with Euler-Bernoulli beam elements. This type of elements is commonly used to construct complex finite element models and different alternatives such as the condensation of degrees of freedom can help substitute other types of elements (membrane-type behavior of the bridge deck in Chapter 5). However, it is acknowledged here that the capabilities of the framework, in terms of efficiency and quality of results, need to be tested with other types of elements.

Perhaps one of the immediate steps that can be taken to further develop the methodology is the implementation of a standard way to quantify the localized damage. As presented, the framework issues a damage warning whenever a portion of the structure (associated with an element of the ID-model) consistently reveals the loss of a predefined percentage of stiffness (5% in the numerical case of Chapter 5). However, and even though a different course of action is probably needed when the stiffness reduction is significant, the issued warnings are always equivalent.

To further investigate the advantages of the principal component analysis proposed in Chapter 4, it is necessary to study the effects of various environmental conditions on the modal properties of structures, but mostly on the characterizations obtained from them. For instance, although variations of temperature alter the modulus of elasticity of steel, other side effects such as residual stresses generated by differential thermal expansion of materials and restricting boundary conditions need to be investigated. Moreover, both humidity and gradual variations of mass may have an impact that can potentially be accommodated with the statistically based analysis proposed.

One of the main advantages of the model updating technique proposed in Chapter 3 is the fact that the objective function used to update the model can be evaluated even when one or more sensors are lost (as long as corresponding modal points are used to calculate the MAC values). It is obvious that the accuracy of the technique is altered as each point contains information about the state of the structure. However, a study on the fault tolerance of the framework should be conducted, indicating the rate in which the results deteriorate with the loss of sensors.

## References

- [1] Abe M. and Siringoringo D.M. 2003. Structural health monitoring of long span bridges. *Structural Health Monitoring and Intelligent Infrastructure*, Balkema. 171–179.
- [2] Abdelghani M., Verhaegen M., Van Overchee P. and De Moor B. 1998. Comparison study of subspace identification methods applied to flexible structures. *Mechanical Systems and Signal Processing*. **12**(5): 679–692.
- [3] Allemang R.J. and Brown D.L. 1982. A correlation coefficient for modal vector analysis. *Proceedings of the 1st International Modal Analysis Conference*. Orlando, FL.
- [4] American Institute of Steel Construction, Inc. 2001. Manual of Steel Construction, Third Edition.
- [5] Andersen P. 1997. Identification of Civil Engineering Structures Using ARMA models. Ph.D. Dissertation. University of Aalborg. Denmark.
- [6] Asmussen J.C. 1997. Modal analysis based on the random decrement technique - application to civil engineering structures. Ph.D. Dissertation. University of Aalborg. Denmark.
- [7] Bedewi N.E. 1986. The mathematical foundation of the auto and cross random decrement technique and the development of a system identification technique for detection of structural deterioration. Ph.D. Dissertation. University of Maryland.
- [8] Bendat J.S. and A.G. Piersol. 1980. *Engineering Applications of Correlation and Spectral Analysis*, John Wiley and Sons, New York, NY.
- [9] Bernal D. 2002. Load vectors for damage localization. *Journal of Engineering Mechanics*. **128**(1):7–14.
- [10] Bertsekas D.P. 1995. Nonlinear programming. Belmon, MA. Athena Scientific. ISBN 1-886529-14-0.

- [11] Bertsekas D.P. and Tsitsiklis J.N. 1996. Neuro-dynamic programming. Belmon, MA. Athena Scientific. ISBN 1-886529-10-8.
- [12] Brinker R., De Stefano A., and Piombo B. 1996. Ambient data to analyze the dynamic behavior of bridges: A first comparison between different techniques. *Proceedings of the 14th International Modal Analysis Conference*. Dearborn, MI. February.
- [13] Bohle K. and Fritzen C.P. 2003. Results obtained by minimizing natural frequency and MAC value errors of a plate model. *Mechanical Systems and Signal Processing*, **17**(1): 55–64.
- [14] Caicedo J.M. 2003. *Structural Health Monitoring of Flexible Civil Structures*. Ph.D. Dissertation, Washington University. St. Louis, MO.
- [15] Caicedo J.M. and Dyke S.J. 2002. Determination of member stiffnesses for structural health monitoring. *Proceedings of the 3rd World Conference in Structural Control*. Como, Italy, April 7-12.
- [16] Caicedo J.M., Dyke S.J., and Johnson E.A. 2004. NExT and ERA for phase I of the IASC-ASCE benchmark problem. *Journal of Engineering Mechanics* (ASCE). **130**(1):49–60.
- [17] Caicedo J.M., Dyke S.J. and Mizumori A. 2004. Characterization of traffic excitation for numerical studies in structural health monitoring. *Proceedings of the 17th Engineering Mechanics Conference* (ASCE). Newark, DE. June 13-16.
- [18] Ching J. and Beck J.L. 2003. Two-stage bayesian structural health monitoring approach for phase II ASCE experimental benchmark studies. *Proceedings of the 16th Engineering Mechanics Conference* (ASCE). Seattle, WA. July 16-18.
- [19] Cole H.A. 1968. On-the-line analysis of random vibrations. *Journal of the American Institute of Aeronautics and Astronautics*. paper No 68-288.
- [20] Cole H.A. 1971. Failure detection of a space shuttle wing by random decrement. NASA TMX-62,041.
- [21] Cole H.A. 1973. Online failure detection and damping measurements of aerospace structures by random decrement signature. NASA CR-2205.
- [22] Desforges M.J., Cooper J.E., and Wrigth J.R. 1995. Spectral and modal parameter estimation from output-only measurements. *Mechanical Systems and Signal Processing*. **9**(2): 169–186.

- [23] Doebling S.W., Farrar C.R., and Prime M.B. 1998. A summary review of vibration-based damage identification methods. *The Shock and Vibration Digest*. **30**(2):91–105.
- [24] Doebling S.W., Farrar C.R., and Prime M.B. 1998. A summary review of vibration-based damage identification methods, *The Shock and Vibration Digest*. **30**(2):91–105.
- [25] Dyke S.J., Bernal D., Beck J., and Ventura C. 2003. Experimental phase of the structural health monitoring benchmark problem, *Proceedings of the 16th Engineering Mechanics Conference* (ASCE). Seattle, WA. July 16-18.
- [26] Fletcher R. 1987. Practical methods for optimization. J. Wiley & Sons, New York, NY. ISBN 0471494631.
- [27] Fox R.L. and Kapoor M.P. 1968. Rates of change of eigenvalues and eigenvectors. *Journal of the American Institute of Aeronautics and Astronautics*. **6**(12):2426–2429.
- [28] Gil P.E., Murray W., and Wright M.H. 1981. Practical Optimization. Academic press. London.
- [29] Giraldo D., Caicedo J.M., and Dyke S.J. 2003. Experimental phase of the SHM benchmark studies: Damage detection using NExT and ERA. *Proceedings of the 16th Engineering Mechanics Conference* (ASCE). Seattle, WA, July 15-18.
- [30] Giraldo D. and Dyke S.J. 2004. Damage localization in benchmark structure considering temperature effects. *Proceedings of the 7th International Conference on Motion and Vibration Control*. St. Louis, MO. August 8-11.
- [31] Guyan R.J. 1965. Reduction of stiffness and mass matrices. *Journal of the American Institute of Aeronautics and Astronautics*. **3**(2):380.
- [32] Hestenes M.R. and Stiefel. 1952. Methods of Conjugate Gradients for Solving Linear Systems. J. Res. Natl. Bur. Stand. **49**:409–436.
- [33] Heylen W. and Janter T. 1988. Applications of the modal assurance criterion in dynamic model updating. *Proceedings of the 13th International Conference on Noise and Vibration Engineering*. Leuven, Belgium, September.
- [34] <http://planetmath.org/encyclopedia/ConjugateGradientAlgorithm.html> (December, 2005).

- [35] <http://wusceel.cive.wustl.edu/asce.shm/benchmarks.htm> (May, 2005)
- [36] <http://www.faqs.org/faqs/ai-faq/neural-nets/part2/section-5.html> (December, 2005).
- [37] Hu X. and Shenton H.W. 2003. Damage identification in a two span continuous beam. *Structural Health Monitoring and Intelligent Infrastructure*. Balkema. 431–436.
- [38] Ibrahim S.R. 1977. Random decrement technique for modal identification of structures. *Journal of Spacecraft*. **14**(11):696–700.
- [39] Ibrahim S.R., Brinker R., and Asmussen J.C. 1996. Modal parameter identification from responses of general unknown random inputs. *Proceedings of the International Modal Analysis Conference*. Dearborn, MI. February.
- [40] Ibrahim S.R. and Mikulcik E.C. 1977. A method for the direct determination of vibration parameters from free responses. *Shock and Vibration Bulletin*. **47**(4):183–198.
- [41] Ito S., Onishi H., Matsui S., and Okuno M. 2003. Study on monitoring of deterioration of RC slab with optical fiber. *Structural Health Monitoring and Intelligent Infrastructure*, Balkema. 247–251.
- [42] Jaishi B. and Ren W.X. 2005. Structural finite element model updating using ambient vibration test results. *Journal of Structural Engineering*. **131**(4):617–628.
- [43] James G.H., Carne T.G., and Lauffer J.P. 1993. The natural excitation technique for modal parameter extraction from operating wind turbines. SAND92-1666, UC-261, Sandia National Laboratories.
- [44] Johnson E.A., Lam H.F., Katafygiotis L., and Beck J. 2000. A benchmark problem for structural health monitoring and damage detection. *Proceedings of the 14th Engineering Mechanics Conference* (ASCE). Austin, TX. May 21-24.
- [45] Johnson E.A., Lam H.F., Katafygiotis L., and Beck J. 2004. Phase I IASC-ASCE structural health monitoring problem using simulated data. *Journal of Engineering Mechanics* (ASCE). **130**(1):3–15.
- [46] Johnson L.M. 2004. Damage detection using static responses and unconstrained, non-linear optimization. M.S. Thesis, Washington University, Civil Engineering Department, St. Louis, MO.

- [47] Juang J.N. Cooper J.E., and Wright J.R. 1988. An eigensystem realization algorithm using data correlations (ERA/DC) for modal parameter identification. *Control theory and Advanced Technology*, **4**(1):5–14.
- [48] Juang J.N. and Pappa R.S. 1985. An eigensystem realization algorithm for modal parameter identification and model reduction, *Journal of Guidance and Control*, **8**(5):620–627.
- [49] Kirkegaard P.H. and Andersen P. 1997. State space identification of civil engineering structures from output measurements. *Proceedings of the 15th International Modal Analysis Conference*. Orlando, FL.
- [50] Kullaa J. 2001. Elimination of environmental influences from damage-sensitive features in a structural health monitoring system, *Structural Health Monitoring: The Demands and Challenges*, edited by F.-K. Chang, 742-749, CRC Press. Boca Raton, FL.
- [51] Lei Y., Kiremidjian A.S., Nair K.K., Lynch P.P., Law K.H., Kenny T.W., Carryer E., and Kottapalli A. 2003. Statistical damage detection using time series analysis on a structural health monitoring benchmark problem. *Proceedings of the 9th international conference on applications of statistics and probability in civil engineering*. San Francisco, CA. July.
- [52] Lew J.S., Juang J.N., and Longman R.W. 1993. Comparison of Several System Identification Methods for Flexible Structures. *Journal of Sound and Vibration*. **167**(3):461–480.
- [53] Ljung L. 1997. System Identification - Theory for the User. Prentice Hall. Englewood Cliffs.
- [54] Marwala T. and Heyns S. 1998. Multiple criterion method for determining structural damage. *Journal of the American Institute of Aeronautics and Astronautics*. **36**(8):1494–1501.
- [55] Matlab. Version 7.0. 2005. The MathWorks, Inc.
- [56] McConnell K.G. 1995. Vibration Testing: Theory and Practice. J. Wiley & Sons, New York, NY. ISBN 0-471-30435-2.
- [57] Moller P.W. and Friberg O. 1998. Updating large finite element models in structural dynamics. *Journal of the American Institute of Aeronautics and Astronautics*. **36**(10): 1861–1867.

- [58] Nelder J.A. and Mead R. 1965. Simplex method for function optimization. *Computer Journal*. **7**:308–313.
- [59] Nelson R.B. 1976. Simplified calculation of eigenvector derivatives. *Journal of the American Institute of Aeronautics and Astronautics*. **14**(9):1201–1205.
- [60] Pandey A.K., Biswas M., and Samman M. 1991. Damage detection from changes in curvature mode shapes. *Journal of Sound and Vibration*. **145**(2):321–332.
- [61] Parloo E., Guillaume P., and Van Overmere M. 2003. Damage Assessment Using Mode Shape Sensitivities. *Journal of Mechanical systems and Signal Processing*. **17**(3):499–518.
- [62] Petsounis K.A. and Fassois S.D. 2001. Parametric time-domain methods for the identification of vibrating structures: A critical comparison and assessment. *Journal of Mechanical Systems and Signal Processing*. **15**(6):1031–1060.
- [63] Poudel U.P., Fu G.K., and Ye J. 2004. Structural damage detection using digital video imaging and wavelet transformation. *Proceedings of the SEM International Congress and Exposition on Experimental and Applied Mechanics*. Costa Mesa, CA. June 7-10.
- [64] Ren W.X. and Zong Z.H. 2004. Output-only modal parameter identification of civil engineering structures. *International Journal of Structural Engineering and Mechanics*. **17**(3-4):429–444.
- [65] Rytter A. 1993. Vibration Based Inspection of Civil Engineering Structures. Ph.D. Dissertation, Department of Building Technology and Structural Engineering, Alborg University, Denmark.
- [66] Shen J.Y. and Sharpe L.Jr. 2000. Damage detection using residual modal forces and modal sensitivity. *Proceedings of 14th Engineering Mechanics Conference* (ASCE). Austin, TX. May.
- [67] Shewchuk J.R. 1994. An introduction to the conjugate gradient method without the agonizing pain. School of Computer Science. Carnegie Mellon University, Pittsburgh, PA.
- [68] Sohn H. and Farrar C.F. 2001. Damage diagnosis using time series analysis of vibration signals. *Smart Materials and Structures*. **10**(3):446–451.

- [69] Sohn H., Worden K., and Farrar C.F. 2001. Novelty detection under changing environmental conditions, *SPIE's 8th Annual International Symposium on Smart Structures & Materials*. Newport Beach, CA. (LA-UR-01-1894).
- [70] Sumitro S., Kurokawa S., Shiano K., Hida K., and Wang M.L. 2003. Monitoring based maintenance by utilizing actual-stress sensory technology. *Structural Health Monitoring and Intelligent Infrastructure*, Balkema. 937–945.
- [71] Tarassenko L., Nairac A., Townsend N., Buxton I., and Cowley Z. 2000. Novelty detection for the identification of abnormalities. *International Journal of Systems Science*. **31**(11):1427–1439.
- [72] Vandiver J.K., Dunwoody A.B., Campbell R.B., and Cook M.F. 1982. A mathematical basis for the random decrement vibration signature analysis technique. *Journal of Mechanical Design*. **10**(april).
- [73] Van Overchee P. and De Moor B. 1996. Subspace Identification for Linear Systems: Theory, Implementation and Applications. Kluwer Academic Publishers, Dordrecht, Netherlands.
- [74] Worden K., Manson G. and Fieller N.R.J. 2000. Damage detection using outlier analysis, *Journal of Sound and Vibration*. **229**(3):647–667.
- [75] Xiang Y.Q., Weng S.L., Song Y., and Yao Y.D. 2003. Health monitoring and assessment management systems of Wenhui Bridge. *Structural Health Monitoring and Intelligent Infrastructure*, Balkema. 913–920.
- [76] Yan A.M., Kerschen G., De Boe P., and Golinval J.C. 2005. Structural damage diagnosis under changing environmental conditions – Part 1: Linear analysis. *Journal of Mechanical Systems and Signal Processing*. **19**(4):847–864.
- [77] Yan A.M., Kerschen G., De Boe P., and Golinval J.C. 2003. Structural damage diagnosis under changing environmental conditions – Part 2: Local PCA for nonlinear cases. *Journal of Mechanical Systems and Signal Processing*. **19**(4):865–880.
- [78] Yokoyama K., and Rafiquzzaman A.K.M. 2003. Bridge damage detection from operating vehicle load. *Structural Health Monitoring and Intelligent Infrastructure*, Balkema. 415–422.

## Vita

### Diego F. Giraldo

<b>Date of Birth</b>	September 26, 1975
<b>Place of Birth</b>	Buga, Valle, Colombia
<b>Degrees</b>	B.S. Civil Engineering, May 1998 M.S. Civil Engineering, 2003 D.Sc. Civil Engineering, 2006
<b>Affiliations</b>	Earthquake Engineering Research Institute (EERI) American Society of Civil Engineers (ASCE) Chi-Epsilon, Civil Engineering Honor Society
<b>Publications</b>	<p>Giraldo D., Yoshida O., Dyke S.J., and Giacosa L. (2004). Control-oriented system identification using ERA. <i>Journal of Structural Control</i>, <b>11</b>(4):239-257.</p> <p>Giraldo D., Dyke S.J., and Caicedo J.M. (2005). Damage detection accommodating varying environmental conditions. <i>Structural Health Monitoring: An International Journal</i>. (In press).</p> <p>Giraldo D., Dyke, S.J. (2005). Control of an elastic continuum when traversed by a moving oscillator. <i>Journal of Structural Control and Health Monitoring</i>. (In press).</p> <p>Giraldo D., Caicedo J.M., Song W., Mogan B., and Dyke S.J. (2006). Modal Identification through Ambient Vibration: A Comparative Study. (In preparation).</p>

May 2006

Short Title: Health Monitoring of Structures

Giraldo, D.Sc. 2006